

**Vortex pairs on surfaces:
can it be a tool for topology in the large?**

Jair Koiller

Universidade Federal de Juiz de Fora, Brazil

joint with

**Umberto Hryniewicz, Alejandro Cabrera, Anilatmaja Aryasomayajula
Adriano Regis Rodrigues, Cesar Castilho**



UNIVERSITÀ
DEGLI STUDI
DI PADOVA

**Geometry, Dynamics and Mechanics
Seminar**

June 8, 2021

Aim of this talk:
propagandizing a research program

**Geometry, Dynamics and Mechanics
of vortices on surfaces**

classical (+ statistical + quantum ?)

Thanks

Stefanella Boatto

Clodoaldo Ragazzo, Humberto Viglioni

Support

**CAPES/CNPq/PVE11-2012
with Darryl Holm/Tudor Ratiu**

**CAPES/CNPq/PVE089-2013
with Richard Montgomery/Alain Albouy**

UFJF, Senior Visitor, 2018-.....

Timeline

Aristotle discussed how typhoons are formed.

Leonardo da Vinci depicted turbulence in fluids - even vortices generated by the aortic valve!

René Descartes: “vortex theory of everything” .

Euler: Mathematical formulation of vorticity

Subsequent generations of mathematical physicists

Helmholtz, Kirchhoff

W. Thomson (Kelvin) + Tait, J.J. Thomson...

Arnold (1966): Euler equations

solid body \sim perfect fluids

Ebin-Marsden (1970): the hard analysis

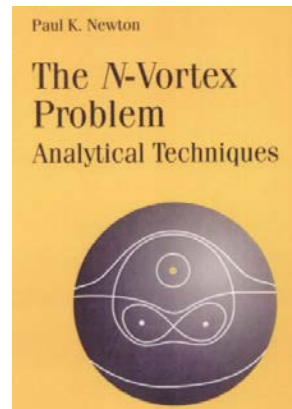
Marsden-Weinstein (1983):

vorticity is a momentum map!

Vorticityists form a large community

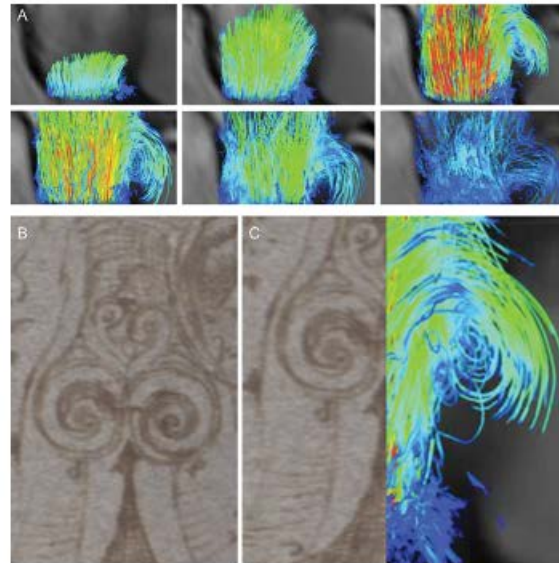
**Mathematicians, Physicists
Engineers, Biologists**

For mathematicians (I fear forgetting many):



**P. Newton, Point vortex dynamics in the post-Aref era
2014 Fluid Dyn. Res. 46 031401**

Flow vortices in the aortic root: in vivo 4D-MRI confirms predictions of Leonardo da Vinci



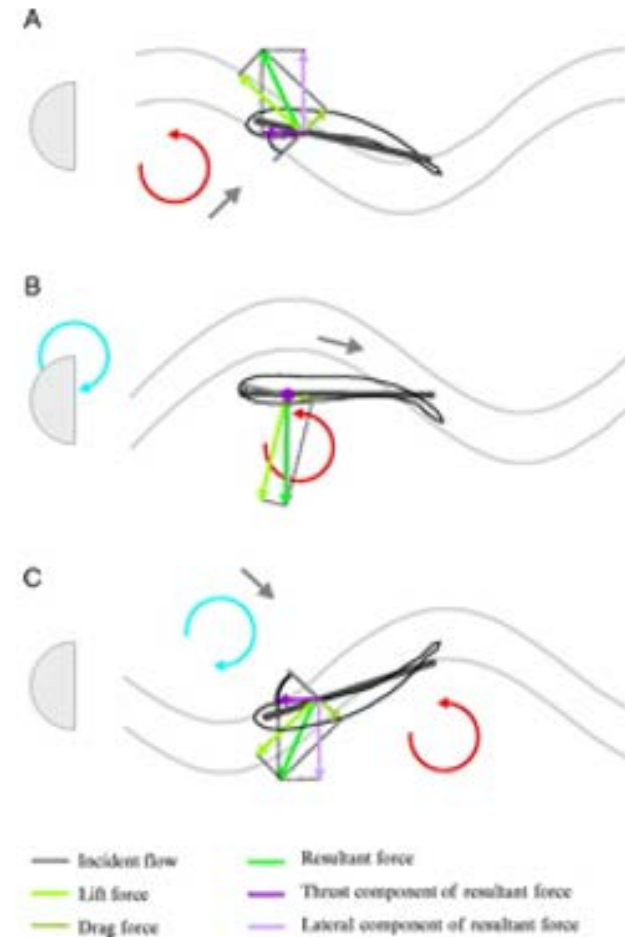
Eur Heart J, Volume 35, Issue 20, 21 May 2014, Page 1344, <https://doi.org/10.1093/eurheartj/ehu011>
The content of this slide may be subject to copyright: please see the slide notes for details.

OXFORD
UNIVERSITY PRESS



Rainbow trout use only their anterior muscles when swimming between vortices in water flow. The assist that the fish get from the vortices supports a hydrodynamic explanation for fish distributions in schools and in current-swept habitats.

[J. C. Liao et al.]



Observation of Vortex Dipoles in an Oblate Bose-Einstein Condensate

T. W. Neely, E. C. Samson, A. S. Bradley, M. J. Davis, and B. P. Anderson

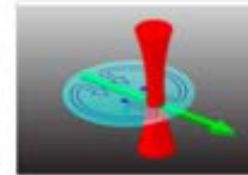
Phys. Rev. Lett. **104**, 160401 (2010)

Published April 19, 2010

Viewpoint: Observing the dance of a vortex–antivortex pair, step by step

Peter Engels, Department of Physics and Astronomy, Washington State University, Pullman, WA 99163, USA
April 23, 2010 • Physics 1, 33

New experiments create pairs of vortices of opposite circulation by forcing a Bose-Einstein condensate to flow past an obstacle.

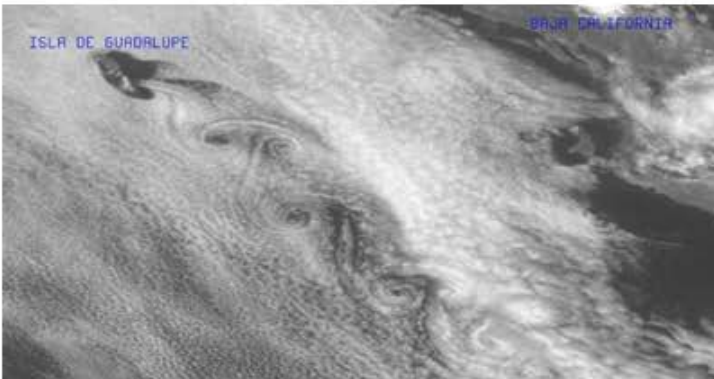


We nucleate pairs of vortices of opposite charge (vortex dipoles) by forcing superfluid flow around a repulsive Gaussian obstacle within the BEC. By controlling the flow velocity we determine the critical velocity for the nucleation of a single vortex dipole, with excellent agreement between experimental and numerical results. We present measurements of vortex dipole dynamics, finding that the vortex cores of opposite charge can exist for many seconds and that annihilation is inhibited in our trap geometry.



Streets formed by two opposite vortices were first studied by von Kármán in 1911 and motivated by a troubled experiment about the wake on flows past a cylinder that was being done in L. Prandtl's lab.

“What I really contributed to the aerodynamic knowledge of the observed phenomenon is twofold: I think I was the first to show that the symmetric arrangement of vortices (upper), which would be an obvious possibility to replace the vortex sheet is unstable. I found that only the asymmetric arrangement (lower) could be stable, and only for a certain ratio of the distance between the rows and the distance between two consecutive vortices of each row. Also, I connected the momentum carried by the vortex system with the drag and showed how the creation of such a vortex system can represent the mechanism of the wake drag” (Aerodynamics, von Kármán, 1963).



Tribute to Engineers

Prandtl, von Kármán (see next)

Bénard, Coanda

Joukowski, Korolev

Taylor, Lighthill

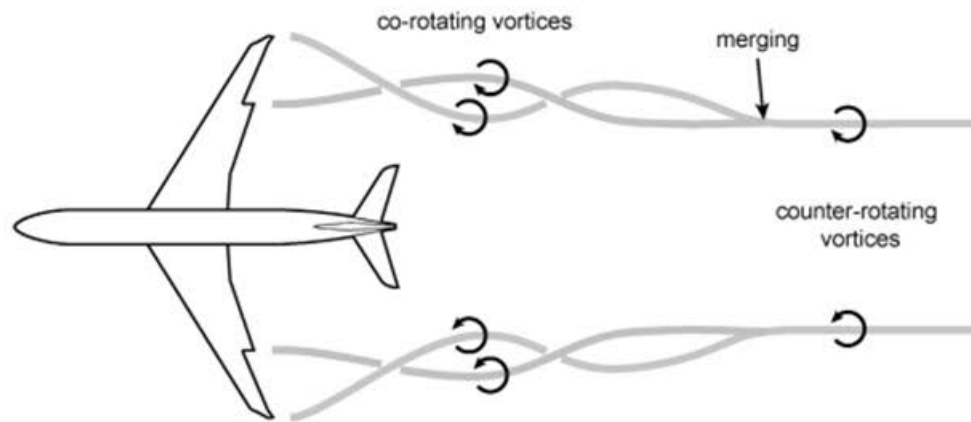


Even a scientist gets time off to meet celebrities.

<http://allanellenberger.com/dr-theodore-von-karman-father-of-the-supersonic-age/>



P. Meunier et al. / C. R. Physique 6 (2005) 431–450



Experimental and numerical study of vortex couples in two-dimensional flows

By **Y. COUDER**

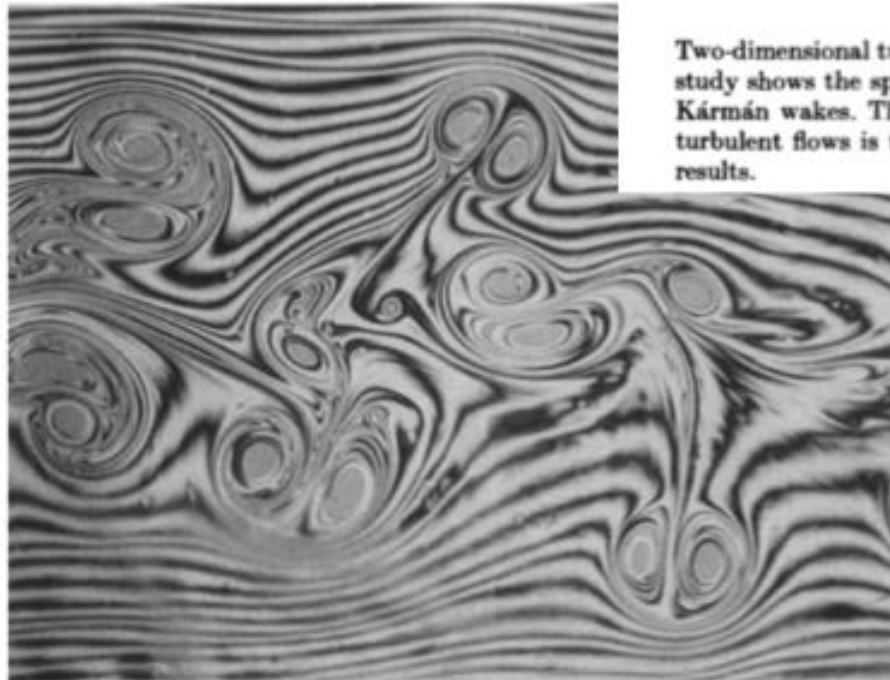
Groupe de Physique des Solides, Ecole Normale Supérieure, 24, rue Lhomond,
75231 Paris Cedex 05, France

AND **C. BASDEVANT**

Laboratoire de Météorologie Dynamique, Ecole Normale Supérieure, 24, rue Lhomond,
75231 Paris Cedex 05, France

(Received 26 March 1986)

Two-dimensional turbulence is investigated experimentally in thin liquid films. This study shows the spontaneous formation of couples of opposite-sign vortices in von Kármán wakes. The structure of these couples, their behaviour and their role in turbulent flows is then studied using both a numerical simulation and laboratory results.



My *fu* paper

**(topic suggested by Marsden and Aref in my
post-doc, 1982)**

Non-Integrability of the 4-Vortex System: Analytical Proof

Jair Koiller^{1,*} and Sonia P. Carvalho²

¹ Laboratório Nacional de Computação Científica, Caixa Postal 56018, 22290 Rio de Janeiro, RJ, Brazil

¹ Instituto de Matemática da UFRJ, Caixa Postal 68530, 21944 Rio de Janeiro, RJ, Brazil

² Departamento de Matemática da UFMG, ICEX, Pampulha, Belo Horizonte, MG, Brazil, 30000

Abstract. An analytical proof is given that the motion of n point vortices in the plane is non-integrable for $n > 3$. The basic geometric configuration, which models a situation often found experimentally, consists of two opposite strong vortices and two advected weak vortices. We use “Melnikov’s method,” as presented by Holmes and Marsden [Commun. Math. Phys. **82**, 523–544 (1982)]. The Melnikov integral is explicitly evaluated, by residues, in the limiting situation where one of the weak vortices is very close to one of the primaries.

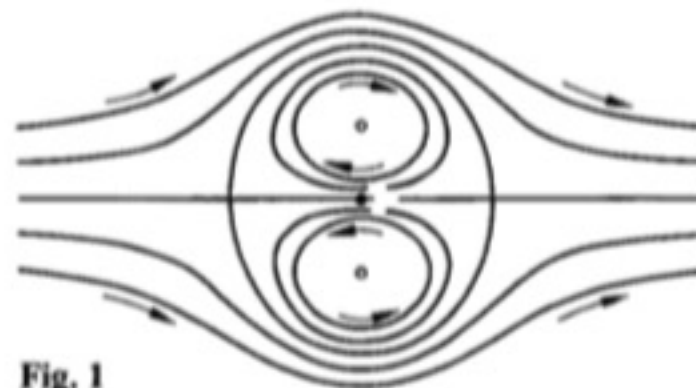


Fig. 1

II. Short review:

Vortices on Surfaces

Vortices on the sphere

Gromeka (1851-1889, MR0056525), Zermelo (1899)
Bogomolov (1977), Kimura/Okamoto (1987),

Many papers appeared since the 2000's

Aref, Borisov/Mamaev, Cabral, Newton, Boatto,
Dritschel, Simo, Kidambi, Montaldi, Marsden, Patrick,
Pekarsky, Roberts, Schmidt, Tronin, Naranjo, García-
Azpeitia, ...

(SORRY FOR MANY OMISSIONS!)

EDOs for vortices in a sphere of radius R

$$\dot{\mathbf{x}}_i = \frac{1}{4\pi R} \sum_{j=1}^N \frac{\Gamma_j (\mathbf{x}_j \times \mathbf{x}_i)}{(R^2 - \mathbf{x}_i \cdot \mathbf{x}_j)}.$$

If the sum $\sum \Gamma_j \neq 0$ there is an uniform counter-vorticity in the background.

Bogomolov, Dynamics of vorticity at a sphere, 1977

<https://link.springer.com/article/10.1007/BF01090320>

The Hamiltonian involves the Green function of spherical Laplacian.

Planar vortices in domains with boundary

C.C. Lin (1916-2013)

<https://history.aip.org/phn/11603035.html>

PhD in Aeronautics, 1944

**California Institute of Technology, Pasadena,
under von Kármán.**



C.C.Lin's theorems (PNAS, 1941)

Vortex dynamics in planar regions

THEOREM I. *For the motion of vortices of strengths κ_i ($i = 1, 2, \dots, n$) in a general region R bounded by fixed boundaries, there exists a Kirchhoff-Routh function $W(x_1, y_1; x_2, y_2; \dots; x_n, y_n)$ such that*

$$\left. \begin{aligned} \kappa_i \frac{dx_i}{dt} &= \kappa_i u_i = - \frac{\partial W}{\partial y_i}, \\ \kappa_i \frac{dy_i}{dt} &= \kappa_i v_i = \frac{\partial W}{\partial x_i}, \end{aligned} \right\} \quad (4.3)$$

where $P_i(x_i, y_i)$ ($i = 1, 2, \dots, n$) are the instantaneous positions of the vortices. The function W is given by

$$W = \sum_{i=1}^n \kappa_i \psi_0(x_i, y_i) + \sum_{\substack{i,j=1 \\ (i>j)}}^n \kappa_i \kappa_j G(x_i, y_i; x_j, y_j) + \frac{1}{2} \sum_{i=1}^n \kappa_i^2 g(x_i, y_i; x_i, y_i). \quad (4.4)$$

W = Kirchhoff-Routh function G = Green function
 g = desingularization of G ψ_0 = external agents

ON THE MOTION OF VORTICES IN TWO DIMENSIONS—II
SOME FURTHER INVESTIGATIONS ON THE KIRCHHOFF-
ROUTH FUNCTION

BY C. C. LIN

DEPARTMENT OF APPLIED MATHEMATICS, UNIVERSITY OF TORONTO

Communicated October 20, 1941

5. *Conformal Transformation.*—We shall now investigate the behavior of the Kirchhoff-Routh function (whose existence we have established in the preceding article) under a conformal transformation of fluid motion.

THEOREM II (*Generalized Routh's theorem*).—*Under a conformal transformation*

$$\bar{z} = f(z) \quad (5.1)$$

which derives the motion in the \bar{z} -plane from that in the z -plane, the Kirchhoff-Routh function for the new motion is given by

$$\bar{W} = W + \sum_{i=1}^n \frac{\kappa_i^2}{4\pi} \log \left| \frac{dz}{d\bar{z}} \right|_{P_i} \quad (5.2)$$

the added term is the log a conformal factor

J. Hally (J. Math. Phys. 21:1, 211-217, 1980)

$$ds^2 = h^2(z, \bar{z}) |dz|^2$$

$$h^2(z_n, \bar{z}_n) \dot{\bar{z}}_n = \sum_{k \neq n}^N -i \frac{\Gamma_k}{z_n - z_k} + i \Gamma_n \frac{\partial}{\partial z_n} \ln(h(z_n, \bar{z}_n)), \quad n = 1, \dots, N$$

Hally suggests that for a closed genus zero surface one could use the stereographic projection, $\Sigma \equiv \mathbb{C} \cup \infty = S^2$. and the above equations would be still OK.

Caveat: when $\sum_{i=1}^N \Gamma_i \neq 0$ there is an extra term, that is nonlocal: it involves $\Delta^{-1}h$ (JK and Stefanella Boatto).

Motivation for vortices on curved surfaces

REVIEWS OF MODERN PHYSICS

[Recent](#) [Accepted](#) [Authors](#) [Referees](#) [Search](#) [Press](#) [About](#) [Staff](#) 

Vortices on curved surfaces

Ari M. Turner, Vincenzo Vitelli, and David R. Nelson
Rev. Mod. Phys. **82**, 1301 – Published 30 April 2010

[Article](#) [References](#) [Citing Articles \(99\)](#) [PDF](#) [HTML](#) [Export Citation](#)

[>](#)

ABSTRACT

Topological defects in thin films coating a deformed substrate interact with the underlying curvature. This coupling mechanism influences the shape of biological structures and provides a new strategy for the design of interfaces with prescribed functionality. In this article, a mathematical formalism based on the method of conformal mapping that is presented permits the calculation of the energetics of disclinations, dislocations, and vortices on rigid substrates of spatially varying Gaussian curvature. Special emphasis is placed on determining the geometric force exerted on vortices in curved superfluid films. This force, which attracts (repels) vortices towards regions of negative (positive) Gaussian curvature, is an illustration of how material shape can influence quantum mechanical degrees of freedom.

Vortices in Superfluid Films on Curved Surfaces

Ari M. Turner¹, Vincenzo Vitelli¹ and David R. Nelson^{*}

^{*}Department of Physics, Harvard University, Cambridge MA 02138

¹Department of Physics, University of California, Berkeley CA 94720 and

¹Department of Physics and Astronomy, University of Pennsylvania, Philadelphia PA 19104

(Dated: October 22, 2018)

We present a systematic study of how vortices in superfluid films interact with the spatially varying Gaussian curvature of the underlying substrate. The Gaussian curvature acts as a source for a geometric potential that attracts (repels) vortices towards regions of negative (positive) Gaussian curvature independently of the sign of their topological charge. Various experimental tests involving rotating superfluid films and vortex pinning are first discussed for films coating gently curved substrates that can be treated in perturbation theory from flatness. An estimate of the experimental regimes of interest is obtained by comparing the strength of the geometrical forces to the vortex pinning induced by the varying thickness of the film which is in turn caused by capillary effects and gravity. We then present a non-perturbative technique based on conformal mappings that leads an exact solution for the geometric potential as well as the geometric correction to the interaction between vortices. The conformal mapping approach is illustrated by means of explicit calculations of the geometric effects encountered in the study of some strongly curved surfaces and by deriving universal bounds on their strength.

Contents		D. Consumer's Guide to Green's Functions on Compact Surfaces	42
I. Introduction	1	E. Approximations for Long Surfaces of Revolution	43
II. Fluid Dynamics and Vortex-Curvature Interactions	4	F. Derivations of Bounds Valid Even for Strong Distortions	47
A. Anomalous force on rotationally symmetric surfaces	6	References	49
B. Vortex-trapping surfaces	8		
C. Negative curvature which does not trap	10		
D. Hysteresis of vortices and trapping strength	12		
III. Rotating Superfluid Films on a Corrugated Substrate	12	I. INTRODUCTION	
A. The effect of rotation	12	In superfluid helium, vortices form when the helium is rotated rapidly or when there is turbulence (Tilley and Tilley, 1990; Vinen, 1969). Though such vortices are similar to the vortices that make up a vortex street behind the wings of an airplane or to the funneled clouds of tornadoes, they are only an Angstrom or two across (Guyon <i>et al.</i> , 2001). A more essential difference is that the vortices in a superfluid do not need a constant source of energy to survive. In fact, a vortex is long-lived because the strength of its flow is fixed by the quantization of angular momentum. Thus, the dissipative mechanisms of a conventional fluid are absent.	
B. Single defect ground state	13	In this article, we focus on forces that the vortices experience as a result of geometric constraints, with an emphasis on those encountered in thin layers of liquid helium wetting a curved substrate with spatially varying Gaussian curvature. As a result of the broken translational invariance of the underlying curved space, the energy of a single vortex with circulation quantum number n_i at position \mathbf{u}_i includes both a divergent term and a position dependent self-energy, $E_s(\mathbf{u}_i)$, given by (Vitelli and Turner, 2004)	
C. Multiple defect configurations	14		
D. Abrikosov lattice on a curved surface	16		
IV. Experimental Considerations	17		
A. The Van der Waals force and thickness variation	18		
B. Parameters for the rotation experiment	20		
C. Films of varying thickness from the three-dimensional point of view	21		
D. Vortex Depinning	22		
V. Complex Surface Morphologies	23		
A. Using conformal mapping	24		
B. Vortices on a "Soap Film" Surface	27		
C. Periodic surfaces	28		
D. Band-flows on elongated surfaces	30		
E. Interactions on a closed surface	33		
VI. Limits on the Strength and Range of Geometrical Forces	36		
VII. Conclusion	38		
VIII. Acknowledgments	38		
A. Nearly Flat Surfaces	38		
B. The Saddle Surface's Potential	40		
C. Van der Waals Attraction on a Curved Surface	41		

$$E_s(\mathbf{u}_i) = -\pi K n_i^2 U_G(\mathbf{u}_i), \quad (1)$$

where $K = \frac{\rho_s \kappa^2}{m^2}$ is the superfluid stiffness expressed in

arXiv:0802.4313v1 [math.SG] 29 Feb 2008

Vortices on closed surfaces

Stefanella Boatto

Departamento de Matemática Aplicada da UFRJ

C.P. 68530, Cidade Universitária

Rio de Janeiro, RJ, 21945-970, Brazil (boatto@impa.br)

Jair Koiller*

Núcleo de Matemática Aplicada, Fundação Getulio Vargas

Praia de Botafogo 190

Rio de Janeiro, RJ, 22250-040, Brazil (jkoiller@fgv.br)

Contents

1 Introduction	3
1.1 Vortex history on a capsule	3
1.2 Vortices on curved surfaces	3
2 Laplace-Beltrami operator and 2-dimensional hydrodynamics	4
2.1 Complex and symplectic geometry	4
2.2 Poisson's equation and Green functions for the Laplace operator	5
3 Point vortex equations	6
3.1 Eppur si muove: vortex drift under its own stream	6
3.2 Collective vortex motions: Hamiltonian description	7
3.3 How Green and Robin functions change under conformal transformations	8
3.4 Jordan domains, Schottky doubles	9
4 When the total vorticity vanishes	10
4.1 Riemann surface Green functions	10
4.2 Surfaces conformal to S^2	11
4.3 Proof of Kimura's conjecture on dipole motion	12
5 Final Remarks	12
5.1 Robin's function and vortex drift	12
5.2 Batman's function and integrable vortex pair problems on Liouville surfaces	12
5.3 Time dependent problems	13
5.4 Higher dimensional extensions	13
5.5 Vortices for a proof of Riemann hypothesis?	13

*Supported in part by a grant from Nehama gestão de ativos.

Vortices on compact surfaces Σ (any genus)

$$H = \sum_{1 \leq i < j \leq N} \kappa_i \kappa_j G_g(s_i, s_j) + \sum_{\ell=1}^N \frac{1}{2} \kappa_\ell^2 R_g(s_\ell)$$

$$\Omega_{\text{collective}}(s_1, \dots, s_N) = \sum_{\ell=1}^N \kappa_\ell \Omega(s_\ell)$$

$G_g(s_1, s_2)$ = Green function of Laplace-Beltrami operator

$R_g(s) = \lim_{s' \rightarrow s} G(s', s) - \frac{1}{2\pi} \ln d(s', s)$ (Robin function)

Ω_g = area form of the metric g .

Boatto/Koiller, Vortices on Closed Surfaces, Fields Institute 73, 2015

https://link.springer.com/chapter/10.1007/978-1-4939-2441-7_10

Metrics related by a conformal factor $\tilde{g} = h^2 g$

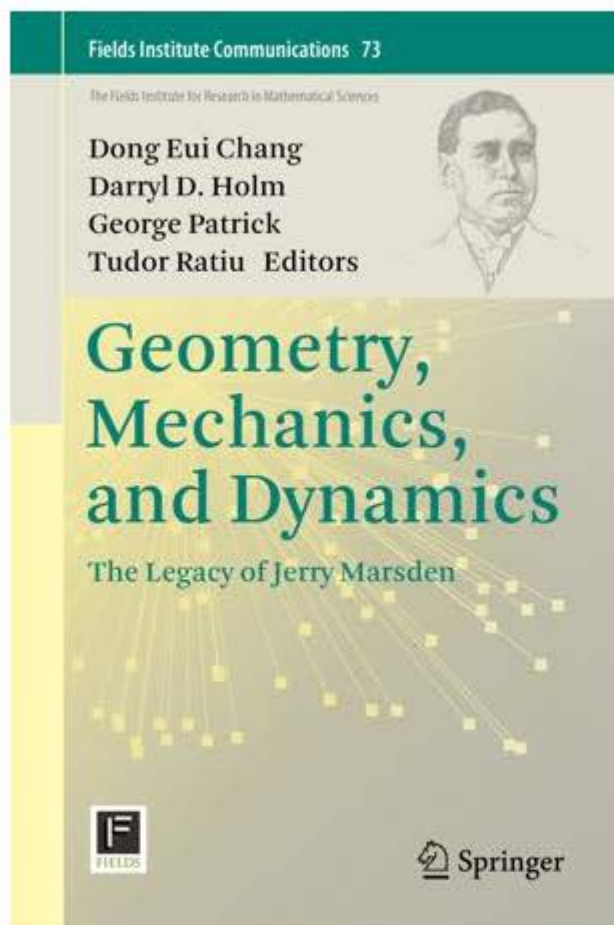
$$\tilde{\Omega}_{\text{collective}}(s_1, \dots, s_N) = \sum_{\ell=1}^N \kappa_{\ell} h^2(s_{\ell}) \omega(s_{\ell}) .$$

$$\tilde{H} = H(s_1, \dots, s_N) - \frac{1}{4\pi} \sum_{\ell=1}^N \kappa_{\ell}^2 \log(h(s_{\ell})) - \frac{\kappa}{\tilde{A}(S)} \sum_{\ell=1}^N \kappa_{\ell} \Delta_g^{-1} h^2(s_{\ell})$$

where

$$\kappa = \sum_{\ell=1}^N \kappa_{\ell} .$$

The last term vanishes when the sum of the vorticities is zero (which is the case for the vortex pair systems).



Vortices on Closed Surfaces

Stefanella Boatto and Jair Koeller

Dedicated to the memory of Jerry Marsden

Abstract It was recognized, since the seminal papers of Arnold (Ann Inst Grenoble 16:319–361, 1966) and Ebin-Marsden (Ann Math Ser 2 92(1):102–163, 1970), that Euler’s equations are the right reduction of the geodesic flow in the group of volume preserving diffeomorphisms. In 1983 Marsden and Weinstein (Physica D 7:305–323, 1983) went one step further, pointing out that vorticity evolves on a coadjoint orbit on the dual of the infinite dimensional Lie algebra consisting of divergence free vectorfields. Here we pursue a suggestion of that paper, namely, to present an intrinsic Hamiltonian formulation for a special coadjoint orbit, which contains the motion of N point vortices on a closed two dimensional surface S with Riemannian metric g . Our main results reformulate the problem on the plane, mainly C.C. Lin’s works (Lin, Proc Natl Acad Sci USA 27:570–575; Lin, Proc Natl Acad Sci USA 27:575–577, 1941) about vortex motion on multiply connected planar domains. Our main tool is the Green function $G_g(s, s_0)$ for the Laplace-Beltrami operator of (S, g) , interpreted as the stream function produced by a unit point vortex at $s_0 \in S$. Since the surface has no boundary, the vorticity distribution ω has to satisfy the global condition $\iint_S \omega \Omega = 0$, where Ω is the area form. Thus the Green function equation has to include a background of uniform counter-vorticity. As a consequence, vortex dynamics is affected by global geometry. Our formulation satisfies Kimura’s requirement (Kimura, Proc R Soc Lond A 455:245–259, 1999) that a vortex dipole describes geodesic motion. A single vortex drifts on the surface, with Hamiltonian given by Robin’s function, which in the case of topological spheres is related to the Gaussian curvature (Steiner, Duke Math J 129(1):63–86, 2005). Results on numerical simulations on flat tori, the catenoid and in the triaxial

S. Boatto

Departamento de Matemática Aplicada, Instituto de Matemática da UFRJ, C.P. 68530, Cidade Universitária, 21945-970 Rio de Janeiro, RJ, Brazil
e-mail: boatto.stefanella@gmail.com

J. Koeller 

Instituto Nacional de Metrologia, Qualidade e Tecnologia (INMETRO), Nossa Senhora das Graças 50, 25250-020 Duque de Caxias, RJ, Brazil
e-mail: jairkoeller@gmail.com

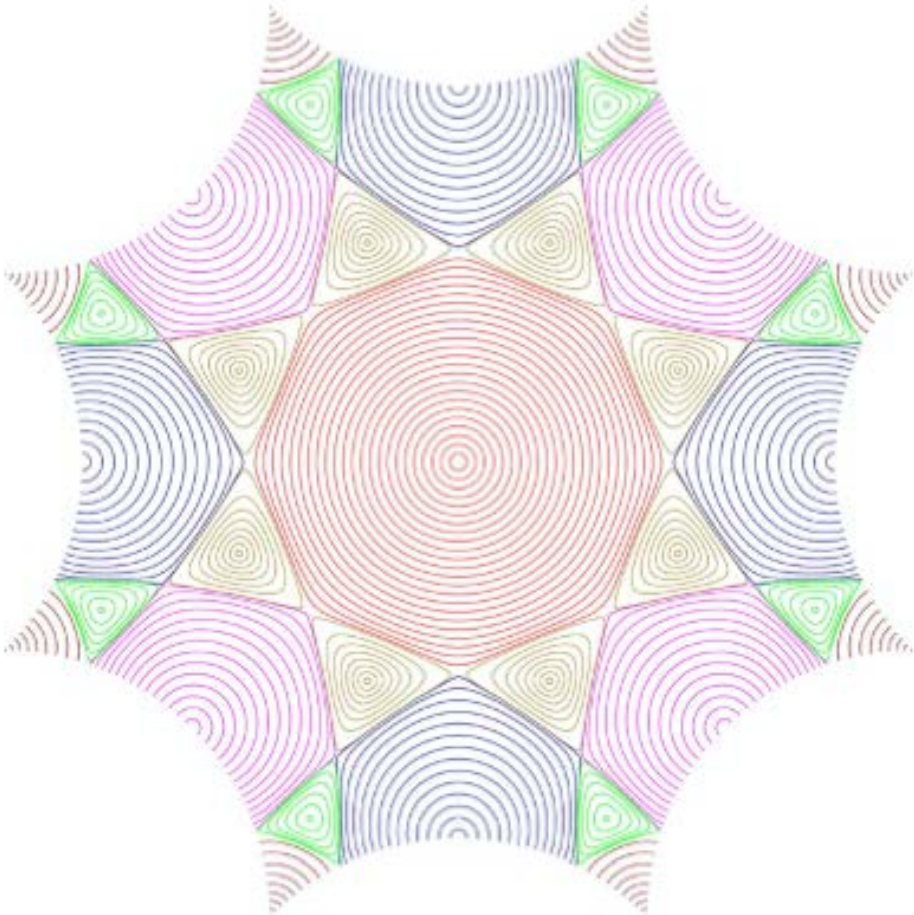
C.Ragazzo: single vortex moving on genus ≥ 2

***R* is not constant for Bolza's surface**

(genus 2 having most discrete symmetries)

C. Ragazzo, The motion of a vortex on a closed surface of constant negative curvature, Proc. Royal Society A Math. Phys. Eng. Sci. 473(2206):20170447 (2017)

The orbits of a single vortex on the Bolza surface restricted to the fundamental domain



C. Grotta Ragazzo Proc. R. Soc. A 2017;473:20170447

Experimental project
(being planned by our group + Ragazzo)

Numerical study of vortex pairs on Bolza's surface.

Motivation: on a compact manifold of constant negative curvature the geodesic flow is chaotic.

(Anosov flows are not only mixing, they are even Bernoullian.)

But the vortex pair problem on a compact surface is never fully chaotic.

What insights could this study produce?

**Remark: 'Steady' hydrodynamical metrics
on noncompact surfaces**

**Given prescribed circulations at its ends there is a
(unique) metric such that R is constant.**

**This theorem extends a result by Gustafsson for
planar domains.**

C. Ragazzo, H. Vighioni, Hydrodynamic Vortex on Surfaces, J. Nonlinear Sci 27, 1609-1640 (2017)

Gustafsson, B.: On the motion of a vortex in two-dimensional flow of an ideal fluid in simply and multiply connected domains, (Technical Report, <http://www.math.kth.se/~gbjorn/theorem>) (1979)



Hydrodynamic Vortex on Surfaces

Clodoaldo Grotta Ragazzo¹  ·
Humberto Henrique de Barros Viglioni²

Received: 21 April 2016 / Accepted: 24 March 2017
© Springer Science+Business Media New York 2017

Abstract The equations of motion for a system of point vortices on an oriented Riemannian surface of finite topological type are presented. The equations are obtained from a Green's function on the surface. The uniqueness of the Green's function is established under hydrodynamic conditions at the surface's boundaries and ends. The hydrodynamic force on a point vortex is computed using a new weak formulation of Euler's equation adapted to the point vortex context. An analogy between the hydrodynamic force on a massive point vortex and the electromagnetic force on a massive electric charge is presented as well as the equations of motion for massive vortices. Any noncompact Riemann surface admits a unique Riemannian metric such that a single vortex in the surface does not move ("Steady Vortex Metric"). Some examples of surfaces with steady vortex metric isometrically embedded in \mathbb{R}^3 are presented.

(Rescaled) Hamiltonian system for a vortex pair

$$\Omega_{pair} = \pi_1^* \omega - \pi_2^* \omega$$

$$F(s_1, s_2) = \exp(-H) = \frac{\exp(G(s_1, s_2))}{\sqrt{\exp(R(s_1))} \sqrt{\exp(R(s_2))}}$$

Alternative expression for F

$$F(s_1, s_2) = d(s_1, s_2) \exp(B(s_1, s_2))$$

$$B(s_1, s_2) = \left[G(s_1, s_2) - \frac{\log d(s_1, s_2)}{2\pi} \right] - \frac{R(s_1) + R(s_2)}{2}$$

Diagonal stability for all time

Suppose that Batman's function is bounded from below. When the initial positions of the vortex pair are taken sufficiently near the diagonal, then the dynamics stays forever close to the diagonal.

Proof. It is immediate. We have $d(s_1(t), s_2(t)) \leq F_o M_o$, where F_o is the initial value of F and

$$M_o = \max_{S \times S} \exp(-B(s_1, s_2)).$$

Therefore we can make $d(s_1(t), s_2(t)) < \epsilon$ for all time, by choosing an initial condition with

$$0 \leq F_o < \epsilon/M_o.$$

□

This is not true when S has boundaries.

The simplest example is a vortex pair in the half plane $y \geq 0$ with the euclidian metric.

Approaching the boundary in a symmetric way, they split apart in opposite directions.

Query

The discrete symmetry

$$(s_1, s_2) \rightarrow (s_2, s_1)$$

reverses time.

One may consider the quotient space

$$S \times S / \{(s_1, s_2) \equiv (s_2, s_1)\}$$

Advantage for topological arguments?

For differential geometry 'in the large'

$\text{Max } F = \text{'hydrodynamical diameter'}$.

Must Estimate!!!

Observe that F is smooth. Nonsmoothness of d and B "cancel out" at conjugate (cut) locus.

Critical values of F are the equilibrium points.
When is F a Morse function?

$F = 0$ at the diagonal and $F > 0$ outside of it.

Query: Let $T =$ small tubular neighborhood of diagonal. Compute $H^*(S \times S/T)$.

Query: Morse functions on $S \times S$ - diagonal

Let S a closed surface of genus κ . Poincaré polynomials:

$$p_S = 1 + 2\kappa x + x^2$$

$$p_{S \times S} = (1 + 2\kappa x + x^2)^2 = 1 + 4\kappa x + 2(1 + 2\kappa^2)x^2 + 4\kappa x^3 + x^4$$

$F^c = \{F \leq c\} =$ tubular neighborhood of S for small $c > 0$.

Let $M = \max F$.

$$H_*(F^c) = H_*(S) \text{ for small } c > 0, \quad H_*(F^M) = H_*(S \times S)$$

We know the Betti numbers at the minimum and maximum.

Question: Can we infer the possible number and types of critical points that should occur in between?

Question for symplectic field theorists

One would like to re-build $S \times S$ starting with T , the small tubular neighborhood of the diagonal.

What would be a "minimal" Morse function?
(smallest number of critical points)

For an index j , how a "handle" $D^j \times D^{4-j}$ is going to be added?

When is $F = d \exp(B)$ Morse?

Implications for vortex pair dynamics?

Batman function
governs the motion of a vortex pair

$$B(s_1, s_2) = \left[G(s_1, s_2) - \frac{\log d(s_1, s_2)}{2\pi} \right] - \frac{R(s_1) + R(s_2)}{2}$$

- B is well defined in $S \times S$ and is symmetric
- B vanishes along the diagonal, as well as dB , the differential
- Smooth within the injectivity radius

B is an yet unexplored object
in geometric function theory.

For a general metric its expansion near the diagonal may require tools from elliptic operators à la Hormander (using a parametrix).

One can reduce the study to constant curvature metrics.

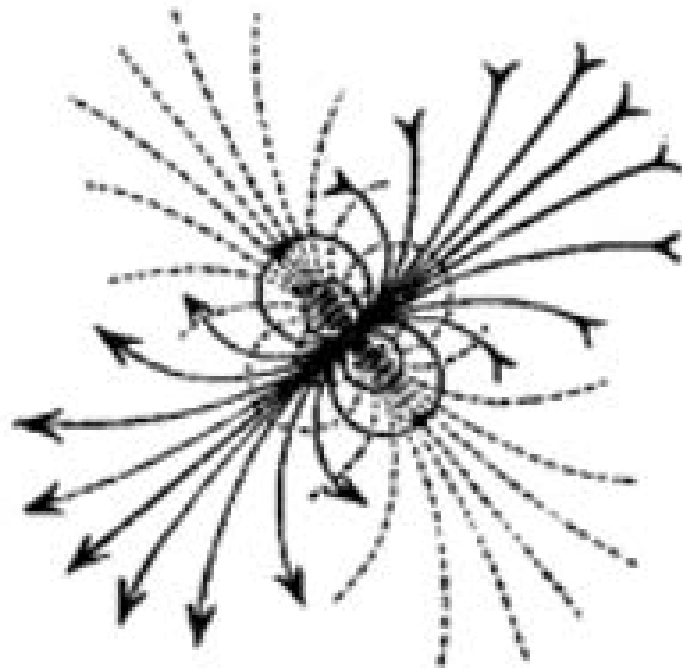
For genus ≥ 2 and curvature -1 :
Anilatmaja Aryasomayajula is computing bounds
for G, R, B, F in terms of injectivity radius and first
eigenvalues of Laplacian.

III. Aim of this talk:

We go (slightly) beyond Y. Kimura's assertion:

"vortex dipoles do geodesics"

Gestalt kleiner, geschlossener, kreisähnlicher Ovale.—Für den imaginären Theil des Ausdrucks rechter Hand und also die Curven $v = \text{Const.}$ gilt eine ähnliche Discussion. Der Unterschied ist nur der, dass jetzt die Richtung $\varphi = \psi$ von allen Curven berührt wird. Hiernach wird die folgende Figur, in welcher die Niveau-curven wieder punctirt, die Strömungscurven ausgezogen sind, verständlich sein:



Figur 4.

Ueber Riemann's Theorie der Algebraischen Functionen

by Felix Klein

In 1999 Yoshifumi Kimura mentioned in his paper 'Vortex motion on surfaces with constant curvature' ([//doi.org/10.1098/rspa.1999.0311](https://doi.org/10.1098/rspa.1999.0311)) that a vortex dipole (two infinitesimally close opposite vortices) on a curved surface should move along a geodesic: "curvature checker", as he interestingly defined.

A proof outline was given in 2008 by Stefanella Boatto and JK (arXiv:0802.4313, [//link.springer.com/book/10.1007/978-1-4939-2441-7](https://link.springer.com/book/10.1007/978-1-4939-2441-7)). In this talk I present some results of ongoing work with Umberto Hryniewicz, Alejandro Cabrera and Anilatmaja Aryasomayajula. Regarding vortex pairs at a small finite distance, we show that close-by pairs can actually be called "topology checkers".

In fact we suggest the idea that, very much like geodesics (perhaps only more so), the study of vortex pair dynamics could be a good way to probe the topology in the large. This is because the Hamiltonian for vortex dynamics on surfaces involves the Laplace Beltrami operator Green's function and its regularizations (Robin's function and its partner, Batman).

Time permitting I will briefly review joint work with Adriano R. Rodrigues and Cesar Castilho ([//doi.org/10.1063/1.3146241](https://doi.org/10.1063/1.3146241), doi: 10.3934/jgm.2018007, <http://mi.mathnet.ru/eng/rcd389>) on far-away vortices on a surface with antipodal symmetry. I will also advertise work by Clodoaldo Ragazzo and Humberto Viglioni ([//doi.org/10.1098/rspa.2017.0447](https://doi.org/10.1098/rspa.2017.0447), [//link.springer.com/article/10.1007/s00332-017-9380-7](https://link.springer.com/article/10.1007/s00332-017-9380-7)) on the motion of a single vortex.

During the talk we will make some queries for the audience, and research suggestions will be presented in the end.

Vortex motion on surfaces with constant curvature

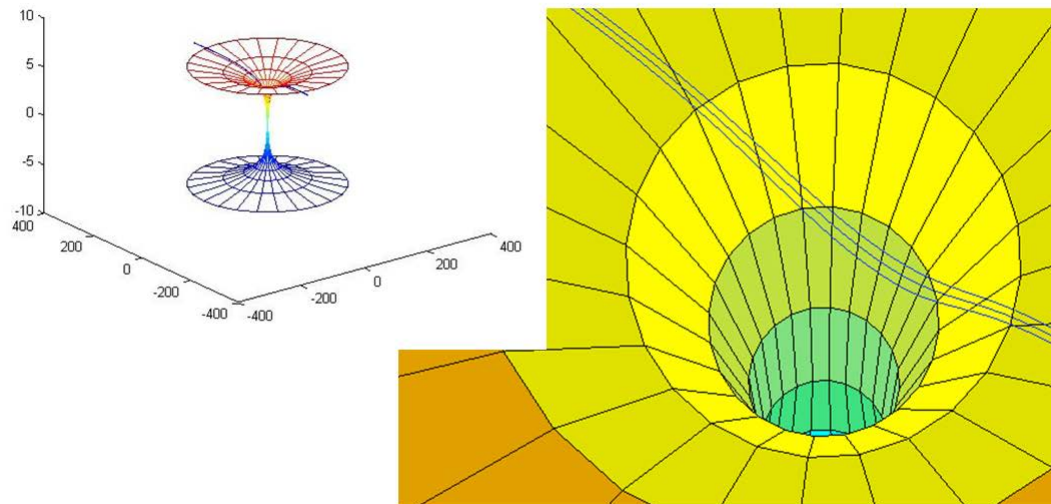
Yoshifumi Kimura

Proc. R. Soc. Lond. A 1999 **455**, 245-259

doi: 10.1098/rspa.1999.0311

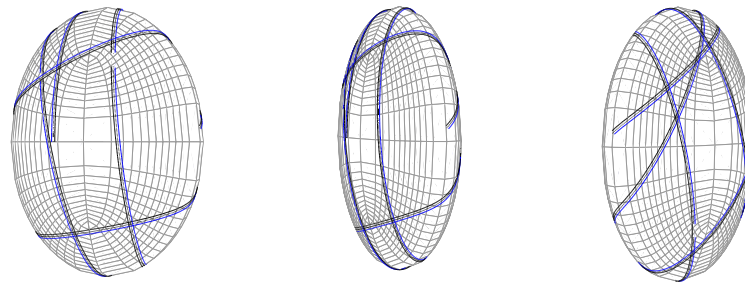
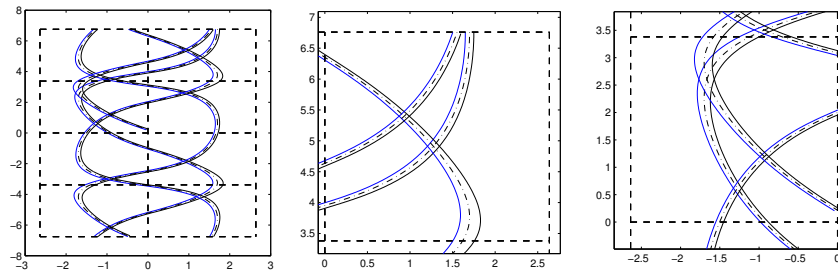
We have seen that a vortex pair (or a vortex dipole in the exact sense) moves on a geodesic on S^2 and H^2 . In a sense, the equation of motion for a vortex dipole coincides with the geodesic equation on either S^2 or H^2 . It is interesting to note that the former is a set of two first-order ODEs while the latter is a set of second-order ODEs in general. The motion of a vortex dipole comes from the fact that it moves in the direction perpendicular to the line connecting two vortices or, in other words, parallel to its axis, which contrasts with electric or magnetic dipoles. It may generally be conjectured that a vortex dipole moves along a geodesic even on a two-dimensional surface with non-constant curvature, if that surface can be covered with the net of orthogonal coordinates. Then a vortex dipole may be used as a geometry checker on such surfaces.

Testing Kimura's conjecture: the catenoid (for short times)



**JK and Stefanello Boatto, Vortex pairs on surfaces
AIP Conference Proceedings 1130, 77 (2009)**

Testing Kimura's conjecture on the triaxial ellipsoid (short times)



Ellipsoid $a = 1$, $b = 6$, $c = 9$.

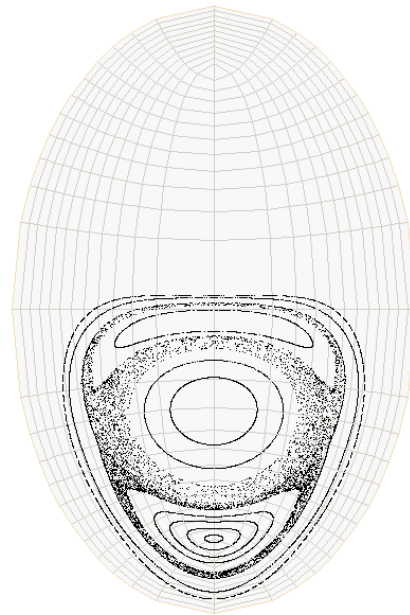
Integrability of triaxial ellipsoid geodesics

Letter from Jacobi to Bessel December 28 1838

“Ich habe vorgestern die geodätische Linie für ein *Ellipsoid mit drei ungleichen Achsen* auf Quadraturen zurückgeführt. Es sind die einfachsten Formeln von der Welt, Abelsche Integrale, die ich in die bekannten elliptischen verwandeln, wenn man 2 Achsen gleich setzt.”

The day before yesterday, I reduced to quadrature the problem of geodesic lines on an ellipsoid with three unequal axes. They are the simplest formulas in the world, Abelian integrals, which become the well known elliptic integrals if 2 axes are set equal.”

Vortex pairs at a distance



Poincaré map. $a = 1$, $b = 4$, $c = 9$, $H = -60$

VORTEX PAIRS ON A TRIAXIAL ELLIPSOID AND KIMURA'S CONJECTURE

ADRIANO REGIS RODRIGUES

Departamento de Matemática
Universidade Federal Rural de Pernambuco
Recife, PE CEP 52171-900 Brazil

CÉSAR CASTILHO*

Departamento de Matemática
Universidade Federal de Pernambuco
Recife, PE CEP 50740-540 Brazil

JAIR KOILLER

Departamento de Matemática
Universidade Federal de Juiz de Fora
Juiz de Fora, MG CEP 36036-900 Brazil

(Communicated by James Montaldi)

ABSTRACT. We consider the problem of point vortices moving on the surface of a triaxial ellipsoid. Following Hally's approach, we obtain the equations of motion by constructing a conformal map from the ellipsoid into the sphere and composing with stereographic projection. We focus on the case of a pair of opposite vortices. Our approach is validated by testing a prediction by Kimura that a (infinitesimally close) vortex dipole follows the geodesic flow. Poincaré sections suggest that the global flow is non-integrable.

In another talk ...

**some results for vortex pairs on genus zero surfaces
with Cesar Castilho and Adriano R. Rodrigues**

- **Equilibria of vortex pairs: linearization**
- **Antipodal symmetry: an invariant submanifold.**
- **Triaxial ellipsoid ; Double faced elliptical region**
- **Surfaces of revolution**

Vortex Pairs on the Triaxial Ellipsoid: Axis Equilibria Stability

Jair Koiller^{1*}, César Castilho^{2**}, and Adriano Regis Rodrigues^{3***}

¹*Departamento de Matemática, Universidade Federal de Juiz de Fora
Juiz de Fora, MG, 36036-900 Brazil*

²*Departamento de Matemática, Universidade Federal de Pernambuco
Recife, PE, 50740-540 Brazil*

³*Universidade Federal Rural de Pernambuco
Recife, PE CEP, 52171-900 Brazil*

Received October 15, 2018; revised January 02, 2019; accepted January 04, 2019

Abstract—We consider a pair of opposite vortices moving on the surface of the triaxial ellipsoid $\mathbb{E}(a, b, c) : x^2/a + y^2/b + z^2/c = 1$, $a < b < c$. The equations of motion are transported to $S^2 \times S^2$ via a conformal map that combines confocal quadric coordinates for the ellipsoid and sphero-conical coordinates in the sphere. The antipodal pairs form an invariant submanifold for the dynamics. We characterize the linear stability of the equilibrium pairs at the three axis endpoints.

**Main result in this talk:
perturbation of dipole geodesic using a blow-up**

$$v_s \in T^1(S) = U(S) , \alpha \in (-r, r)$$

$$s_- = \exp(-\alpha J v_s) , s_+ = \exp(+\alpha J v_s)$$

$2r =$ injectivity radius

$J = \pi/2$ rotation

**$M = U(S) \times (-r, r)$ maps to a large neighborhood
of the diagonal of $S \times S$.**

**It blows up the diagonal, keeping the direction of
approach.**

Theorem 1.

Denote $D =$ Levi-Civita covariant derivative.

$$\dot{s} = v_s + \alpha^2 \left[(3m_2(v_s) + \frac{1}{2} K(s)) v_s - dm_2(V_1) Jv_s \right] + O(\alpha^4)$$

$$D_{\dot{s}} v_s = -\alpha^2 \left[dm_2(V_3) + \frac{1}{6} (\nabla K \cdot Jv_s) + O(\alpha^2) \right] Jv_s$$

$$\dot{\alpha} = -\alpha^3 dm_2(V_2) + O(\alpha^5)$$

This proves Kimura's assertion for dipoles:

$$\alpha \equiv 0 \text{ implies } D_{\dot{s}} \dot{s} \equiv 0$$

Will explain (in next slides)

Frame V_1, V_2, V_3 and its dual $\theta_1, \theta_2, \theta_3$ (geometry)

Quadratic term $m_2 : U(S) \rightarrow \mathbb{R}$ (topology)

V_i are used customarily in 'tensor tomography', and is a nice way to describe the Levi-Civita connection in $U(S)$.

m_2 is the leading term in the Batman function expansion. It captures, in the small (i.e, for closeby vortex pairs) the influence of the manifold topology.

Hamiltonian structure in $M = U(S) \times (-r, r)$ (explicit formulae/proofs in extra slides)

Theorem 2. Using the frame V_1, V_2, V_3 one can make explicit the pull back of $\omega(s_+) - \omega(s_-)$ in $S \times S$ to the modified phase space M via

$$(v_s, \alpha) \mapsto (\exp(-\alpha Jv_s), \exp(+\alpha Jv_s))$$

where $\alpha \in (-r, r)$ is a dynamic variable (distances to the diagonal) and $2r$ is the injectivity radius.

M is a folded symplectic space at $\alpha = 0$ (blow up at the diagonal).

Symplectic form involves Jacobi fields along geodesic s_- to s_+ .

Its expansion in powers of α can be done at any desired order.

The Hamiltonian expands as $F = 2\alpha(1 + \alpha^2 m_2(v_s) + O(\alpha^4))$.

Pull back to TS together with a dummy scaling ϵ

Let $v_s \in TS \mapsto E(v_s) = (\exp(-Jv_s), \exp(Jv_s)) \in S \times S$ and then take the rescaling $v_s \rightarrow \epsilon v_s$. Denote $g_b : TS \rightarrow T^*S$ the Legendre transform, and $\Omega_o = g_b^* \Omega_{can}$ the pullback of the canonical form of T^*S .

Theorem 3. (suited for Hamiltonian perturbation methods)

$$E_\epsilon^* \Omega_{pair} / 2\epsilon \sim d \left[|v_s|^2 \left(1 - \frac{1}{6} K(s) \epsilon^2 \right) \theta_2 + \dots \right] = \Omega_o + \epsilon^2 \Omega_1 + O(\epsilon^4)$$

$$\Omega_o = |v_s|^2 (\theta_1 \wedge \theta_3 + 2\theta_4 \wedge \theta_2) \quad , \quad \Omega_1 = -\frac{1}{6} K(s) \Omega_o + \frac{|v_s|^2}{6} (\nabla K \cdot Jv_s) \theta_2 \wedge \theta_3$$

$$F/2\epsilon = |v_s| \exp(B) \quad , \quad B(v_s, \epsilon) = m_2 \left(\frac{v_s}{|v_s|} \right) |v_s|^2 \epsilon^2 + O(\epsilon^4)$$

For $\epsilon = 0$ we recover the geodesic flow $(\Omega_o, |v|)$.

The frame V_1, V_2, V_3 in $T_r(S)$

$$T_r(S) = \{v \in TS \mid |v| = r\}, \quad T_1(S) = U(S)$$

$P_{\gamma(t)}$ = parallel transport operator along γ .

$\Phi_1(t)$: rotation of angle t in $T_r S$: $v_s \rightarrow R_t v_s$

$$\Phi_2(t) = (\gamma_o(t), \dot{\gamma}_o(t)), \quad \gamma_o(t) = \exp(v_s, t)$$

(geodesic flow: $\dot{\gamma}_o(t) = P_{\gamma_o(t)}(v_s)$)

$\Phi_3(t)$: parallel transport of v_s along geodesic γ_1 with initial condition $J v_s$

$$\Phi_3(t) = (\gamma_1(t), P_{\gamma_1(t)}(v_s)), \quad \gamma_1(t) = \exp(Jv_s, t).$$

V_i = infinitesimal generators of the $\Phi_i(t)$

Bundle picture: Levi-Civita

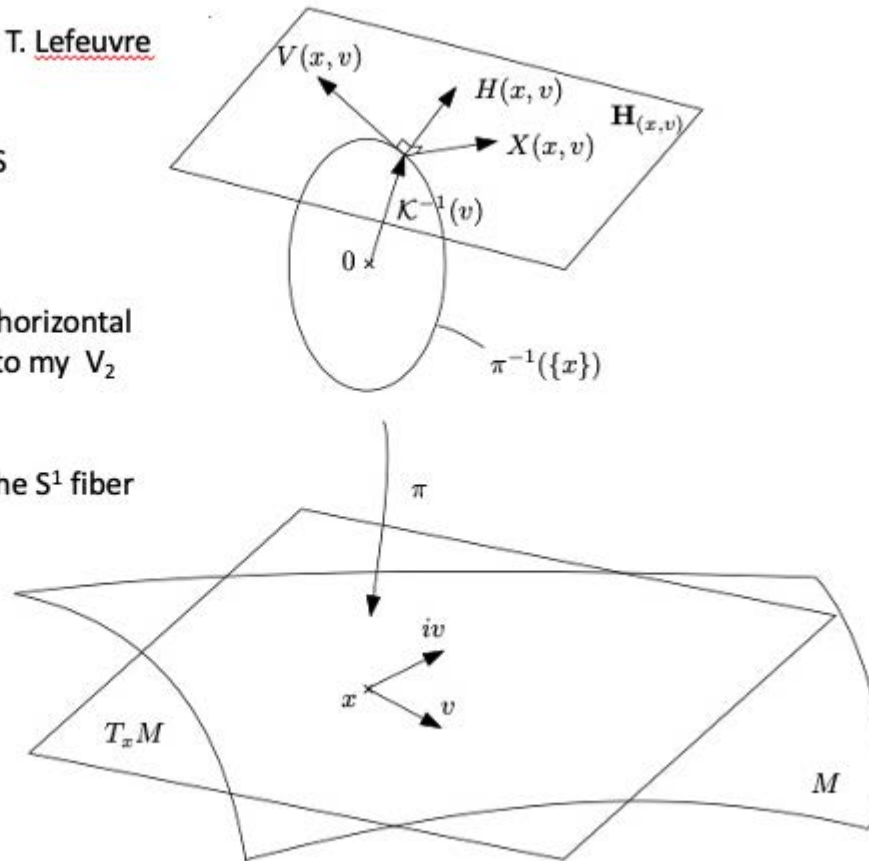
Notations change from T. Lefeuvre

x in M becomes s in S

$i v$ becomes $J v$

X and H generate the horizontal space and correspond to my V_2 and V_3

V is our V_1 tangent to the S^1 fiber of $U(S) \rightarrow S$



Commutation relations

V_1 is tangent to the fibers of the principal bundle

$$S^1 \hookrightarrow T_r(S) \rightarrow S$$

V_2 and V_3 span horizontal spaces, projecting to v_s and Jv_s .

$$[V_1, V_2] = V_3, \quad [V_3, V_1] = V_2, \quad [V_2, V_3] = \frac{K(s)}{r^2} V_1,$$

Denoting $\theta_1, \theta_2, \theta_3$ the dual coframe of V_1, V_2, V_3

$$d\theta_1 = -\frac{K(s)}{r^2} \theta_2 \wedge \theta_3, \quad d\theta_2 = -\theta_3 \wedge \theta_1, \quad d\theta_3 = -\theta_1 \wedge \theta_2.$$

T. Leveuvre (section 2.4.2 (2.28)-(2.30))

<https://thibaultlefeuvre.files.wordpress.com/2016/04/memoire.pdf>

The function m_2 : quadratic part of B

$$F = 2|\alpha| \exp(B)$$

$$B(v_s, \alpha) = m_2(v_s) \alpha^2 + O(\alpha^4)$$

The influence of the global topology is encoded in

$$m_2 : U(S) \rightarrow \mathbb{R}.$$

and the directional derivatives $dm_2(V_i)$.

Examples of m_2 and validation of the ODEs

- Round sphere ($K = 1$): $m_2 \equiv -1/6$
- Hyperbolic half plane ($K = -1$): $m_2 \equiv -1/3$
- Half plane with $K = 0$: $m_2 = -\frac{1}{y_o^2}$

$y_o =$ from midpoint

Independent of direction v_s

We checked the ODEs in $U(S) \times \mathbb{R}$ with the vortex pair equations in $S \times S$ for validation. See the extra slides.

Round cylinder and flat tori

Group symmetry: the pair keeps the same relative positions in the covering plane.

Cylinder Green function: by elementary functions.

$$X = (x, y) \in \mathbb{R} \times S^1, \quad y \equiv y + 2\pi, \quad V = (a, b), \quad a^2 + b^2 = 1$$

Exponential map: $X_{\pm} = X \pm \alpha J(a, b) = (x, y) \pm \alpha (-b, a)$.

We computed using the Green function:

$$m_2 = \frac{1}{6} (b^2 - a^2)$$

Tori: require elliptic functions but the behavior is similar.

There is a steady drift from the instantaneous geodesic.

Curvature is not enough to capture the dynamics.

The cylinder topology matters even in the small.

Conclusions

Vortex pairs divorce approaching boundaries.

On a compact boundaryless surface closeby vortex pairs remain close for all time.

As predicted by Kimura, dipoles follow geodesics.

However, for vortex pairs at a small distance, the dynamics drifts as $O(\text{distance}^2)$.

Even in the small, vortex pairs are topology probers.

Very much like geodesics, vortex pairs could be a tool for differential geometry in the large.

Only more so!

Up for grabs:

Vortex pairs on compact surfaces of genus ≥ 2 .

Continuation of periodic geodesics for $F = c > 0$, small c .

Applying symplectic field theory methods for global results.

Thank you!

(many extra slides now follow
please circulate with care: everything to be submitted...
But collaborations are welcome!!)

Contents of extra slides

A. Vortex pair in the round cylinder: steady drift from geodesic.

B. Informations on Green and Robin functions.

C. Details on the pull back map $E : TS \rightarrow S \times S$. See pg. 69 for the deformation

$$\frac{1}{2\epsilon} E_\epsilon^* \Omega_{pair} \sim d \left[|v_s|^2 \left(1 - \frac{1}{6} K(s) \epsilon^2 \right) \theta_2 \right] = \Omega_o + \epsilon^2 \Omega_1 + O(\epsilon^4)$$

$$\Omega_o = \Omega_g = g_b^* \Omega_{can} = |v_s|^2 (\theta_1 \wedge \theta_3 + 2\theta_4 \wedge \theta_2)$$

$$\Omega_1 = -\frac{1}{6} K(s) \Omega_g + \frac{|v_s|^2}{6} (\nabla K \cdot J v_s) \theta_2 \wedge \theta_3$$

D. Blow up approach: $M = U(S) \times (-r, r)$ and the symplectic form matrix via Jacobi fields.

E. Examples of computing m_2 and Theorem validations in examples.

F. Some papers mentioned in the presentation.

G. Outline of numerical projects.

H. A note on von Kármán.

A. Some details for the round cylinder

Educated guess: the midpoint $s(t)$ does a cylinder geodesic. However, there is no obligation to do it at right angle with the direction from s_- to s_+ .

In fact, we will find the angle between the trajectory of the center point s and the direction of the relative position between the vortices as a function of α , that will be constant.

$$G(X_1, X_2) = \frac{1}{2\pi} \log \sqrt{\cosh z - \cos \theta}, \quad z = x_2 - x_1, \quad \theta = y_2 - y_1$$

Dropping the $1/2\pi$, the ODEs with $F = \exp(G) = \sqrt{\cosh z - \cos \theta}$ are

$$\begin{aligned} \dot{x}_1 &= -\frac{\partial F}{\partial y_1} = -\frac{1}{F} \sin(y_1 - y_2), & \dot{x}_2 &= \frac{\partial F}{\partial y_2} = \frac{1}{F} \sin(y_2 - y_1) \\ \dot{y}_1 &= \frac{\partial F}{\partial x_1} = \frac{1}{F} \sinh(x_1 - x_2), & \dot{y}_2 &= -\frac{\partial F}{\partial x_2} = -\frac{1}{F} \sinh(x_2 - x_1) \end{aligned}$$

Denote $s = (x, y)$, $v_s = (a, b)$ and for $0 \leq \alpha < \pi$,

$$\boxed{(x_{\pm}, y_{\pm}) = (x, y) \pm \alpha J(a, b) = (x, y) \pm \alpha (-b, a), \quad a^2 + b^2 = 1, .}$$

Then $s = (x, y)$ satisfies

$$\dot{s} = (\dot{x}, \dot{y}) = \frac{1}{F} (\sin(2a\alpha), \sinh(2b\alpha)), \quad F = \sqrt{\cosh(2b\alpha) - \cos(2a\alpha)}.$$

Robin function is constant (and we may set to zero) and a quick computation gives

$$F = \sqrt{2}\alpha \left(1 + \frac{1}{6}(b^2 - a^2)\alpha^2 + O(\alpha^4) \right)$$

$$m_2 = \frac{1}{6}(b^2 - a^2) \text{ with } a^2 + b^2 = 1.$$

Thus we see that m_2 does not depend on the center point $s = (x, y)$, BUT it depends on direction $v_s = (a, b)$.

Checking the pulled back ODES:

Expanding $(\sin(2a\alpha), \sinh(2b\alpha))/F$ and neglecting the innocuous factor $\sqrt{2}$:

$$\dot{s} = (\dot{x}, \dot{y}) = \left(1 - \frac{\alpha^2}{6}(b^2 - a^2) + O(\alpha^4) \right) \left[(a, b) + \frac{2}{3}\alpha^2(-a^3, b^3) + O(\alpha^5) \right]$$

$$\dot{s} = (\dot{x}, \dot{y}) = \left(1 - \frac{\alpha^2}{6}(b^2 - ab^2) \right) (a, b) + \frac{2}{3}\alpha^2(-a^3, b^3) + \dots$$

Now, we may decompose, since $a^2 + b^2 = 1$, $(-a^3, b^3) = (b^2 - a^2)(a, b) + ab(-b, a)$.

$$\dot{s} = \left(1 + \left(-\frac{1}{6} + \frac{2}{3} \right) (b^2 - a^2)\alpha^2 \right) (a, b) + \frac{2}{3}ab\alpha^2 J(a, b) + \dots$$

Validations

$$\dot{s} = \left(1 + \frac{1}{2}(b^2 - a^2)\alpha^2\right) (a, b) + \frac{2}{3}ab\alpha^2 J(a, b) + \dots$$

The term with $(-\frac{1}{6} + \frac{2}{3})(b^2 - a^2) = \frac{1}{2}(b^2 - a^2)$ coincides with the predicted $3m_2$ and moreover,

$$\frac{2}{3}ab = 2(-b, a) \begin{bmatrix} -1/6 & 0 \\ 0 & 1/6 \end{bmatrix} \begin{bmatrix} a \\ b \end{bmatrix} = -dm_2(V_1),$$

again as predicted. Also note that the parallel transport for flat metrics is trivial, so $dm_2(V_2) = dm_2(V_3) \equiv 0$.

Historical note

The study of vortex motions on the flat cylinder has a notable history, starting with von Karman's papers on his vortex pair "streets". From our calculations we confirm that the street moves in the y -direction when $a = 0$ (the parallel configuration) or $\alpha a = \pi/2$ (staggered).

von Karman showed that relative to the moving frame with velocity \dot{y} , the former is unstable, but the latter is stable: it is a ubiquitous phenomenon in fluids. Several papers have been published for streets of more than two vortices (Aref and Stremler).

Flat tori

Double periodic arrays have also been observed in Nature (see the papers by Stremler/Aref).

Let $T = \mathbb{C}/L$, where L is the lattice generated by 1 and

$$\tau = a + bi, \quad b > 0.$$

Denote $q = e^{\pi i \tau}$ so $|q| = e^{-\pi b} < 1$. Up to a constant $C(\tau)$, the Green function $G(z, w)$ for the Laplace operator on T is given by

$$G(z, w) = -\frac{1}{2\pi} \ln |\theta_1(z - w)| + \frac{1}{2b} (\text{Im}(z - w))^2 + C(\tau),$$

where the theta function $\theta_1(z; \tau)$ is the exponentially convergent series

$$\theta_1(z; \tau) = 2 \sum_{n=0}^{\infty} (-1)^n q^{(n+1/2)^2} \sin((2n+1)\pi z), \quad z = x + iy.$$

Robin's functions are constant (Boatto and K.).

... continues

Place z at the center of a fundamental domain. These Green functions have always three critical points on w : one of them corresponding to the vertices of the fundamental domain, and the other two are the half periods.

It was shown shown (Lin-Wang, Ann. of Math. 172:2 (2010), 911–954) that there are special 1-parameter families in τ with an extra pair of singular points.

Humberto Viglioni described the structure of these families inside the modular surface.

We leave as a challenge computing the coefficient $m_2(a, b; \tau)$ for a pair

$$s_{\pm} = (x, y) + \alpha(-b, a).$$

One needs to expand $G(s_+, s_-) - \log |2\alpha|/2\pi$, which requires some expertise in elliptic functions. As in the case of the cylinder, m_2 does not depend on position of the midpoint (x, y) . The issue is the dependence on τ .

For the Green function of the “true” (curved) torus in \mathbb{R}^3 see J. S. Marshall, Proc. R. Soc. A **469**, (2013) 20120479.

B. Green function of Laplace-Beltrami operator

S = closed orientable two-dimensional surface (without boundary) with a Riemannian metric g .

$\omega = dS$ = area form

$\Delta = \Delta_g$ = Laplace-Beltrami operator

$d(s, s_0)$ = geodesic distance with respect to g .

$$\Delta G(s, s_0) = -\frac{1}{\text{Area}(S)} + \delta(s, s_0) \ , \quad \int_S G(p, q) dS = 0 \ ,$$
$$G(s, s_0) - \log d(s, s_0)/2\pi \text{ bounded,} \quad G(s, s_0) = G(s_0, s).$$

$G(s, s_0)$ smooth outside diagonal. Diverges logarithmically.

G = kernel of the integral operator for Poisson's equation:

$$\Delta^{-1}f(s) = \int_S G(s, r) f(r) dS .$$

Declare $\Delta^{-1}\text{constant} = 0$ by convention, so

$$\int_S \Delta^{-1}f dS = 0, \forall f \in L^2(S).$$

$$G(s_1, s_2) = \sum_{\lambda_i \in \text{spectrum}} \frac{1}{\lambda_i} \phi_i(s_1) \phi_i(s_2) .$$

where $\{\phi_i\}$ is a normalized eigenbasis.

Robin's function

$$R_g(s_o) = \lim_{s \rightarrow s_o} G_g(s, s_o) - \log d_g(s, s_o)/2\pi$$

R is an interesting constant for the round sphere and flat genus 1 (any modulus).

The fact that R is constant for flat tori requires some thought, but it is not hard to prove.

J. Steiner, K. Okikiolu: spectral invariants!

Jean Steiner, A geometrical mass and its extremal properties for metrics on S^2 .
Duke Math. J. 129(1): 63-86 (2005)

K. Okikiolu, A Negative Mass Theorem for Surfaces of Positive Genus
Communications in Mathematical Physics 290(3):1025-1031 (2009)

For any metric g on S^2 , up to constant,

$$R_g(s) = \frac{1}{2\pi}(\Delta_g^{-1}K_g)(s)$$

For any metric $g_\phi = \exp(2\phi)g_{can}$ on a torus (any modulus), up to a constant,

$$R_g(s) = \frac{1}{2\pi}(\Delta_g^{-1}K_g)(s) - \frac{1}{2\pi}\Delta^{-1}\exp(2\phi)$$

More generally, for any genus χ , up to a constant,

$$R_g(s) = \frac{1}{2\pi}(\Delta_g^{-1}K_g)(s) - \frac{\chi}{2\pi}\Delta^{-1}\exp(2\phi) + R_{can}(s)$$

Batman function
governs the motion of a vortex pair

$$B(s_1, s_2) = \left[G(s_1, s_2) - \frac{\log d(s_1, s_2)}{2\pi} \right] - \frac{R(s_1) + R(s_2)}{2}$$

- B is well defined in $S \times S$ and is symmetric
- B vanishes along the diagonal, as well as dB , the differential
- Smooth within the injectivity radius

B is an yet unexplored object in geometric function theory.

For a general metric its expansion near the diagonal may require tools from elliptic operators à la Hormander (using a parametrix).

One can reduce the study to constant curvature metrics.

For genus ≥ 2 and curvature -1 :

Anilatmaja Aryasomayajula is computing bounds for G, R, B in terms of injectivity radius and first eigenvalues of Laplacian.

C. The map

$$E : v_s \in TS \rightarrow (\exp(-v_s), \exp(v_s))$$

and the pullback of the two form

$$\omega(s_+) - \omega(s_-)$$

A neighborhood of the zero section of TS is mapped to a neighborhood of the diagonal of $S \times S$ via the centered exponential map

$$E : v_s \in TS \rightarrow (\exp(-v_s), \exp(v_s)).$$

Combine with the $\pi/2$ rotation $J : T_s S \rightarrow T_s S$.

$$E_{\text{symp}} = E \circ J$$

$$v_s \in TS \xrightarrow{J} u_s = Jv_s \in TS \xrightarrow{E} (s_-, s_+) \in S \times S$$

$$s_{\pm} = \exp(\pm u_s) = \exp(\pm Jv_s)$$

Kimura's assertion

Pulled back to TS , the vortex pair system is

$$E_{\text{symp}}^* \Omega_{\text{pair}} (= J^* E^* \Omega_{\text{pair}}), \quad F = F(\exp(-Jv_s), \exp(Jv_s))$$

Introduce dummy parameter ϵ (no dynamical meaning)

$$\text{Scaling : } v_s \rightarrow \epsilon v_s$$

and expand in powers of ϵ :

- Will show (tricky): leading term of the pull back

$$E_{\epsilon}^{\text{symp}} = E \circ J \circ \epsilon \text{ scaling}$$

is 2ϵ times the canonical 2-form of T^*S .

(as seen in TS via Legendre's transformation.)

- Easy: leading term of F is: $2\epsilon|v_s|$.

Computing next order terms of the deformation

We use a 'magic formula' by Alejandro Cabrera to compute the pullback by E_{sym}^* of the 2-form on $S \times S$

- To implement the magic formula, use frame V_1, V_2, V_3
- Find its commutation relations and rewrite in coframe: θ_i
- Expand the magic formula in a scaling ϵv_s
- Make use of $L_X = i_X d + di_X$, $X =$ geodesic flow

The frame V_1, V_2, V_3 in $T_r(S)$

$$T_r(S) = \{v \in TS \mid |v| = r\}, \quad T_1(S) = U(S)$$

$P_{\gamma(t)}$ = parallel transport operator along γ .

$\Phi_1(t)$: rotation of angle t in $T_r S$: $v_s \rightarrow R_t v_s$

$$\Phi_2(t) = (\gamma_o(t), \dot{\gamma}_o(t)), \quad \gamma_o(t) = \exp(v_s, t)$$

(geodesic flow: $\dot{\gamma}_o(t) = P_{\gamma_o(t)}(v_s)$)

$\Phi_3(t)$: parallel transport of v_s along geodesic γ_1 with initial condition $J v_s$

$$\Phi_3(t) = (\gamma_1(t), P_{\gamma_1(t)}(v_s)), \quad \gamma_1(t) = \exp(Jv_s, t).$$

V_i = infinitesimal generators of the $\Phi_i(t)$

Bundle picture: Levi-Civita

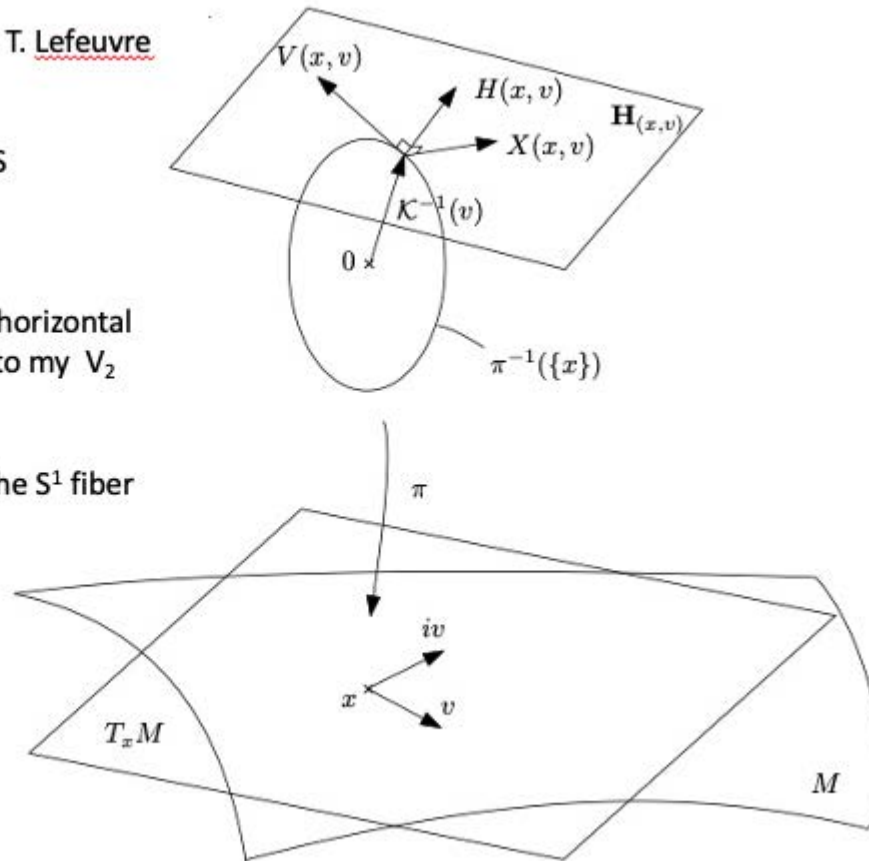
Notations change from T. Lefeuvre

x in M becomes s in S

$i v$ becomes $J v$

X and H generate the horizontal space and correspond to my V_2 and V_3

V is our V_1 tangent to the S^1 fiber of $U(S) \rightarrow S$



Commutation relations

V_1 is tangent to the fibers of the principal bundle

$$S^1 \hookrightarrow T_r(S) \rightarrow S$$

V_2 and V_3 span the horizontal spaces, projecting respectively to v_s and Jv_s .

$$[V_1, V_2] = V_3, \quad [V_3, V_1] = V_2, \quad [V_2, V_3] = \frac{K(s)}{r^2} V_1,$$

Denoting $\theta_1, \theta_2, \theta_3$ the dual coframe of V_1, V_2, V_3

$$d\theta_1 = -\frac{K(s)}{r^2} \theta_2 \wedge \theta_3, \quad d\theta_2 = -\theta_3 \wedge \theta_1, \quad d\theta_3 = -\theta_1 \wedge \theta_2.$$

Summary: symplectic form expansion up to ϵ^2

$$\begin{aligned} \frac{1}{2\epsilon} E_\epsilon^* \Omega_{pair} &\sim d \left[|v_s|^2 \left(1 - \frac{1}{6} K(s) \epsilon^2 \right) \theta_2 \right] = \\ &= \Omega_o + \epsilon^2 \Omega_1 + O(\epsilon^4) \end{aligned}$$

$$\Omega_o = \Omega_g = g_b^* \Omega_{can} = |v_s|^2 (\theta_1 \wedge \theta_3 + 2\theta_4 \wedge \theta_2)$$

$$\Omega_1 = -\frac{1}{6} K(s) \Omega_g + \frac{|v_s|^2}{6} (\nabla K \cdot J v_s) \theta_2 \wedge \theta_3$$

Expanding the Hamiltonian: function m_2

$$\frac{1}{2\epsilon} F = |v_s| \exp(B)$$

$$B(v_s, \epsilon) = Q_2(v_s, v_s)\epsilon^2 + O(\epsilon^4)$$

$$Q_2(v_s, v_s) = m_2 \left(\frac{v_s}{|v_s|} \right) |v_s|^2$$

The main influence of the topology is encoded in

$$m_2 : U(S) \rightarrow \mathbb{R}.$$

and the directional derivatives $dm_2(V_i)$.

D. Blow up approach: $M = U(S) \times (-r, r)$

$$s_{\pm} = \exp(\pm \alpha J v_s), \quad V_4 = \partial / \partial \alpha$$

$2r =$ injectivity radius.

$D =$ Levi-Civita covariant derivative.

$K =$ curvature. $V_i =$ vectorfields in $U(S)$

$$B(-\alpha, \alpha) = B(\exp(-\alpha J v_s), \exp(\alpha J v_s)) = \alpha^2 m_2(v_s) + O(\alpha^4)$$

$$\dot{s} = v_s + \alpha^2 \left[(3m_2(v_s) + \frac{1}{2} K(s)) v_s - dm_2(V_1) J v_s \right] + O(\alpha^4)$$

$$D_{\dot{s}} v_s = -\alpha^2 \left[dm_2(V_3) + \frac{1}{6} dK(J v_s) + O(\alpha^2) \right] J v_s$$

$$\dot{\alpha} = -\alpha^3 dm_2(V_2) + O(\alpha^5)$$

Will show: this has a folded Hamiltonian structure.

Step1: sketch the images in $S \times S$ via E_*^{folded} of the frame in M

$$V_i, \quad 1 \leq i \leq 4.$$

Step2: compute symplectic brackets

$$\Omega_{pair}(E_*^{folded}V_i, E_*^{folded}V_j)$$

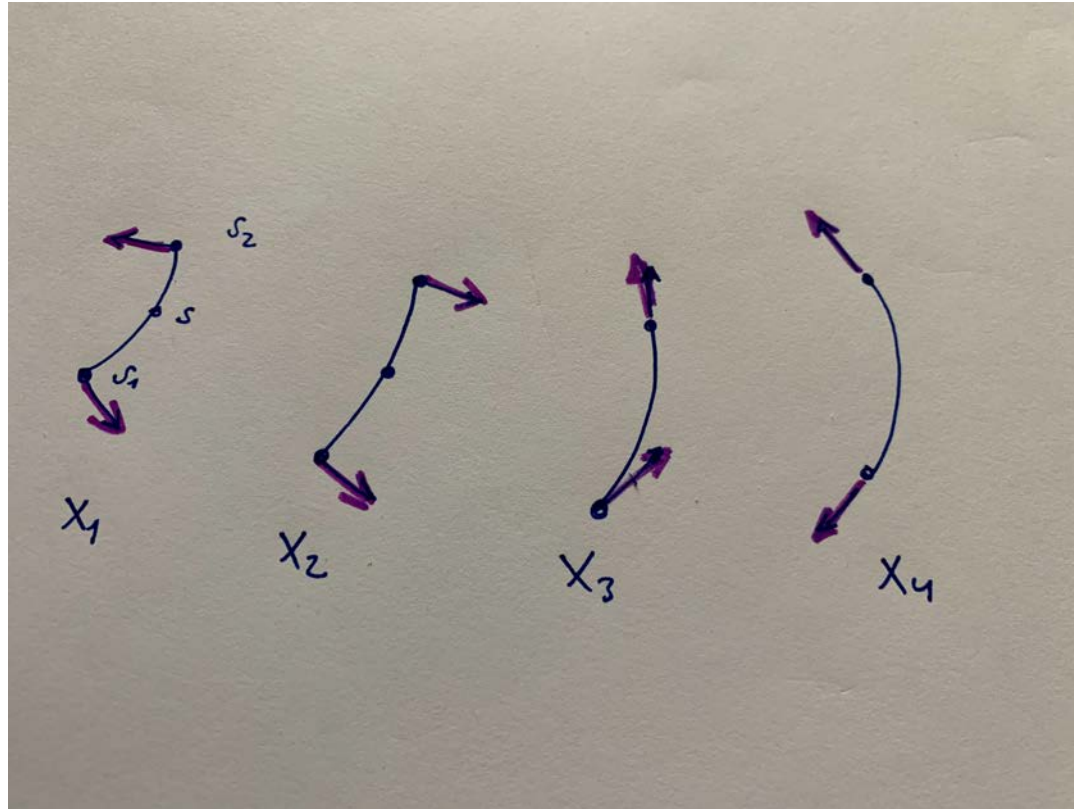
**These images frame almost all of $S \times S$.
(Out: diagonal and conjugate-cut locus)**

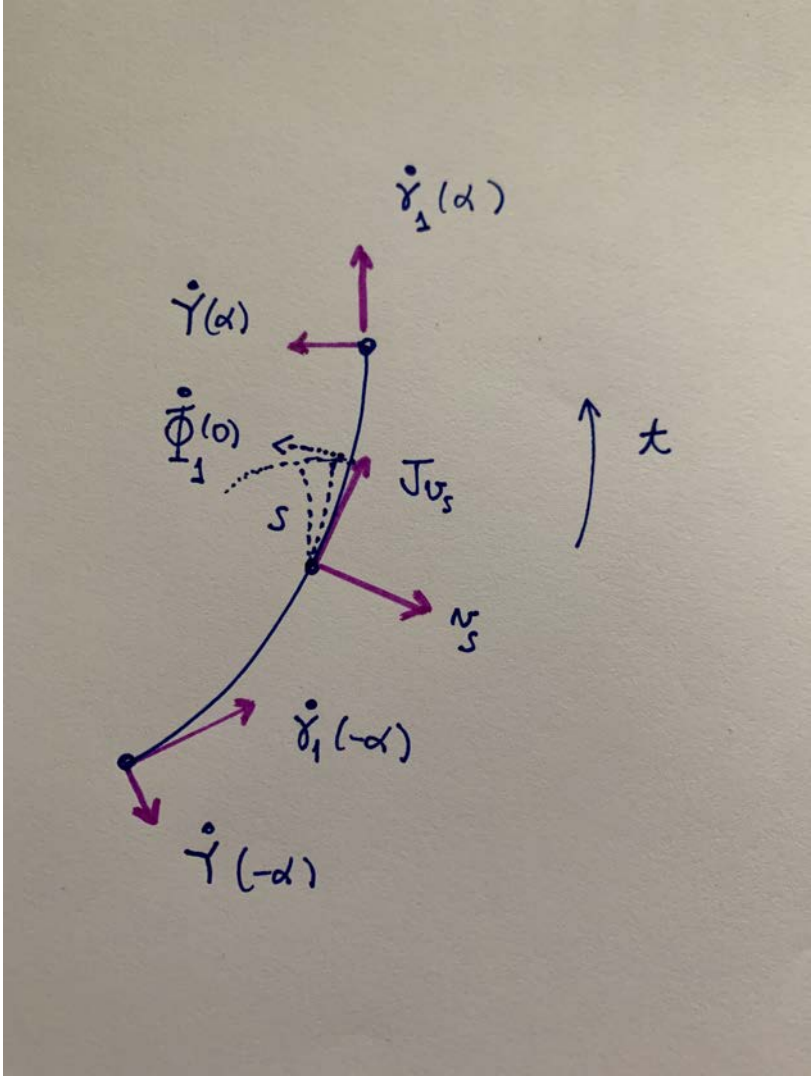
Differentiating *exp*: Jacobi fields shall appear ...

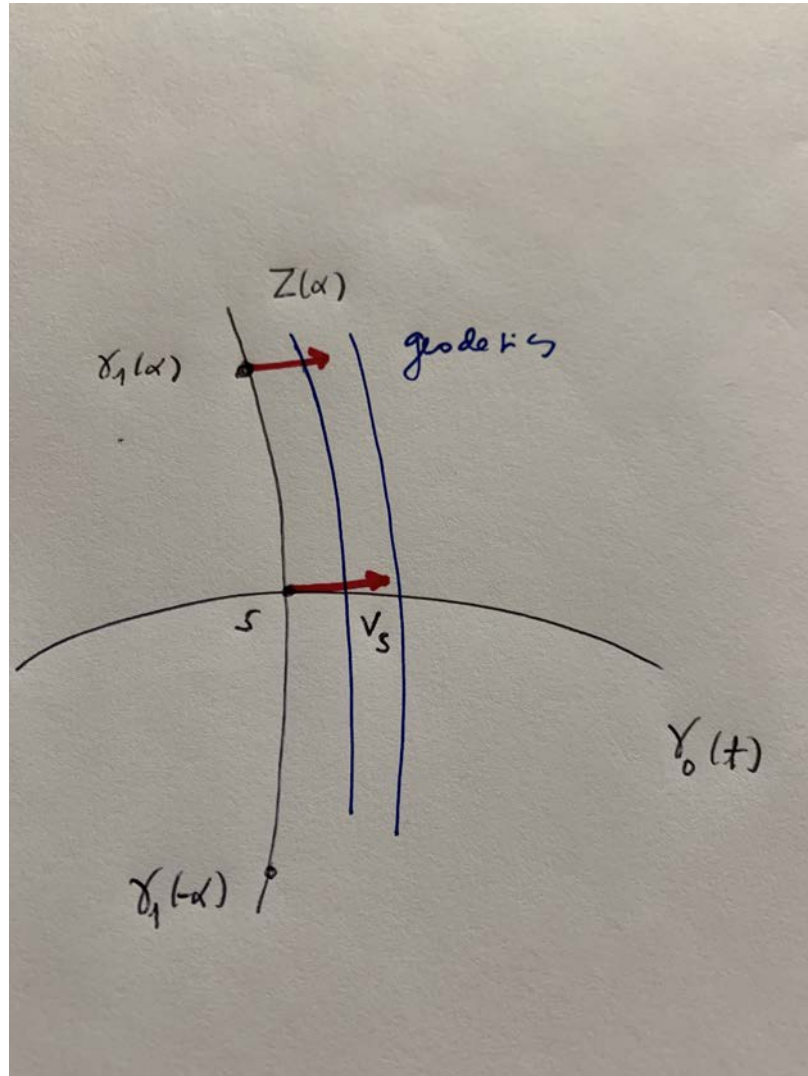
$Y, Z =$ Jacobi fields along the geodesic connecting s_{\pm} (starting at s in the direction Jv_s) with initial conditions

$$Y(0) = 0, \quad Y'(0) = -v_s$$

$$Z(0) = v_s, \quad Z'(0) = 0$$







End result: relative to frame V_1, V_2, V_3, V_4

$$\begin{aligned}\Omega_{13} &= -\Omega_{31} = -(|Y(\alpha)| + |Y(-\alpha)|) \\ \Omega_{14} &= -\Omega_{41} = -|Y(\alpha)| + |Y(-\alpha)| \\ \Omega_{23} &= -[\Omega]_{32} = |Z(\alpha)| - |Z(-\alpha)| \\ \Omega_{24} &= -[\Omega]_{42} = |Z(\alpha)| + |Z(-\alpha)|\end{aligned}$$

$$[\Omega] = \begin{bmatrix} 0 & 0 & \Omega_{13} & \Omega_{14} \\ 0 & 0 & \Omega_{23} & \Omega_{24} \\ -\Omega_{13} & -\Omega_{23} & 0 & 0 \\ -\Omega_{14} & -\Omega_{24} & 0 & 0 \end{bmatrix}$$

$$Y(0) = 0, Y'(0) = -v_s, Z(0) = v_s, Z'(0) = 0.$$

Using the expansions of the norm of Jacobi fields

$$\Omega_{13} = -2\alpha + \frac{1}{3}K(s)\alpha^3 + O(\alpha^5)$$

$$\Omega_{14} = O(\alpha^4)$$

$$\Omega_{23} = -\frac{1}{3}(\nabla K \cdot Jv_s)\alpha^3 + O(\alpha^5)$$

$$\Omega_{24} = 2 - K(s)\alpha^2 + O(\alpha^4)$$

Summary of the blow up approach:

$M = U(S) \times (-r, r)$ is folded symplectic

$$E^* \Omega_{pair} = 2\theta_2 \wedge d\alpha - 2\alpha \theta_1 \wedge \theta_3 - \alpha^2 K(s) \theta_2 \wedge d\alpha + \\ + \alpha^3/3 [K(s) \theta_1 \wedge \theta_3 - (\nabla K \cdot Jv_s) \theta_2 \wedge \theta_3] + O(\alpha^4)$$

$$E^* \Omega_{pair} = d\omega_M + O(\alpha^4)$$

$$\omega_M = 2(-\alpha + \frac{1}{6}K(s)\alpha^3) \theta_2$$

$$F = 2\alpha \exp(B(-\alpha, \alpha)) = 2\alpha (1 + m_2(v_s)\alpha^2 + O(\alpha^4))$$

Maybe a bit more: an educated guess

$$E^* \Omega_{pair} = d(\omega + O(\alpha^4))$$

$$\omega = 2\left(-\alpha + \frac{1}{6}K(s)\alpha^3\right)\theta_2$$

We posit that $E^* \Omega_{pair}$ is exact, namely

$$E^* \Omega_{pair} = d[f(v_s, \alpha)\theta_2],$$

with a $f(v_s, \alpha)$ in M that can be expressed in terms of multiindices derivatives in Jv_s .

Details of symplectomorphism approach

A neighborhood of the zero section of TS is mapped to a neighborhood of the diagonal of $S \times S$ via the centered exponential map

$$E : v_s \in TS \rightarrow (\exp(-v_s), \exp(v_s)).$$

Combine with the $\pi/2$ rotation $J : T_s S \rightarrow T_s S$.

$$E_{\text{symp}} = E \circ J$$

$$v_s \in TS \xrightarrow{J} u_s = Jv_s \in TS \xrightarrow{E} (s_-, s_+) \in S \times S$$

$$s_{\pm} = \exp(\pm u_s) = \exp(\pm Jv_s)$$

Two Bundle isomorphisms $T^*S \cong TS$

θ_{can} = the canonical 1 – form in T^*S

$g^b : TS \rightarrow T^*S, v \mapsto v^b = g(v, \cdot)$ (Legendre)

$\omega^b : TS \rightarrow T^*S, v \mapsto v^{Jb} = g(Jv, \cdot)$.

$\theta_g = (g^b)^* \theta_{can}, \Omega_g = (g^b)^* \Omega_{can} = d\theta_g$

$\theta_\omega = (\omega^b)^* \theta_{can}, \Omega_\omega = (\omega^b)^* \Omega_{can} = d\theta_\omega$

Recall J is compatible with Riemannian metric g ,

$$\omega(v_1, v_2) = g(Jv_1, v_2).$$

Alejandro's magic formula

$P = TS - 0_S$, $\Phi : P \times \mathbb{R} \rightarrow P$ the geodesic flow.

$$E_t(v_s) = (\exp(-tv_s), \exp(tv_s)).$$

$$E_t^* \Omega_{pair} = \int_{-t}^t \Phi_u^* \Omega_\omega du = d \int_{-t}^t \Phi_u^* \theta_\omega du$$

$$\theta_\omega = (\omega^b)^* \theta_{can}, \quad \Omega_\omega = (\omega^b)^* \Omega_{can} = d\theta_\omega$$

Proof. Alejandro says is just the fundamental theorem of Calculus. But it is kind of tricky!!! □

ϵ -expansion

With $X =$ generator of geodesic flow,

$$E_\epsilon(v_s) = (\exp(-\epsilon v_s), \exp(-\epsilon v_s)).$$

$$\begin{aligned} \frac{1}{2\epsilon} E_\epsilon^* \Omega_{pair} &= \sum_{n=0}^{\infty} \frac{\epsilon^{2n}}{(2n+1)!} L_X^{2n} \Omega_\omega \\ &= d \left(\sum_{n=0}^{\infty} \frac{\epsilon^{2n}}{(2n+1)!} L_X^{2n} \theta_\omega \right) \quad (\text{recall } \Omega_\omega = d\theta_\omega) \end{aligned}$$

Proof. Lie bracket expansion of flows. □

Kimura's assertion

We can show that for $\epsilon = 0$

$$\Omega_g = d\theta_g, \quad F_o = |v_s|$$

We can go further:

How to compute the $L_X^{2n} \theta_\omega$?

Answer in next slides: we can write, in principle, the ϵ -expansion for the symplectic form and of the vortex pair Hamiltonian to any desired order.

The moving frame V_1, V_2, V_3 in $T_r(S)$

$$T_r(S) = \{v \in TS \mid |v| = r\}, \quad T_1(S) = U(S)$$

$P_{\gamma(t)}$ = parallel transport operator along γ .

$\Phi_1 : v_s \rightarrow R_t v_s$, rotation of angle t in $T_r S$.

$$\Phi_2(t) = (\gamma_o(t), \dot{\gamma}_o(t)), \quad \gamma_o(t) = \exp(v_s, t)$$

(geodesic flow: $\dot{\gamma}_o(t) = P_{\gamma_o(t)}(v_s)$)

Φ_3 : parallel transport of v_s for time t along geodesic γ_1 with initial condition $J v_s$

$$\Phi_3(t) = (\gamma_1(t), P_{\gamma_1(t)}(v_s)), \quad \gamma_1(t) = \exp(J v_s, t).$$

The $V_i, i = 1, 2, 3$ are the infinitesimal generators.

Commutation relations

V_1 is tangent to the fibers of the principal bundle

$$S^1 \hookrightarrow T_r(S) \rightarrow S$$

V_2 and V_3 span the horizontal spaces, projecting respectively to v_s and Jv_s .

$$[V_1, V_2] = V_3, \quad [V_3, V_1] = V_2, \quad [V_2, V_3] = \frac{K(s)}{r^2} V_1,$$

Denoting $\theta_1, \theta_2, \theta_3$ the dual coframe of V_1, V_2, V_3

$$d\theta_1 = -\frac{K(s)}{r^2} \theta_2 \wedge \theta_3, \quad d\theta_2 = -\theta_3 \wedge \theta_1, \quad d\theta_3 = -\theta_1 \wedge \theta_2.$$

Proof. See T. Leveuvre (section 2.4.2 (2.28)-(2.30))
<https://thibaultlefeuvre.files.wordpress.com/2016/04/memoire.pdf>

Computations are done in conformal coordinates.

Actually his derivation was done just for $U(S)$. For the general situation consider the scaled metric $\tilde{g} = g/r^2$ that has the same Euler-Lagrange equations - thus the same parametrized geodesics and *same flows* Φ_j .

Then $T_{r,g}S = U_{\tilde{g}}S$ in the rescaled metric. Therefore we can apply the same formulas, replacing $K(s)$ by $K(s)/r^2$. □

Completing the frame with V_4

$$V_4 = V_4^{fold} \text{ on } M = U(S) \times \mathfrak{R}, \quad V_4 = V_4^{symp} \text{ on } P = TS - 0_S.$$

$$V_4^{folded}(v_s, \alpha) = \partial/\partial\alpha, \quad V_4^{symp}(v_s) = v_s.$$

In the latter, used in the symplectomorphism approach, V_4^{symp} is the infinitesimal generator of $\Phi_4(v_s, t) = e^t v_s$.

In both cases the Lie bracket with the $V_i, i = 1, 2, 3$ vanishes. If we correspond M with P via their images in $S \times S$, we may write, with some abuse of language,

$$V_4^{symp} = |v_s| V_4^{folded}, \quad |v_s| = \alpha > 0.$$

$$\text{Coframe : } \{\theta_i\}, \quad 1 \leq i \leq 4 \text{ add : } d\theta_4 = 0.$$

Outline of derivations

Use Cartan's $L_X = i_X d + di_X$ in

$$\theta_g = |v_s|^2 \theta_2$$

and the structure equations for the $\theta_i, i = 1, 2, 3, 4$.

Take into account also:

$$J_*(V_1) = V_1, \quad J_*(V_2) = -V_3, \quad J_*(V_3) = V_2, \quad J_*(V_4) = V_4$$

$$J^*(\theta_1) = \theta_1, \quad J^*(\theta_2) = -\theta_3, \quad J_*(\theta_3) = \theta_2, \quad J_*(\theta_4) = \theta_4 .$$

Standard notations

We will denote the projections by

$$q : TQ \rightarrow Q \quad \text{and} \quad \pi : T^*Q \rightarrow Q$$

θ_{can} = the canonical 1 – form in T^*S

$g^b : TS \rightarrow T^*S, \quad v \mapsto v^b = g(v, \cdot)$ (Legendre)

$\omega^b : TS \rightarrow T^*S, \quad v \mapsto v^{Jb} = g(Jv, \cdot)$.

$\theta_g = (g^b)^* \theta_{can}, \quad \Omega_g = (g^b)^* \Omega_{can} = d\theta_g$

$\theta_\omega = (\omega^b)^* \theta_{can}, \quad \Omega_\omega = (\omega^b)^* \Omega_{can} = d\theta_\omega$

**Symplectic forms via the coframe θ_i , $i = 1, 2, 3, 4$
(Here we are working in $P = TS - 0_S$)**

$$\theta_g(V_{v_s}) = g(v_s, q_* V_{v_s}) \text{ for } V_{v_s} \in T_{v_s}(TS)$$

$$\theta_g(V_2(v_s)) = |v_s|^2$$

$$\text{In fact : } \theta_g = |v_s|^2 \theta_2$$

$$d|v_s| = |v_s| \theta_4$$

$$\Omega_g = d(|v_s|^2 \theta_2) = |v_s|^2 (\theta_1 \wedge \theta_3 + 2\theta_4 \wedge \theta_2)$$

Proof. The first is just trivial abstract nonsense from the definitions.

For the second note that the values of the 1-form θ_g on V_1 and V_4 vanish because the flows do not move the base point. Since $\pi_*(V_3) = Jv_s$, it follows that θ_g must also annihilate V_3 .

Third: The three directional derivatives $i = 1, 2, 3$ of v_s vanish because the flows of the $V_i, i = 1, 2, 3$, do not change norms in P . It is easy to see that for $V_4 = V_4^{symp}$

$$V_4|v_s| = |v_s| \text{ hence } d|v_s| = |v_s| \theta_4.$$

Finally $d(|v_s|^2 \theta_2) = |v_s|^2 \theta_1 \wedge \theta_3 + d|v_s|^2 \wedge \theta_2.$ □

Kimura's assertion

As $\epsilon \rightarrow 0$, the time rescaled vortex system tends to the geodesic system. More precisely, for $\epsilon = 0$

$$\Omega_g = d\theta_g, \quad F_0 = |v_s|. \quad \text{Its generator is } \frac{1}{2|v_s|} V_2.$$

Proof. Factors $(2\epsilon)^{-1}$ in front of the expansions of F and $J^* E_\epsilon^* \Omega_{pair}$ mutually cancel. To leading order

$$dF \sim d|v_s| = |v_s| \theta_4 .$$

Claim: the leading term of the symplectic form is

$$J^* d\theta_\omega = \Omega_g = |v_s|^2 (\theta_1 \wedge \theta_3 + 2\theta_4 \wedge \theta_2)$$



Why?

Why:

$$J^*d(|v|^2 \theta_3) = J^*(2|v_s|^2 \theta_4 \wedge \theta_3) + |v^2| J^*(\theta_2 \wedge \theta_1)$$

We claim that this equals to

$$\Omega_g = |v_s|^2 (\theta_1 \wedge \theta_3 + 2\theta_4 \wedge \theta_2)$$

An useful observation:

$$\begin{aligned} J_*(V_1) &= V_1, & J_*(V_2) &= -V_3, & J_*(V_3) &= V_2, & J_*(V_4) &= V_4 \\ J^*(\theta_1) &= \theta_1, & J^*(\theta_2) &= -\theta_3, & J^*(\theta_3) &= \theta_2, & J^*(\theta_4) &= \theta_4. \end{aligned}$$

Proof. Simply by doing mental pictures of the corresponding vectorfields along geodesic curves in S with initial conditions v_s or Jv_s . For instance we compute $J_*(V_3)$ mentally: we keep the base curve (the geodesic in the direction of Jv_s) and rotate the vectorfield along the curve, (which is the parallel transport of v_2) by $\pi/2$. Hence obtaining the geodesic field determined by Jv_s , ie.,

$$(J_*)_{v_s}(V_3(v_s)) = V_2(Jv_s).$$

□

Computation of the Lie derivatives

Lie derivatives can be computed to any desired order. The starting point is: $\theta_\omega = |v_s|^2 \theta_3$. Let us compute the ϵ^2 term $(L_X)^2 (|v_s|^2 \theta_3)$ with $X = V_2$.

$$\begin{aligned} L_X(|v_s|^2 \theta_3) &= (i_X d)(|v_s|^2 \theta_3) + d i_X(|v_s|^2 \theta_3) = \\ &= i_X(2|v_s|^2 \theta_4 \wedge \theta_3) + i_X(|v_s|^2 \theta_2 \wedge \theta_1) = |v_s|^2 \theta_1 \end{aligned}$$

Differentiating once more,

$$(L_X)^2 (|v_s|^2 \theta_3) = L_X(|v_s|^2 \theta_1) = -|v_s|^2 K(s) \theta_3.$$

Since $J^* \theta_3 = \theta_2$, we get finally ...

Symplectic form expansion up to ϵ^2

$$\begin{aligned} \frac{1}{2\epsilon} E_\epsilon^* \Omega_{pair} &\sim d \left[|v_s|^2 \left(1 - \frac{1}{6} K(s) \epsilon^2 \right) \theta_2 \right] = \\ &= \Omega_o + \epsilon^2 \Omega_1 + O(\epsilon^4) \end{aligned}$$

$$\Omega_o = \Omega_g = g_b^* \Omega_{can} = |v_s|^2 (\theta_1 \wedge \theta_3 + 2\theta_4 \wedge \theta_2)$$

$$\Omega_1 = -\frac{1}{6} K(s) \Omega_g + \frac{|v_s|^2}{6} (\nabla K \cdot Jv_s) \theta_2 \wedge \theta_3$$

Educated guess for the 1-form

The expansion of the pulled back 1-form is

$$\left(1 - \frac{1}{6} K(s) \epsilon^2 + O(\epsilon^4)\right) \theta_g, \quad \theta_g = |v_s|^2 \theta_2$$

Claim that inside the parenthesis one gets higher order multi-index derivatives of $K(s)$ in the direction of Jv_s for all even powers of ϵ .

Thus we are quite sure that we will get a function in TS multiplying θ_2 . None of the forms $\theta_1, \theta_3, \theta_4$ will appear.

Another approach: working in $M = U(S) \times (-r, r)$

$$E_{folded} : (v_s, \alpha) \mapsto (\exp(-\alpha v_s, \alpha v_s), |v_s| = 1)$$

$V_i, i = 1, 2, 3$ Levi Civita frame in $U(S)$, $V_4 = \partial/\partial\alpha$.

$\theta_i, i = 1, 2, 3$ are now restricted to $U(S)$, $\theta_4 = d\alpha$.

$0 \leq |\alpha| \leq r$, $2r =$ the injectivity radius

$$F = 2\alpha \exp(B), \quad B(v_s, \alpha) = m_2(v_s)\alpha^2 + O(\alpha^4)$$

$$E_{folded}^* \Omega_{pair} = \Omega_{13} \theta_1 \wedge \theta_3 + \Omega_{14} \theta_1 \wedge \theta_4 + \\ + \Omega_{23} \theta_2 \wedge \theta_3 + \Omega_{24} \theta_2 \wedge \theta_4$$

Next: the coefficients $\Omega_{ij}(v_s, \alpha)$: Jacobi fields!!!

For $\alpha = 0$ the only nonzero is $\Omega_{24} = 2$

folded symplectic

Notations in $M = U(S) \times (-r, r)$

$0 \leq |\alpha| \leq r$, $2r =$ the injectivity radius

$E_{folded} : (v_s, \alpha) \mapsto (\exp(-\alpha v_s), \exp(\alpha v_s))$, $|v_s| = 1$.

V_i , $i = 1, 2, 3$ the Levi Civita frame on $U(S)$

$V_4 = \partial/\partial\alpha$.

Let Y, Z the Jacobi fields with initial conditions

$$Y(0) = 0, Y'(0) = -v_s, Z(0) = v_s, Z'(0) = 0$$

(along the geodesic γ_1 with initial condition Jv_s connecting s_{\pm} .)

Folded symplectic: $M = U(S) \times (-r, r)$

$$\begin{aligned}\Omega_{13} &= -\Omega_{31} = -(|Y(\alpha)| + |Y(-\alpha)|) \\ \Omega_{14} &= -\Omega_{41} = -|Y(\alpha)| + |Y(-\alpha)| \\ \Omega_{23} &= -[\Omega]_{32} = |Z(\alpha)| - |Z(-\alpha)| \\ \Omega_{24} &= -[\Omega]_{42} = |Z(\alpha)| + |Z(-\alpha)|\end{aligned}$$

$$[\Omega] = \begin{bmatrix} 0 & 0 & \Omega_{13} & \Omega_{14} \\ 0 & 0 & \Omega_{23} & \Omega_{24} \\ -\Omega_{13} & -\Omega_{23} & 0 & 0 \\ -\Omega_{14} & -\Omega_{24} & 0 & 0 \end{bmatrix}$$

$$Y(0) = 0, Y'(0) = -v_s, Z(0) = v_s, Z'(0) = 0.$$

Using the expansions of the norm of Jacobi fields

$$\Omega_{13} = -2\alpha + \frac{1}{3}K(s)\alpha^3 + O(\alpha^5)$$

$$\Omega_{14} = O(\alpha^4)$$

$$\Omega_{23} = -\frac{1}{3}(\nabla K \cdot Jv_s)\alpha^3 + O(\alpha^5)$$

$$\Omega_{24} = 2 - K(s)\alpha^2 + O(\alpha^4)$$

$$E^* \Omega_{pair} = 2\theta_2 \wedge d\alpha - 2\alpha \theta_1 \wedge \theta_3 - \alpha^2 K(s) \theta_2 \wedge d\alpha + \\ + \alpha^3/3 [K(s) \theta_1 \wedge \theta_3 - (\nabla K \cdot Jv_s) \theta_2 \wedge \theta_3] + O(\alpha^4)$$

$$E^* \Omega_{pair} = d\omega + O(\alpha^4)$$

$$\omega = 2(-\alpha + \frac{1}{6}K(s)\alpha^3) \theta_2$$

Educated guess

$$E^* \Omega_{pair} = d(\omega + O(\alpha^4))$$

$$\omega = 2\left(-\alpha + \frac{1}{6}K(s)\alpha^3\right)\theta_2$$

We posit that $E^* \Omega_{pair}$ is exact, namely

$$E^* \Omega_{pair} = d[f(v_s, \alpha)\theta_2],$$

with a $f(v_s, \alpha)$ in M that can be expressed in terms of multiindices derivatives in Jv_s .

Summary: Vortex pair equations to leading orders

$$\dot{s} = v_s + \alpha^2 \left[(3m_2(v_s) + \frac{1}{2}K(s)) v_s - dm_2(V_1) Jv_s \right] + O(\alpha^4)$$

$$D_{\dot{s}} v_s = -\alpha^2 \left[dm_2(V_3) + \frac{1}{6} (\nabla K \cdot Jv_s) + O(\alpha^2) \right] Jv_s$$

$$\dot{\alpha} = -\alpha^3 dm_2(V_2) + O(\alpha^5)$$

D = Levi-Civita covariant derivative.

E. Computation of m_2 : some simple examples

a) Half plane $\{(x, y) \mid y \geq 0\}$ with euclidian metric

$$G(z_1, z_2) = \frac{1}{2\pi} (\log(|z_1 - z_2|) - \log(|z_1 - \bar{z}_2|))$$

$$R(z) = -\frac{1}{2\pi} \log(2y)$$

$$4\pi B(z_1, z_2) = \log(4y_1y_2) - \log((x_1 - x_2)^2 + (y_1 + y_2)^2).$$

Substituting

$$x_{1,2} = x_o \pm a \cos \theta, \quad y_{1,2} = y_o \pm a \sin \theta$$

we get

$$4\pi B = -\log(1 + a^2 \cos^2 \theta / y_o^2) + \log(1 - a^2 \sin^2 \theta / y_o^2) = -\frac{1}{y_o^2} a^2 + O(a^4).$$

$$m_2 = -\frac{1}{y_o^2} \quad (\text{independent of direction}).$$

As the pair approaches the boundary in an inclined way it shall perform a sharp turn, similar to a billiard. But when the pair approaches the boundary in the perpendicular direction, they split in two opposite directions, while their geometric center comes to a halt asymptotically. One way to interpret this phenomenon is as follows: in the full plane, the image pair comes along from the negative side. The two pairs swap partners and change directions by 90 degrees.

The same behavior will occur for a vortex pair inside the unit disk $D : |z| \leq 1$, for which the Green function is

$$G(z_1, z_2) = \frac{1}{2\pi} (\log |z_1 - z_2| - \log(|z_1 - z_2^*||z_2|)) \quad , \quad z_2^* = z_2/|z_2|^2 .$$

Similar computations give analogous results. In the case of the unit disk, suppose that the pair approaches the boundary with symmetric positions relative to a diameter. The geometric center stops and then reverses direction, while the pair splits apart, running close to the boundary but in opposite ways. They reunite on the other side: a perennial cycle of “love and hate”.

In conclusion: B blows up as one approaches the boundary, due to the mirror vortex pair coming from the other side. B contains contributions from this, as we saw explicitly in the case of the upper half plane. For surfaces one can do this formally using the Schottky double (we thank Björn Gustafsson for this observation).

b) The round sphere: $m_2 = -1/6$

$$G(x, y) = \log |X - Y|$$

where one takes the euclidian distance between X, Y .

Their midpoint is well defined when they are not antipodal. Denote $0 < \alpha < \pi/2$ the angle between each of vectors X, Y with s .

$$d_{S^2}(x, y) = 2\alpha, \quad G(X, Y) = \log(2 \sin \alpha).$$

$$B(X, Y) = \log |X - Y| - \log d_{S^2}(X, Y) = \log(2 \sin \alpha) - \log(2\alpha) = \log\left(\frac{\sin \alpha}{\alpha}\right),$$

since Robin's function vanishes identically. We can expand

$$B(X, Y) = \log\left(1 - \frac{1}{6}\alpha^2 + \dots\right) = -\frac{1}{6}\alpha^2 + \dots, \text{ so}$$

$$\boxed{m_2 \equiv -\frac{1}{6}.$$

Validating the results using the round sphere

When we put $K = 1$, $m_2 = -1/6$, $e_1 = e_2 = e_3 = 0$, then

$$3m_2 + K/2 \equiv 0.$$

Hence the central geodesic does not sense any perturbation.

Let us verify again with the full vortex equations.

$$H = -\log(2 \sin \alpha)$$

without rescaling, or

$$F = \exp(-H) = 2 \sin \alpha$$

after rescaling. The vorticities are $\kappa = \pm 1$.

Without loss of generality we may take the initial conditions

$$s_o = (1, 0, 0), v_o = (0, 1, 0) \text{ so that } Jv_o = s_o \times v_o = (0, 0, 1).$$

$$s_{\pm}(\alpha) = \exp(s_o, \pm \alpha Jv_o) = (\cos \alpha, 0, \pm \sin \alpha), 0 \leq \alpha \leq \pi/2.$$

The Jacobi fields are tangent to the parallels, with norm

$$|Y(\pm\alpha)| = \sin \alpha, \quad |Z(\pm\alpha)| = \cos \alpha.$$

... continues

The symplectic matrix is

$$[\Omega] = 2 \begin{bmatrix} 0 & 0 & \sin \alpha & 0 \\ 0 & 0 & 0 & \cos \alpha \\ -\sin \alpha & 0 & 0 & 0 \\ 0 & -\cos \alpha & 0 & 0 \end{bmatrix}.$$

The differential of the rescaled Hamiltonian is

$$[dF] = (0, 0, 0, 2 \cos \alpha)$$

Solving for X_F in $\Omega(X_F, \bullet) = -dF$ we get, as expected, the well known fact: the centerpoint s runs the equator, and the vortices s_{\pm} the parallels with latitude $\pm\alpha = \text{const}$.

In this rescaling the period of all orbits is constant, $T_{resc} = 2\pi$. If we go to the original time, the period is obtained multiplying 2π by $\sin \alpha$. The motion is infinitely fast for dipoles, and the velocity slows down to zero at the poles.

c) Hyperbolic half plane ($K = -1$): $m_2 = -1/3$

$$ds_H^2 = |dz|^2/y^2 \text{ in } H : y > 0.$$

$$\cosh d_H(z_1, z_2) = 1 + \frac{|z_1 - z_2|^2}{2y_1 y_2}.$$

$$G(z_1, z_2) = \frac{1}{2\pi} \log(\tanh(\frac{\rho}{2})) = \frac{1}{4\pi} \log \frac{\cosh \rho - 1}{\cosh \rho + 1}.$$

$$\text{Initial conditions } z_- = -\beta + i, z_+ = \beta + i.$$

The trajectories stay symmetric with respect to the y -axis, which is a geodesic.

The vortex $z_+(t)$ traces the line

$$x = \beta y, y > 0$$

with constant distances $\rho = d(z_-(t), z_+(t))$ given by $\cosh \rho = 1 + 2\beta^2$.

In first order, $\rho \sim \sinh \rho \sim 2\beta$. The geodesic joining $z_{\pm}(t)$ is an arc of the semicircle centered at the origin and radius

$$r(t) = |z_+(t)| = \sqrt{x^2(t) + y^2(t)} = \sqrt{1 + \beta^2} y(t).$$

Thus the mid point of $s_-(t)$ and $s_+(t)$ is $(0, r(t))$, and

$$\frac{\dot{r}}{r} = \frac{\dot{y}}{y}.$$

... continues

\dot{y} is governed by the differential equation

$$\frac{\dot{y}}{y^2} = \kappa \frac{\partial F}{\partial x}.$$

where we take the rescaled Hamiltonian (dropping the $1/2\pi$ factor)

$$F = \exp(-H) = \exp(G) = \sqrt{\frac{\cosh \rho - 1}{\cosh \rho + 1}} = \tanh\left(\frac{\rho}{2}\right).$$

A quick computation gives at the symmetric pair:

$$F_x = \sqrt{\frac{\cosh \rho + 1}{\cosh \rho - 1}} \frac{(\cosh \rho)_x}{(\cosh \rho + 1)^2}$$

where $(\cosh \rho)_x = 2x/y^2$. Thus

$$\frac{\dot{y}}{y^2} = \sqrt{\frac{\cosh \rho + 1}{\cosh \rho - 1}} \frac{2x/y^2}{(\cosh \rho + 1)^2}, \quad \cosh \rho = 1 + 2\beta^2, \quad x = \beta y.$$

Simplifying, we get

$$v_r = \frac{\dot{r}}{r} = \frac{\dot{y}}{y} = \frac{v_o}{(1 + \beta^2)^{3/2}}, \quad v_o = 1/2.$$

Adjusting the vorticity κ we can assume $v_o = 1$.

As expected, that the velocity v_r of the midpoint (same as the vertical component of the vortices) is constant, when measured in the hyperbolic metric.

But the velocity depends on the separation parameter β .

When $\beta \rightarrow \infty$ then $v_r \rightarrow 0$, which is what one expects: they do not see each other. For small β the Taylor expansion starts as

$$v_r = v_o \left(1 - \frac{3}{2}\beta^2 + \dots\right)$$

where v_o is the velocity of the dipole (infinitesimal separation) in the time scale of the Hamiltonian $F = \exp(G)$.

Claim: $m_2 = -1/3$. This gives rise to the coefficient $-3/2$ above as predicted, by adding

$$3m_2 + K/2 = 3(-1/3) - 1/2.$$

We use the Poincaré disk model just to do a double check. The Green function for the metric

$$ds_D^2 = 4 \frac{|dw|^2}{(1 - |w|^2)^2} \text{ in } D : |w| < 1$$

is given by

$$G(w_1, z_2) = \frac{1}{2\pi} \log \frac{|w_1 - w_2|}{|w_1 \bar{w}_2 - 1|} = \frac{1}{2\pi} \log \left(\tanh\left(\frac{\rho}{2}\right) \right) = \frac{1}{4\pi} \log \frac{\cosh \rho - 1}{\cosh \rho + 1}$$

where the hyperbolic distance is

$$\rho = d_D(w_1, w_2) = 2 \tanh^{-1} |(w_1 - w_2)/(w_1 \bar{w}_2 - 1)|.$$

Robin function is constant. We expand

$$\begin{aligned} G &= \frac{1}{4\pi} \log \left(\frac{\rho^2/2 + \rho^4/4! + \dots}{2 + \rho^2/2 + \rho^4/4! + \dots} \right) = \\ &= \frac{1}{2\pi} \log \rho + \frac{1}{4\pi} \log \left(\frac{1/2 + \rho^2/4! + \dots}{2 + \rho^2/2 + \rho^4/4! + \dots} \right) \end{aligned}$$

$$B = G - \frac{1}{2\pi} \log \rho = \frac{1}{4\pi} \log \left[\left(1 + \frac{\rho^2}{12} + \dots\right) \left(1 - \frac{\rho^2}{4} + \dots\right) \right] = -\frac{1}{2\pi} \frac{\rho^2}{12} + \dots$$

Replacing $\rho = 2\alpha$, where α is the distance to the midpont, and neglecting the $1/2\pi$ we get indeed

$$m_2 \equiv -1/3$$

d) Surfaces of Revolution

For surfaces of revolution one can construct a global coordinate system (x, y) with metric of the form

$$ds^2 = h^2(x) (dx^2 + dy^2) , \quad y \equiv y + 2\pi.$$

Both the geodesic system and the vortex pair are completely integrable, with momentum maps of the S^1 symmetry given by

$$p_y = 2h^2(x)\dot{y}$$

for the geodesic problem and

$$J = \int_{x_2}^{x_1} h^2(x) dx$$

for the vortex pair problem in $S \times S$.

Project: comparative study in the catenoid. The natural parametrization is already conformal,

$$\begin{aligned} X(x, \phi) &= (\cos \phi \cosh x, \sin \phi \cosh x, x) , \\ \text{Metric } g &: ds^2 = \cosh^2(x)(d\phi^2 + dx^2) . \end{aligned}$$

with x running linearly along the surface-axis, and with $h = \cosh(x)$ equal to the radius of circles forming the parallels. The geodesics were described using elliptic functions.

Topologically, the catenoid is a cylinder, with underlying Green function for the constant curvature metric given by (). The vortex pair problem can be reduced to quadratures (see appendix B), with

$$J = \frac{1}{4} [(\sinh(2x_2) + 2x_2) - (\sinh(2x_1) + 2x_1)]$$

The reduction will involve the transcendental equation

$$x + \frac{1}{2} \sinh(2x) = a, \quad \text{where } a = 2J + x_1 + \frac{1}{2} \sinh(2x_1)$$

so the development of the project needs to be a mix analytical/numerical.

A question we would be particularly interested: for nearby vortices, how the center point motion drifts from the initial geodesic given by the initial conditions?

e) Round cylinder and flat tori: topology matters

As discussed in extra slides (A). The Green function of the cylinder is given just by elementary functions. The Green functions for flat tori require elliptic functions. Since the feature we want to show is similar in both, we only did the vortex pair problem on the cylinder.

There are two symmetry groups of translations. For the cylinder: coordinates $X = (x, y) \in \mathbb{R} \times S^1$, $y \equiv y + 2\pi$. The groups are the real line itself in the x direction, and S^1 itself for in the slot y . It is trivial to find the conserved (group valued) momenta, although

$$\Omega_{pair} = dx_2 \wedge dy_2 - dx_1 \wedge dy_1$$

is exact only in the x coordinate.

In a flat torus, one identifies points in the plane that differ by integer multiples of two generators. The groups of translations are generated by infinitesimal motions in the direction of the generators. The momenta in both cases are the coordinate differences, the 2π ambiguities are irrelevant.

Momentum conservation entails:

The pair moves keeping fixed the relative position vector.
This implies also $\dot{\alpha} \equiv 0$.

VORTEX PAIRS ON A TRIAXIAL ELLIPSOID AND KIMURA'S CONJECTURE

ADRIANO REGIS RODRIGUES

Departamento de Matemática
Universidade Federal Rural de Pernambuco
Recife, PE CEP 52171-900 Brazil

CÉSAR CASTILHO*

Departamento de Matemática
Universidade Federal de Pernambuco
Recife, PE CEP 50740-540 Brazil

JAIR KOILLER

Departamento de Matemática
Universidade Federal de Juiz de Fora
Juiz de Fora, MG CEP 36036-900 Brazil

(Communicated by James Montaldi)

ABSTRACT. We consider the problem of point vortices moving on the surface of a triaxial ellipsoid. Following Hally's approach, we obtain the equations of motion by constructing a conformal map from the ellipsoid into the sphere and composing with stereographic projection. We focus on the case of a pair of opposite vortices. Our approach is validated by testing a prediction by Kimura that a (infinitesimally close) vortex dipole follows the geodesic flow. Poincaré sections suggest that the global flow is non-integrable.

1. Introduction. The equations describing the motion of N -point vortices on an ideal planar fluid were introduced in 1867 by Helmholtz [15] and described as an Hamiltonian system in 1876 by Kirchhoff [24]. Equations for point vortices on the two dimensional sphere were derived independently by I. Gromeka [13] and by E. Zermelo [37] and rediscovered in 1977 by Bogomolov [2]. In 1999 Kimura [23] studied all complete surfaces with constant curvature. *Kimura conjectured that on any surface a pair of infinitesimally close opposite vortices would move along a geodesic.* For the hyperbolic plane a recent study was carried out by Montaldi [27].

In 1980 D. Hally [14] wrote the equations for the point vortex dynamics on a simply connected compact surface (i.e, surfaces diffeomorphic to spheres) using isothermal coordinates. For such a surface with metric $ds^2 = h^2(z, \bar{z})|dz|^2$ where $z \in \mathbb{C} \cup \infty$ represents stereographic coordinates on the sphere, Hally's equations are

$$\dot{z}_n = h^{-2}(z_n, \bar{z}_n) \left[\sum_{k \neq n}^N -i \frac{\Gamma_k}{z_n - z_k} + i \Gamma_n \frac{\partial}{\partial z_n} \ln(h(z_n, \bar{z}_n)) \right], \quad n = 1, 2, \dots, N; \quad (1)$$

2010 *Mathematics Subject Classification.* Primary: 76B99, 34C28; Secondary: 37D99.

Key words and phrases. Fluid Dynamics, Vortex Dynamics, Point Vortices, Riemann Surfaces.

* Corresponding author.

where Γ_k represents the k -th vortex intensity and z_k its coordinates. The notation (z, \bar{z}) should be familiar to the reader, meaning $\operatorname{Re} z = (z + \bar{z})/2$, $\operatorname{Im} z = (z - \bar{z})/(2i)$. The topological constraint of the surface being compact imposes

$$\sum_{i=1}^N \Gamma_i = 0. \quad (2)$$

Bounded domains inside curved surfaces, simply or multiply connected, can be studied on its planar image via Theorem 2 of C.C.Lin's classical paper [19]. Presently, there are powerful methods to produce conformal mappings to the unit circle or the unit circle with circular holes [10].

Recent work. The case of a *compact* Riemann surface S of any genus endowed with an arbitrary metric was addressed by Boatto and Koiller [1]. The constraint (2) can be relaxed. In fact, for compact surfaces, the Green function $G(s_1, s_2)$ of the Laplace-Beltrami operator governing the vortex-vortex interactions, also encodes a background counter-vorticity, uniformly distributed with respect to the metric. The Robin function (desingularization of G) accounts for the self interactions. For vortices in the round sphere there is a sizeable literature (for a fairly complete list see [1]). We now review some work on vortices moving on surfaces with non-constant curvature. In 2008 Castilho and Machado [7] wrote Hally's equations as an Hamiltonian system, with Hamiltonian function

$$H = \sum_{k < n} \Gamma_k \Gamma_n \ln(h(z_k, \bar{z}_k)h(z_n, \bar{z}_n)|z_k - z_n|^2) \quad (3)$$

and symplectic form

$$\Omega = \sum_{n=1}^N \Gamma_n h^2(z_n, \bar{z}_n) dz_n \wedge d\bar{z}_n. \quad (4)$$

Using perturbation theory they obtained first order approximations for Hally's equations for an ellipsoid of revolution $\frac{x^2}{R^2} + \frac{y^2}{R^2} + \frac{z^2}{R^2(1+\epsilon)} = 1$, for small values of ϵ . The ellipsoid's symmetry was used to reduce the dimension of the problem. In 2010 Kim [21] obtained the full equations for any ellipsoid of revolution. Several other surfaces of revolution were considered in [8]. Kimura's conjecture for vortex pairs ($\Gamma_2 = -\Gamma_1$) was first tested in [25]. As for numerical methods: San Miguel [32], used least-squares fitting to obtain discretized conformal mappings between ovaloids and the sphere. He integrated the vortex pair equations using the Gaussian collocation method. The first study on a genus 2 surface was done by C. Ragazzo [30]. Based on a relation between the Laplace-Beltrami Green function and the heat kernel, an algorithm is presented to determine the motion of a single vortex which is governed by Robin's function. The method is applied to compute the motion of a vortex on the Bolza surface, namely a constant curvature genus 2 surface whose fundamental domain is a regular octagon.

Summary of the paper. We study the motion of a vortex pair on the triaxial ellipsoid

$$\mathbb{E}^2(a, b, c) : \frac{x^2}{a} + \frac{y^2}{b} + \frac{z^2}{c} = 1 \quad (5)$$

with $0 < a < b < c$. In section 2 we review Jacobi's confocal conics coordinates λ_1, λ_2 , with $a \leq \lambda_1 \leq b \leq \lambda_2 \leq c$ that parametrize one octant of the ellipsoid.

Jacobi also derived a system of conformal coordinates, but they become singular at the four umbilical points that belong to the ellipse with semiaxis a, c ($y = 0$), corresponding to $\lambda_1 = \lambda_2 = b$. In section 3 we recall the sphero-conical coordinates μ_1, μ_2 for the unit sphere \mathbb{S}^2 ,

$$\xi^2 + \eta^2 + \zeta^2 = 1, \quad (6)$$

that depends on three affine parameters $I_1 < I_2 < I_3$, with $I_1 < \mu_1 < I_2 < \mu_2 < I_3$.

In section 4 we construct a conformal map between the two surfaces, with the help of a simple, but useful lemma 4.1. The sphero-conical parameters I_j are chosen in such a way that one octant of the ellipsoid is mapped exactly into one octant of the sphere under a common isothermal parametrization. There are two relations between the affine triples a, b, c and I_1, I_2, I_3 , given in terms of complete elliptic integrals. Moreover, each λ_i is an elliptic function of their corresponding μ_i , $i = 1, 2$. Dupin's lines of curvature of the ellipsoid is mapped into a topologically equivalent system of curves in the sphere. The umbilics $\lambda_1 = \lambda_2 = b$ map to $\mu_1 = \mu_2 = I_2$. The conformal factor is $(\lambda_2 - \lambda_1)/(\mu_2 - \mu_1)$, which is $0/0$ at the umbilical points. We computed the limit in §5: it is equal to $[(b - a)(c - b)]/[b(I_2 - I_1)(I_3 - I_2)]$.

In section 6 we write the vortex pair equations on the ellipsoid and present our methodology to numerically integrate them. Composing the ellipsoid to sphere map with the stereographic projection from the sphere into the z -complex plane we get the conformal factor $h(z, \bar{z})$ required for Hally's equation.

In section 7 our approach is validated by verifying Kimura's conjecture [23] about the relation between the dipole dynamics and the geodesic flow. We also compute exploratory Poincaré maps for the flow suggesting that it is chaotic. Directions for future research are presented in section 8. In Appendix A (following [1]) two proofs of Kimura's conjecture are outlined. Appendix B outlines Carlson's method for numerically computing elliptic integrals [6].

2. Confocal quadrics coordinates (λ_1, λ_2) on the triaxial ellipsoid. Consider the equation

$$\frac{x^2}{a - \lambda} + \frac{y^2}{b - \lambda} + \frac{z^2}{c - \lambda} = 1. \quad (7)$$

For $P = (x, y, z) \in \mathbb{E}^2$ the above equation has three solutions $\lambda_3 = 0$ and λ_1, λ_2 (called Jacobi's confocal coordinates [18], [28]) such that $a \leq \lambda_1 \leq b \leq \lambda_2 \leq c$. They satisfy

$$\begin{aligned} x^2 &= \frac{a(a - \lambda_1)(a - \lambda_2)}{(a - b)(a - c)}, \\ y^2 &= \frac{b(b - \lambda_1)(b - \lambda_2)}{(b - a)(b - c)}, \\ z^2 &= \frac{c(c - \lambda_1)(c - \lambda_2)}{(c - a)(c - b)}. \end{aligned} \quad (8)$$

Each (closed) *octant* of \mathbb{E}^2 is parametrized by $(\lambda_1, \lambda_2) \in [a, b] \times [b, c]$. See Fig. 2. Clearly, the semiaxis extremes correspond to:

$$\begin{aligned} \lambda_1 = b, \lambda_2 = c &\Rightarrow (\sqrt{a}, 0, 0) \\ \lambda_1 = a, \lambda_2 = c &\Rightarrow (0, \sqrt{b}, 0) \\ \lambda_1 = a, \lambda_2 = b &\Rightarrow (0, 0, \sqrt{c}) \end{aligned} \quad (9)$$

There are four umbilical points located in the middle ellipse ($y = 0$):

$$\left(\pm \sqrt{\frac{a(b-a)}{c-a}}, 0, \pm \sqrt{\frac{c(c-b)}{c-a}} \right) \quad (10)$$

corresponding to $\lambda_1 = \lambda_2 = b$. The following result is classical:

Proposition 1. (*Jacobi, [18]*) *The metric ds^2 induced by the embedding of the ellipsoid in \mathbb{R}^3 is of Liouville type ([4])*

$$ds^2 = \frac{\lambda_2 - \lambda_1}{4} \left[\frac{\lambda_1 d\lambda_1^2}{(\lambda_1 - a)(\lambda_1 - b)(\lambda_1 - c)} - \frac{\lambda_2 d\lambda_2^2}{(\lambda_2 - a)(\lambda_2 - b)(\lambda_2 - c)} \right] \quad (11)$$

(note that the second term is positive).

In a famous paper Jacobi showed that the geodesics on the triaxial ellipsoid are integrable ([17], 1839). In §28 of his *Vorlesungen* ([18], 1866), he presented a derivation using the (now called) Hamilton-Jacobi PDE, that separates using confocal quadrics coordinates¹. In §28 Jacobi also constructed a *local* conformal map from the triaxial ellipsoid to the plane (pp. 215-217 of second edition). Jacobi's map was implemented recently in [29] and [20]. Isothermal coordinates (u, v) on an octant of \mathbb{E}^2 can be constructed using elliptic integrals of the third kind Π (see [5])

$$\Pi(\phi, k, n) = \int_0^\phi \frac{d\theta}{(1 - n \sin^2 \theta) \sqrt{1 - k^2 \sin^2 \theta}}. \quad (12)$$

We define the functions $u = P(\lambda_1)$ (increasing) and $v = Q(\lambda_2)$ (decreasing) by

$$u = P(\lambda_1) = \int_a^{\lambda_1} \sqrt{\frac{t}{(t-a)(t-b)(t-c)}} dt = \frac{2a}{\sqrt{b(c-a)}} \Pi(\phi, k, n) \quad (13)$$

with

$$\phi = \arcsin \sqrt{\frac{b(\lambda_1 - a)}{\lambda_1(b-a)}}, \quad k = \sqrt{\frac{c(b-a)}{b(c-a)}} \quad \text{and} \quad n = \frac{a-b}{b}; \quad (14)$$

$$v = Q(\lambda_2) = \int_{\lambda_2}^c \sqrt{\frac{-t}{(t-a)(t-b)(t-c)}} dt = \frac{2c}{\sqrt{b(c-a)}} \Pi(\phi, k, n) \quad (15)$$

with

$$\phi = \arcsin \sqrt{\frac{b(c-\lambda_2)}{\lambda_2(c-b)}}, \quad k = \sqrt{\frac{a(c-b)}{b(c-a)}} \quad \text{and} \quad n = \frac{c-b}{b}. \quad (16)$$

Proposition 2. *The metric (11) in the ellipsoid (5) induced by its embedding in the euclidian space has, in the first octant, the isothermal coordinates (u, v) in the rectangle $[0, K_1] \times [0, K_2]$. Here $u = P(\lambda_1)$, $v = Q(\lambda_2)$ are given by (13) and (15), with $K_1 = P(b)$ and $K_2 = Q(b)$. Moreover,*

$$ds^2 = h^2(u, v)(du^2 + dv^2), \quad \text{with} \quad h^2(u, v) = \frac{\lambda_2(v) - \lambda_1(u)}{4}. \quad (17)$$

The conformal map becomes singular (because the conformal factor vanishes) when $\lambda_2(v) = \lambda_1(u)$ which occurs only for $u = K_1$, $v = K_2$, precisely the umbilical point.

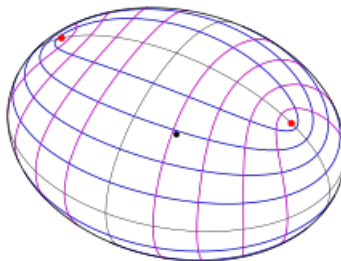


FIGURE 1. Lines of curvature of the triaxial ellipsoid. Cuts along the top and bottom segments joining the umbilical points results (topologically) on an open cylinder. One could as well make the cuts sidewise.

The lines of curvature (of both families) in Fig.1 cannot be given a consistent direction along the middle ellipse². In Fig.2, the top panel shows the transformation from confocal coordinates (λ_1, λ_2) to Jacobi's (u, v) on every octant. The following Proposition explains the middle and bottom panels. An underlined letter means that in the planar map the region appears flipped by 180° but overlap perfectly in the ellipsoid. This observation certainly has not escaped to Jacobi, to whom it must have appeared so trivial that he did not even bothered to put in print.

Proposition 3. *The real elliptic functions*

$$\lambda_1 = \lambda_1(u) \text{ and } \lambda_2 = \lambda_2(v), \quad (18)$$

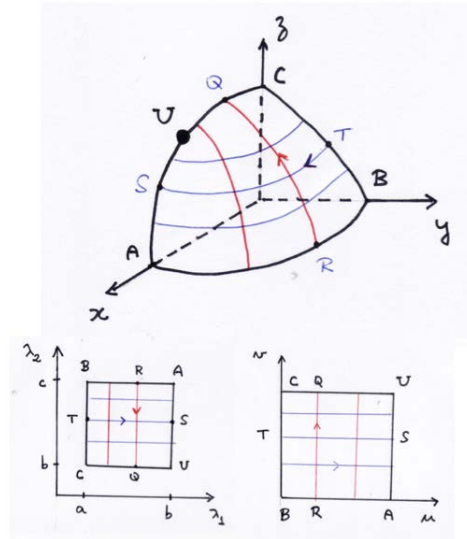
obtained by inverting respectively (13) and (15), give rise to a double (branched) covering of the ellipsoid by a flat torus. The lattice has fundamental domains of sizes $4K_1$ and $4K_2$. Each of the 16 rectangles of sizes $K_1 \times K_2$ in the plane (u, v) corresponds to an octant: the ellipsoid is covered twice.

For the numerical work will not need to use their explicit formulas. Instead, we will be only computing elliptic integrals. Four rectangles in the plane surrounding a point marked U cover twice the sector formed by two octants with a common umbilical point. Rectangles with vertices corresponding to the umbilical points $\pm U_1, \pm U_2$ with centers B (or $-B$) are mapped to sides $y > 0$ or $y < 0$ of the ellipsoid (5). In the next sections we will remedy the defect at the umbilical points.

Remark 1. In contradistinction with geodesics, which depends on the local metric, vortex motion depends on non local effects, which are encoded in the Green function of the Laplace-Beltrami operator of the metric [1]. An early attempt to use Jacobi's coordinates (u, v) in our numerical experiments for the vortex pair problem on the triaxial ellipsoid was not satisfactory. However, for initial conditions where the distance between the vortices was small, we found in §6 that the dynamics tends to move along a geodesic of the ellipsoid, as predicted by Kimura's conjecture. Therefore, in order to study point vortices on the full triaxial ellipsoid a *global* map from the ellipsoid to the sphere is needed.

¹The triaxial ellipsoid geodesics problem also separates in sphero-conical coordinates in §3 applied to $\xi = x/\sqrt{a}, \eta = y/\sqrt{b}, \zeta = z/\sqrt{c}$, but we preferred to use Jacobi's confocal coordinates).

²Source https://en.wikipedia.org/wiki/Umbilical_point



	C2	U2	C	U1	C1
	$x < 0$ $y < 0$ $z > 0$	$x < 0$ $y > 0$ $z > 0$	$x > 0$ $y > 0$ $z > 0$	$x > 0$ $y < 0$ $z > 0$	
	$x < 0$ $y < 0$ $z < 0$	$x < 0$ $y > 0$ $z < 0$	$x > 0$ $y > 0$ $z < 0$	$x > 0$ $y < 0$ $z < 0$	
	-C2	-U2	-C	-U1	-C1

	-U1	-C	-U2	-C	-U1
	<u>i</u>	<u>h</u>	<u>f</u>	<u>e</u>	
A	<u>a</u>	<u>b</u>	<u>c</u>	<u>d</u>	A
U1	d	c	b	a	U1
A	e	f	h	i	A
	-U1	-C	-U2	-C	-U1

FIGURE 2. Scheme for the double branched covering of the torus over the ellipsoid. See Proposition 3.

Our construction of a conformal map from the ellipsoid to the sphere makes use of confocal coordinates in \mathbb{E} and sphero-conical coordinates in \mathbb{S}^2 , that has four “fake” singular points. The distribution of coordinate lines on the two surfaces correspond: in the ellipsoid they are the principal curvature lines, that have the umbilical points as singularities. The umbilics on the ellipsoid are mapped into the singular points of the sphero-conical coordinates. Hence the map will be global.

3. Sphero-conical coordinates (μ_1, μ_2) on the sphere \mathbb{S}^2 [3]. This coordinate system depends on three arbitrary parameters $I_1 < I_2 < I_3$, that will be chosen so that one octant of the ellipsoid (5) gets mapped exactly into one octant of the sphere (6). *This will permit to extend the conformal transformation between the whole surfaces, in such a way that the coordinate lines distributions correspond.*

The parametrization of $(\gamma_1, \gamma_2, \gamma_3) \in \mathbb{S}^2$ is

$$\begin{aligned}\gamma_1^2 &= \frac{(I_1 - \mu_1)(I_1 - \mu_2)}{(I_1 - I_2)(I_1 - I_3)}, \\ \gamma_2^2 &= \frac{(I_2 - \mu_1)(I_2 - \mu_2)}{(I_2 - I_1)(I_2 - I_3)}, \\ \gamma_3^2 &= \frac{(I_3 - \mu_1)(I_3 - \mu_2)}{(I_3 - I_1)(I_3 - I_2)}\end{aligned}\tag{19}$$

with $(\mu_1, \mu_2) \in [I_1, I_2] \times [I_2, I_3]$. Taking $\mu_1 = \mu_2 = I_2$ one gets four distinguished points in the sphere

$$\left(\pm \sqrt{\frac{I_2 - I_1}{I_3 - I_1}}, 0, \pm \sqrt{\frac{I_3 - I_2}{I_3 - I_1}} \right)\tag{20}$$

that will be paired with the ellipsoid umbilics (10) in the conformal transformation between the surfaces.

A quick derivation of this coordinate system on an octant of the sphere comes indirectly from the following problem (see [26]). Let $A = \text{diag}(I_1, I_2, I_3)$. Diagonalize $\langle Ax, x \rangle$, $x \in \mathbb{R}^3$, restricted to the subset $\langle x, \gamma \rangle = 0$; that is, find extremals of $\langle Ax, x \rangle$ constrained to $\|x\|^2 = 1$ and to $\langle x, \gamma \rangle = 0$. The extremals can be located by considering the function $f(x) = \frac{1}{2} \langle Ax, x \rangle$, constrained to the subset of \mathbb{S}^2 defined by $\varphi^{-1}(0, 0)$ where

$$\varphi(x) = \left(\sum x_j^2 - 1, \sum x_j \gamma_j \right).$$

Let μ and k be Lagrange multipliers. We look for solutions of

$$\nabla f(x) = \frac{\mu}{2} \nabla \varphi_1(x) + k \nabla \varphi_2(x).$$

That is

$$x_j = k \frac{\gamma_j}{(I_j - \mu)}, \quad j = 1, 2, 3.\tag{21}$$

Considering that $\sum x_j^2 = 1$ and $\sum x_j \gamma_j = 0$, we obtain $k^2 = 1 / \left[\sum \frac{\gamma_j^2}{(I_j - \mu)^2} \right]$ and

$$\sum_{j=1}^3 \frac{\gamma_j^2}{I_j - \mu} = 0.\tag{22}$$

For each choice of value μ , equation (22) represents an elliptical cone in the Euclidian space of the $(\gamma_1, \gamma_2, \gamma_3)$. The intersection of these cones with the sphere $\langle \gamma, \gamma \rangle = 1$, are curves that represent an orthogonal system of coordinates, since the

extremal vectors (21), are extremals of the quadratic form $\langle Ax, x \rangle$, and are also parallel to the gradient of (22). Equation (22) has two roots

$$I_1 < \mu_1(\gamma, I_1, I_2, I_3) < I_2, \quad I_2 < \mu_2(\gamma, I_1, I_2, I_3) < I_3$$

that are explicitly obtained from a quadratic equation. Conversely, equations (19) for $(\gamma_1, \gamma_2, \gamma_3)$ can be obtained by solving the linear system

$$A(\gamma_1^2 \ \gamma_2^2 \ \gamma_3^2)^t = (1 \ 0 \ 0)^t$$

with

$$A = \begin{pmatrix} 1 & 1 & 1 \\ (I_1 - \mu_1)^{-1} & (I_2 - \mu_1)^{-1} & (I_3 - \mu_1)^{-1} \\ (I_1 - \mu_2)^{-1} & (I_2 - \mu_2)^{-1} & (I_2 - \mu_2)^{-1} \end{pmatrix}.$$

For future reference we observe that

$$\frac{\partial \gamma}{\partial \mu_i} = \frac{1}{2} \left(\frac{\gamma_1}{\mu_i - I_1}, \frac{\gamma_2}{\mu_i - I_2}, \frac{\gamma_3}{\mu_i - I_3} \right). \quad (23)$$

Proposition 4. *The standard metric ds^2 of \mathbb{S}^2 can be written in terms of the sphero-conical coordinates (19) with parameters (I_1, I_2, I_3) as*

$$ds^2 = \frac{\mu_2 - \mu_1}{4} \left[\frac{d\mu_1^2}{\prod_{i=1}^3 (\mu_1 - I_i)} - \frac{d\mu_2^2}{\prod_{i=1}^3 (\mu_2 - I_i)} \right]. \quad (24)$$

For a derivation, see [3]. The coordinates $I_1 < \mu_1 < I_2 < \mu_2 < I_3$ cover each octant of the sphere in a similar fashion as the confocal quadric coordinates do for the triaxial ellipsoid.

4. Constructing the conformal map from $\mathbb{E}^2(a, b, c)$ to the unit sphere.

Two conformal maps from a closed simply connected surface to the sphere differ by Moebius transformations in \mathbb{S}^2 . For the triaxial ellipsoid we found two references: Schering [34] in 1857 and Craig [9] in 1880. Both are quite intricate analytically, so we opted do to an *ab initio* construction, that may have its own interest due to its simplicity. Our map is equivalent to theirs. As this paper was being revised, we found a post in a cartography forum with a similar idea, combining Jacobi's projection of the $y > 0$ side of the ellipsoid, with a projection due to Goyou of half the sphere on a common rectangle in the plane³. Such a map will also makes explicit the (unique) complex structure in $\mathbb{E}^2(a, b, c)$, via the global isothermic coordinates z, \bar{z} obtained by stereographic projection of the sphere over the complex plane.

³Karney, in <http://lists.maptools.org/pipermail/proj/2015-January/006959.html>.

4.1. **A simple lemma.** The following is immediate:

Lemma 4.1. *Let $(\mu_1, \mu_2) \in T = [a_1, b_1] \times [a_2, b_2]$ and $(\lambda_1, \lambda_2) \in \tilde{T} = [\tilde{a}_1, \tilde{b}_1] \times [\tilde{a}_2, \tilde{b}_2]$ local coordinates on surfaces S and \tilde{S} , respectively. Assume that the respective metrics can be written as*

$$ds^2(\mu_1, \mu_2) = f(\mu_1, \mu_2) [g_1^2(\mu_1)d\mu_1^2 + g_2^2(\mu_2)d\mu_2^2], \quad (25)$$

$$d\tilde{s}^2(\lambda_1, \lambda_2) = \tilde{f}(\lambda_1, \lambda_2) [\tilde{g}_1^2(\lambda_1)d\lambda_1^2 + \tilde{g}_2^2(\lambda_2)d\lambda_2^2] \quad (26)$$

and that

$$\int_{a_1}^{b_1} g_1(\mu_1)d\mu_1 = \int_{\tilde{a}_1}^{\tilde{b}_1} \tilde{g}_1(\lambda_1)d\lambda_1 (= r_1), \quad \int_{a_2}^{b_2} g_2(\mu_2)d\mu_2 = \int_{\tilde{a}_2}^{\tilde{b}_2} \tilde{g}_2(\lambda_2)d\lambda_2 (= r_2). \quad (27)$$

Then the correspondence

$$(\mu_1, \mu_2) \mapsto (\lambda_1(\mu_1), \lambda_2(\mu_2)),$$

defined implicitly through

$$\int_{a_1}^{\mu_1} g_1(t)dt = \int_{\tilde{a}_1}^{\lambda_1} \tilde{g}_1(t)dt (= \xi_1), \quad \int_{a_2}^{\mu_2} g_2(t)dt = \int_{\tilde{a}_2}^{\lambda_2} \tilde{g}_2(t)dt (= \xi_2). \quad (28)$$

defines a conformal map between the surfaces

$$d\tilde{s}^2(\mu_1, \mu_2) = h^2(\mu_1, \mu_2) ds^2(\mu_1, \mu_2) \quad (29)$$

with conformal factor h given by

$$h^2 = \frac{\tilde{f}(\lambda_1(\mu_1), \lambda_2(\mu_2))}{f(\mu_1, \mu_2)}. \quad (30)$$

In other words, we use the coordinate patch $(\xi_1, \xi_2) \in R = [0, r_1] \times [0, r_2]$ as common isothermal parameters for the two surfaces,

$$ds^2 = f [d\xi_1^2 + d\xi_2^2], \quad d\tilde{s}^2 = \tilde{f} [d\xi_1^2 + d\xi_2^2] \quad (31)$$

We apply this Lemma using $S = \mathbb{S}^2$ with the sphero-conical coordinates (μ_1, μ_2) and $\tilde{S} = \mathbb{E}^2$ with Jacobi confocal coordinates (λ_1, λ_2) with the corresponding metrics given by (24) and (11). It is VERY important that given $a < b < c$ we chose $I_1 < I_2 < I_3$ such that condition (27) holds. On both coordinate systems and in each octant the coordinate curves meet the great circles perpendicularly, except at the point corresponding to the umbilic points at the ellipsoid.

Theorem 4.2. *The conformal factor between the metric on the ellipsoid to the metric on the sphere is*

$$h^2 = \frac{\lambda_2(\mu_2) - \lambda_1(\mu_1)}{\mu_2 - \mu_1}. \quad (32)$$

The functions $\lambda_2(\mu_2), \lambda_1(\mu_1)$ defining the conformal map are derived from the the metric expressions (11) and (24).

Identifying the corresponding points of the two surfaces on the double coverings by the lattice in the complex plane $w = u + iv$, a global map from \mathbb{E}^2 to \mathbb{S}^2 results. w, \bar{w} are common isothermal coordinates. The umbilical points in the ellipsoid (and the special points in the sphere) are ramification points of order 1/2.

4.2. Technical details. Computing each function $\lambda_i(\mu_i), i = 1, 2$ requires one elliptic integral and one elliptic integrals inversion. Computing the parameters I_1, I_2, I_3 of the sphero-conical coordinates involves a nonlinear system involving two complete elliptic integrals of the first kind. Recall that the standard metric on \mathbb{S}^2 written in the sphero-conical coordinates is given by (24),

$$ds^2 = \frac{\mu_2 - \mu_1}{4} (G_1(\mu_1) d\mu_1^2 + G_2(\mu_2) d\mu_2^2)$$

where

$$G_1(\mu_1) = \frac{1}{(\mu_1 - I_1)(\mu_1 - I_2)(\mu_1 - I_3)}, \quad G_2(\mu_2) = \frac{-1}{(\mu_2 - I_1)(\mu_2 - I_2)(\mu_2 - I_3)}. \quad (33)$$

Define the functions

$$S(\mu_1) = \int_{I_1}^{\mu_1} \sqrt{\frac{1}{(t - I_1)(t - I_2)(t - I_3)}} dt = \frac{2}{\sqrt{I_3 - I_1}} F(\phi, k_1) \quad (34)$$

with

$$\phi = \arcsin \sqrt{\frac{\mu_1 - I_1}{I_2 - I_1}}, \quad k_1 = \sqrt{\frac{I_2 - I_1}{I_3 - I_1}}; \quad (35)$$

$$T(\mu_2) = \int_{\mu_2}^{I_3} \sqrt{\frac{-1}{(t - I_1)(t - I_2)(t - I_3)}} dt = \frac{2}{\sqrt{I_3 - I_1}} F(\phi, k_2), \quad (36)$$

with

$$\phi = \arcsin \sqrt{\frac{I_3 - \mu_2}{I_3 - I_2}}, \quad k_2 = \sqrt{\frac{I_3 - I_2}{I_3 - I_1}} \quad (37)$$

Here F is the elliptic integral of the first kind [5]

$$F(\phi, k) = \int_0^\phi \frac{d\theta}{\sqrt{1 - k^2 \sin^2 \theta}}. \quad (38)$$

Let P and Q as (13) and (15) respectively. The relations (28) become

$$\boxed{P(\lambda_1) = S(\mu_1), \quad Q(\lambda_2) = T(\mu_2)}. \quad (39)$$

We must impose the condition (27) in Lemma 4.1 that assures that one octant of the sphere is mapped exactly over an octant of the ellipsoid. This amounts to

$$\boxed{P(b) = S(I_2), \quad Q(b) = T(I_2)} \quad (40)$$

Given a, b and c , finding I_1, I_2 and I_3 satisfying (40). Note that both triples (a, b, c) and (I_1, I_2, I_3) can be considered as *projective* quantities. Let

$$K(k) = F\left(\frac{\pi}{2}, k\right) \quad (41)$$

be the complete integral of the first type. From (34) and (36) it follows that

$$K(k_1) = \frac{\sqrt{I_3 - I_1}}{2} P(b), \quad K(k_2) = \frac{\sqrt{I_3 - I_1}}{2} Q(b) \quad (42)$$

Observing that k_1 and k_2 are complementary, we get

$$\frac{K(k_1)}{K(k_2)} = \frac{P(b)}{Q(b)}, \quad k_1^2 + k_2^2 = 1. \quad (43)$$

After solving this system for k_1 , k_2 , the parameters I_1 , I_2 and I_3 are obtained from

$$I_3 - I_1 = \left(\frac{2K(k_1)}{P(b)} \right)^2, \quad I_2 - I_1 = (I_3 - I_1) k_1^2. \quad (44)$$

5. Conformality at the umbilical points. The conformal factor is given by (32), with the coordinates implicitly related by (39). Umbilics correspond to $\lambda_1 = \lambda_2 = b$, and at the sphere we have $\mu_1 = \mu_2 = I_2$ in view of (40). Therefore we get a 0/0 indeterminacy. Let $\alpha, \beta > 0$, with $\alpha + \beta = 1$, and take

$$\mu_1 = I_2 - \alpha\epsilon + O(\epsilon^2), \quad \mu_2 = I_2 + \beta\epsilon + O(\epsilon^2), \quad \epsilon > 0.$$

Let's examine the limit

$$\lim_{\epsilon \rightarrow 0^+} (Q^{-1}T(I_2 + \beta\epsilon) - P^{-1}S(I_2 - \alpha\epsilon)) / \epsilon \quad (45)$$

Using l'Hôpital, we should investigate the two limits in the combination

$$\alpha \left[\lim_{\mu_1 \rightarrow I_2} \frac{d}{d\mu_1} P^{-1}S(\mu_1) \right] + \beta \left[\lim_{\mu_2 \rightarrow I_2} \frac{d}{d\mu_2} Q^{-1}T(\mu_2) \right] \quad (46)$$

We will now show that both are equal to $[(b-a)(c-b)]/[b(I_2 - I_1)(I_3 - I_2)]$. We do it for the first:

$$L = \lim_{\mu_1 \rightarrow I_2} d/d\mu_1 [P^{-1}S(\mu_1)] \quad (47)$$

$$\frac{d}{d\mu_1} P^{-1}S(\mu_1) = \frac{dP^{-1}}{du} \Big|_{u=S(\mu_1)} \cdot \frac{dS}{d\mu_1} = \frac{1}{\frac{dP}{d\lambda_1}} \cdot \frac{dS}{d\mu_1}$$

where $dP/d\lambda_1$ is computed at $\lambda_1 = P^{-1}S(\mu_1)$. Therefore

$$\frac{d}{d\mu_1} P^{-1}S(\mu_1) = \left[\frac{1/((I_2 - \mu_1)(I_2 - \mu_1)(I_3 - \mu_1))}{P^{-1}S(\mu_1)/((P^{-1}S(\mu_1) - a)(b - P^{-1}S(\mu_1))(c - P^{-1}S(\mu_1)))} \right]^{1/2}$$

Let's now try to compute this limit as $\mu_1 \rightarrow I_2$. Recall that $P^{-1}S(I_2) = b$. Pulling out (if we may) the factors that have a direct limit we get

$$L = \left[\frac{(b-a)(c-b)}{b(I_2 - I_1)(I_3 - I_2)} \right]^{1/2} \lim_{\mu_1 \rightarrow I_2} \left(1/\sqrt{I_2 - \mu_1} \right) / \left(1/\sqrt{b - P^{-1}S(\mu_1)} \right) \quad (48)$$

The limit in the right is, by a stroke of luck, \sqrt{L} . The second limit is computed analogously and gives, seemingly by another stroke of luck, the same result, but this is indeed what we expect to happen by Riemann surfaces theory.

In passing, we have also shown that for $\mu_1 < I_2 < \mu_2$, both close to I_2 , we have

$$\lambda_1 = b - \gamma(I_2 - \mu_1) + O((I_2 - \mu_1)^2), \quad \lambda_2 = b + \gamma(\mu_2 - I_2) + O((\mu_2 - I_2)^2) \quad (49)$$

with

$$\gamma = h_{\text{umbilic}}^2 = \frac{(b-a)(c-b)}{[b(I_2 - I_1)(I_3 - I_2)]} \quad (50)$$

where a, b, c and I_1, I_2, I_3 are related by (44).

We defined a global map from \mathbb{E}^2 to \mathbb{S}^2 by identifying the corresponding points on the two surfaces (ellipsoid and the sphere) on their double coverings by the same lattice in the complex w -plane ($w = u + iv$). Summarizing:

Proposition 5. *Global isothermal coordinates (z, \bar{z}) on \mathbb{E}^2 (except for the point corresponding to $z = \infty$) are obtained by stereographic projection from the γ -sphere to the complex z -plane, namely:*

$$w = u + iv \rightarrow (p \in \mathbb{E}^2) \leftrightarrow (\gamma \in \mathbb{S}^2) \rightarrow z \in \mathbb{C}.$$

Moreover, $z = z(w)$ is a (complex) elliptic function with quarter periods K_1, iK_2 .

6. The vortex pair on the triaxial ellipsoid \mathbb{E}^2 . The case of a vortex pair is given when $N = 2$ and $\Gamma_1 = -\Gamma_2 = \Gamma$ in Hally's equations (1). The symplectic form and Hamiltonian function are respectively

$$\Omega = \Gamma [h^2(z_1, \bar{z}_1) dz_1 \wedge d\bar{z}_1 - h^2(z_2, \bar{z}_2) dz_2 \wedge d\bar{z}_2], \quad (51)$$

$$H = -\Gamma^2 \ln(h(z_1, \bar{z}_1)h(z_2, \bar{z}_2)|z_1 - z_2|^2). \quad (52)$$

Hamilton's equations are

$$\dot{\bar{z}}_1 = i\Gamma h^{-2}(z_1, \bar{z}_1) \left[\frac{1}{z_1 - z_2} + \frac{\partial}{\partial z_1} \ln(h(z_1, \bar{z}_1)) \right], \quad (53)$$

$$\dot{\bar{z}}_2 = i\Gamma h^{-2}(z_2, \bar{z}_2) \left[\frac{1}{z_1 - z_2} - \frac{\partial}{\partial z_2} \ln(h(z_2, \bar{z}_2)) \right].$$

Let us now discuss how to do the actual computations. Let (z, \bar{z}) denote the stereographic coordinates through the south pole S on $\mathbb{S}^2 \setminus \{S\}$.

$$\mathbb{S}^2 \setminus \{S\} \rightarrow \mathbb{C}, \quad (54)$$

$$(\xi, \eta, \zeta) \mapsto z = \frac{\xi + i\eta}{1 + \zeta}. \quad (55)$$

The standard (round) \mathbb{S}^2 metric is conformal to the Euclidean

$$ds^2 = \frac{4}{(1 + z\bar{z})^2} |dz|^2. \quad (56)$$

The inverse transformation is

$$\xi = \frac{z + \bar{z}}{1 + z\bar{z}}, \quad \eta = \frac{-i(z - \bar{z})}{1 + z\bar{z}}, \quad \zeta = \frac{1 - z\bar{z}}{1 + z\bar{z}}. \quad (57)$$

Recall that the sphero-conical coordinates (μ_1, μ_2) on \mathbb{S}^2 , are obtained from (22) and (57) via

$$\frac{\xi^2}{I_1 - \mu} + \frac{\eta^2}{I_2 - \mu} + \frac{\zeta^2}{I_3 - \mu} = 0.$$

In other words μ_1 and μ_2 are the roots of

$$\mu^2 - \alpha\mu + \beta = 0, \quad (58)$$

where

$$\alpha(z, \bar{z}) = (I_2 + I_3)\xi^2(z, \bar{z}) + (I_1 + I_3)\eta^2(z, \bar{z}) + (I_1 + I_2)\zeta^2(z, \bar{z}),$$

$$\beta(z, \bar{z}) = I_2 I_3 \xi^2(z, \bar{z}) - I_1 I_3 \eta^2(z, \bar{z}) + I_1 I_2 \zeta^2(z, \bar{z}).$$

The ellipsoid metric in stereographic coordinates is given by

$$d\tilde{s}^2 = h^2 |dz|^2, \quad h^2(z, \bar{z}) = \frac{4(\lambda_2 - \lambda_1)}{(\mu_2 - \mu_1)(1 + z\bar{z})^2}. \quad (59)$$

To simplify notation we define

$$L(z, \bar{z}) \equiv \lambda_2(z, \bar{z}) - \lambda_1(z, \bar{z}), \quad M(z, \bar{z}) \equiv \mu_2(z, \bar{z}) - \mu_1(z, \bar{z}) \quad \text{and} \quad r(z, \bar{z}) \equiv 1 + z\bar{z}. \quad (60)$$

We also write $\lambda_i(z, \bar{z}) = \lambda_i(\mu_i(z, \bar{z}))$, $i = 1, 2$. Therefore, we get

Proposition 6. *The conformal factor of the ellipsoid over the z -complex plane is given by*

$$h^2(z, \bar{z}) = \frac{4L}{Mr^2}, \quad (61)$$

$$\frac{\partial}{\partial z} \ln(h(z, \bar{z})) = \frac{1}{2} \frac{\partial}{\partial z} \ln \left(\frac{4L}{Mr^2} \right) = \frac{MrL_z - LrM_z - 2ML\bar{z}}{2LMr}. \quad (62)$$

These determine equations (53). L_z and M_z , are given by

$$\begin{aligned} \frac{\partial \lambda_i}{\partial z} &= \sqrt{\frac{(\lambda_i - a)(\lambda_i - b)(\lambda_i - c)}{\lambda_i(\mu_i - I_1)(\mu_i - I_2)(\mu_i - I_3)}} \frac{\partial \mu_i}{\partial z}, \\ \frac{\partial \mu_i}{\partial z} &= \frac{\alpha_z \mu_i - \beta_z}{2\mu_i - \alpha}, \quad i = 1, 2; \end{aligned}$$

that are obtained through implicit differentiation of (39).

The numerical integration of the dipole problem on \mathbb{E}^2 (53) is done as follows:

- 1) Use (58) to obtain the sphero-conical coordinates $(\mu_1(z_i, \bar{z}_i), \mu_2(z_i, \bar{z}_i))$, $i = 1, 2$.
- 2) Compute the confocal coordinates $(\lambda_1(z_1, \bar{z}_1), \lambda_2(z_1, \bar{z}_1))$ and $(\lambda_1(z_2, \bar{z}_2), \lambda_2(z_2, \bar{z}_2))$ using (28) (inverting P and Q defined in (13) and (15), respectively);
- 3) Using (61) and (62) compute the conformal factors (59) $h^2(z_1, \bar{z}_1)$, $h^2(z_2, \bar{z}_2)$ and its partial derivatives

$$\frac{\partial}{\partial z_1} \ln(h(z_1, \bar{z}_1)) \quad \text{and} \quad \frac{\partial}{\partial z_2} \ln(h(z_2, \bar{z}_2)),$$

- 4) The Hamiltonian ODEs are numerically integrated using a Runge-Kutta 4(5) with adaptative time-step.

7. Numerical experiments. We check Kimura's conjecture by integrating Hally's equations [14] in isothermal coordinates (u, v) given by (17).

$$\dot{\bar{z}}_n = \sum_{k \neq n}^N -i \frac{4\Gamma_k}{(\lambda_2(v_n) - \lambda_1(u_n))(z_n - z_k)} + \Gamma_n \frac{\lambda_2'(v_n) - i\lambda_1'(u_n)}{(\lambda_2(v_n) - \lambda_1(u_n))^2}. \quad (63)$$

In fact,

$$\begin{aligned} \frac{\partial}{\partial z} \ln(h(z, \bar{z})) &= \frac{1}{2} \frac{\partial}{\partial z} \ln(h^2(z, \bar{z})) = \frac{1}{2h^2} \frac{\partial}{\partial z} (h^2(z, \bar{z})) \\ &= \frac{2}{\lambda_2(v) - \lambda_1(u)} \cdot \frac{1}{2} \left(\frac{-\lambda_1'(u) - i\lambda_2'(v)}{4} \right) \\ &= -\frac{1}{4} \cdot \frac{\lambda_1'(u) + i\lambda_2'(v)}{\lambda_2(v) - \lambda_1(u)}. \end{aligned}$$

On the other hand, the geodesic equations in local coordinates (u, v) are given by

$$\begin{aligned} \ddot{u} + \Gamma_{11}^1 \dot{u}^2 + 2\Gamma_{12}^1 \dot{u}\dot{v} + \Gamma_{22}^1 \dot{v}^2 &= 0 \\ \ddot{v} + \Gamma_{11}^2 \dot{u}^2 + 2\Gamma_{12}^2 \dot{u}\dot{v} + \Gamma_{22}^2 \dot{v}^2 &= 0 \end{aligned} \quad (64)$$

The first fundamental form coefficients are

$$E = G = h^2 = \frac{\lambda_2(v) - \lambda_1(u)}{4} \quad F \equiv 0$$

and we obtain the Christoffel symbols

$$\begin{aligned} \Gamma_{11}^1 = \Gamma_{12}^2 = -\Gamma_{22}^1 &= -\frac{2\lambda_1'(u)}{\lambda_2(v) - \lambda_1(u)} \equiv c_1, \\ \Gamma_{11}^2 = -\Gamma_{12}^1 = -\Gamma_{22}^2 &= -\frac{2\lambda_2'(v)}{\lambda_2(v) - \lambda_1(u)} \equiv c_2. \end{aligned} \quad (65)$$

Hence, the geodesic equations are

$$\dot{u} = p, \quad \dot{v} = q, \quad \dot{p} = c_1(q^2 - p^2) + 2c_2pq, \quad \dot{q} = c_2(q^2 - p^2) - 2c_1pq. \quad (66)$$

The numerical integration was performed as follows. Let $v(0)$ and $q(0)$ be initial conditions for some geodesic. If $\gamma(t)$ is its projection over the ellipsoid, integrating numerically determine $p_1 = \gamma(\epsilon/2)$ and $p_2 = \gamma(-\epsilon/2)$. q_1 and q_2 are the initial conditions for the vortex dipole. The geodesics initial conditions are $q(0)$ and $\tilde{v}(0)$ where $\tilde{v}(0)$ is a $\pi/2$ positive rotation of $v(0)$ suitably normalized. In the figures the dashed lines represent the geodesics and solid lines represent the vortices. In the top figures u is the horizontal axis and v is the vertical axis.

Exploratory Poincaré Sections for $H = H(u_1, v_1, u_2, v_2)$ were computed at $v_1 = 0$ using Henon's method [16]. We depicted the stroboscopic positions of one of the vortices.

8. Final comments. In this paper we make a first study about point vortices moving on the surface of a triaxial ellipsoid. We focused on the case of a pair of opposite vortices. Our methodology was validated by testing Kimura's conjecture on close by pairs. The numerical experiments we presented on global behavior are exploratory, and we plan to make a more thorough study in a sequel paper.

1. Domains (simply or multiply connected) in the ellipsoid are mapped in topologically equivalent domains in the plane. Theorem 2 of [19] as geometrized in [1] allow to study confined vortex motion in the planar image.
2. Equilibria and their stability. It is geometrically evident that vortex pairs placed at the ends of the principal axis should remain in equilibrium. Which of the three configurations are stable?
3. One of the referees suggested superposing Poincaré sections of the ellipsoid geodesics system with the sections of the vortex pair. Can the vortex pair system be regarded as a KAM perturbation of the integrable geodesic system on the triaxial ellipsoid when the vortices are sufficiently close? For a surface S , a numerical construction for the symplectomorphism $S \times S - \text{diagonal} \equiv T^*S - \text{zero section}$ is needed (see [1]) but this is not a trivial task.
4. What would be the behavior of a vortex pair placed initially around a point from a geodesic passing through an umbilical point? It is known that the geodesic path will pass successively through the opposite umbilical point, approaching the middle ellipse as $t \rightarrow \pm\infty$. For the geodesic problem the middle ellipse is a periodic orbit with coinciding stable and unstable manifolds. Can

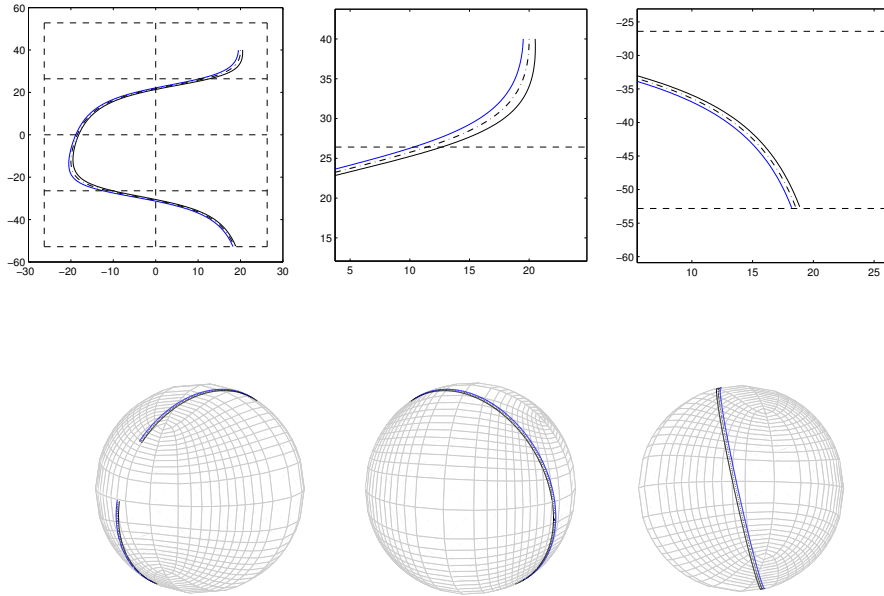


FIGURE 3. Nearly spherical example $a = 1$, $b = 1.01$, $c = 1.02$

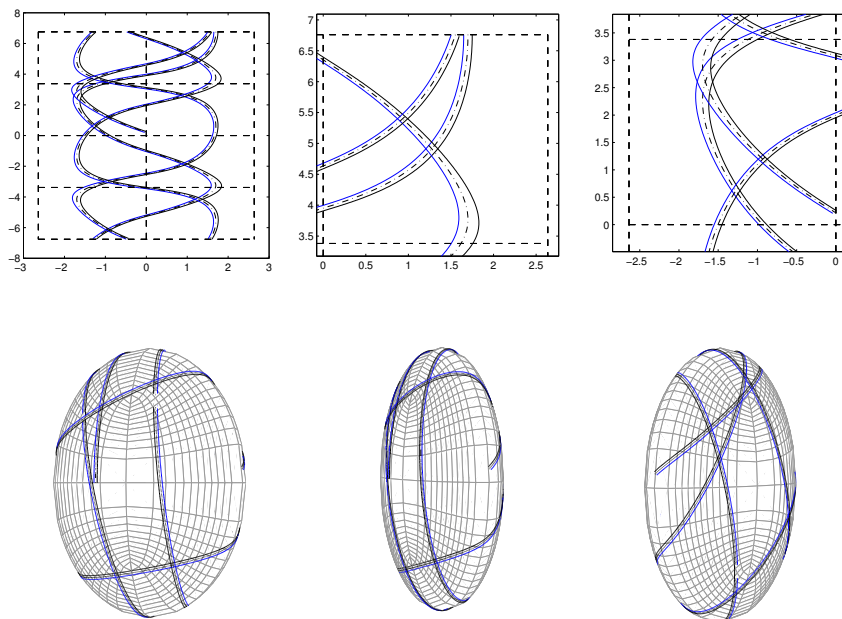


FIGURE 4. Ellipsoid $a = 1$, $b = 6$, $c = 9$.

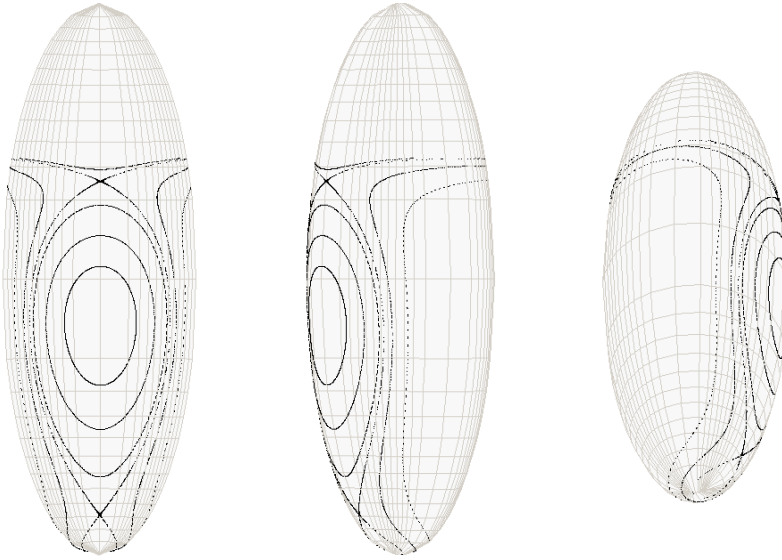


FIGURE 5. Poincaré map. Prolate, nearly symmetrical $a = 1$, $b = 1.1$, $c = 9$, $H = -40$

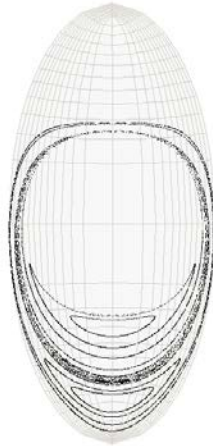


FIGURE 6. Poincaré map. Prolate $a = 1$, $b = 2$, $c = 9$, $H = -36$.

transversality be shown for the vortex pair system regarded as a perturbation of the geodesic system? How about vortex pairs placed at opposite umbilical points? We conjecture that they will traverse a periodic orbit passing through the other pair.

5. We plan to pursue a more thorough investigation of Poincaré sections in the future. One of the referees suggests to make parameters move away from circular symmetry (two equal axis). Chaotic regions should become more and more visible (e.g. take $a=1$, $c=9$, $b=1, 1.1, 1.2, 1.3, \dots$).

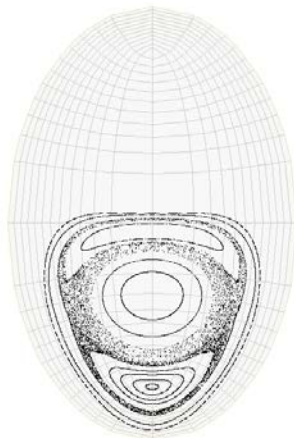


FIGURE 7. Poincaré map. Prolate $a = 1$, $b = 4$, $c = 9$, $H = -60$.

6. The one point vortex problem on a compact surface S of genus zero or 1 (with uniform countervorticity) has the Robin function R as Hamiltonian [1],

$$R(s_o) = \lim_{s \rightarrow s_o} G(s, s_o) - \frac{1}{2\pi} \ln d(s, s_o) \quad (67)$$

where G is the Green function and d is the distance function of the metric. The symplectic 2-form is the area (normalized by vorticity). A remarkable result is (see [35])

$$\Delta R = \frac{1}{2\pi} K \quad (68)$$

where K is the Gaussian curvature function of the surface and Δ the Laplace-Beltrami operator of the metric. It should be possible to solve this Poisson equation using the confocal coordinates.

7. Three point vortices on the sphere are integrable due to the $SO(3)$ symmetry and were studied in [22] and [33]. How is the motion of three vortices affected on a nearly spherical oblate or prolate ellipsoid with two equal axis?
8. We used a Runge-Kutta method in the simulations. A symplectic integrator would be more adequate for very long times. Indeed, one could attempt to apply a symplectic integrator directly on the vortex system in the triaxial ellipsoid. A new numerical method for point vortices in the sphere was proposed in [36]. Can this method be extended to spheroids? Other numerical methods for point vortices on surfaces are in order using discrete differential geometry, implementing numerical conformal maps and Green functions of a discretized Laplacian [12].

Acknowledgements. We thank the three referees for their criticisms and suggestions. This paper contains some of the results from A. Regis' doctoral thesis [31], who wants to thank Prof. Maria Luiza Soares Leite for introducing him to differential geometry. This work was supported by Capes-CNPq Ciência sem Fronteiras grants PV011-2012 and PV089-2013.

Appendix A. Kimura's conjecture. In [1] two proofs were outlined. One of them is based in the following way to rewrite of the vortex pair Hamiltonian:

$$H = -\frac{\ln d(s_1, s_2)}{2\pi} + B(s_1, s_2) \quad (69)$$

where

$$B(s_1, s_2) = \left[\frac{R(s_1) + R(s_2)}{2} - \left(G(s_1, s_2) - \frac{\ln d(s_1, s_2)}{2\pi} \right) \right] \quad (70)$$

Here R is the Robin function and its companion B was called the Batman function. If initially $d(s_1(0), s_2(0)) = O(\epsilon)$ then $B = O(\epsilon^2)$. Suppose the vorticities $\pm\Gamma$ are weak, of order $O(\epsilon)$. Then to first order the contribution of B can be neglected, and we get the truncated system

$$\dot{s}_1 = \epsilon \text{SGrad}_{s_1} \ln d(s_1, s_2), \quad \dot{s}_2 = \epsilon \text{SGrad}_{s_2} \ln d(s_1, s_2)$$

with initially $1/d(s_1(0), s_2(0)) = O(\epsilon^{-1})$. Here SGrad is the symplectic gradient, which is the gradient rotated by $\pi/2$ in the tangent plane. Now the proof ends by writing the EDOs in terms of Gauss coordinates around a central geodesic.

The other proof would have a potential for further developments. It relies on pulling back the symplectic form Ω of $S \times S$ (the phase space of the vortex pair system) to T^*S , the phase space of the geodesic system. Ω is the difference of the area forms (take the vorticity=1). A map $p_s \in T^*S \rightarrow (s_-, s_+) \in S \times S$ is constructed using the exponential map of the metric: using the inverse Legendre transform, write $p_s = \langle v_s, \cdot \rangle$, take the rotation $u_s = J(v_s)$, and define $s_\pm = \exp(\pm \epsilon u_s)$. This map depends on a parameter ϵ that gives the order of proximity of the pair. It is easy to show that the leading term of the expansion of the pullback is precisely the canonical symplectic form of T^*S , while the Hamiltonian has as leading term the norm of the cometric, $|p_s|$, up to a scaling. This proves Kimura's conjecture, at least formally. The task is to compute the next order terms in ϵ of the symplectic form and of the Hamiltonian.

Appendix B. Evaluation of elliptic integrals, following [6]. In the numerical implementations, we computed the elliptical integrals (13), (15), (34) and (36) using

$$R_F(x, y, z) = \frac{1}{2} \int_0^\infty \frac{dt}{\sqrt{(t+x)(t+y)(t+z)}} \quad (71)$$

$$R_J(x, y, z, p) = \frac{3}{2} \int_0^\infty \frac{dt}{(t+p)\sqrt{(t+x)(t+y)(t+z)}}, \quad (72)$$

When p is equal to any of the coordinates x, y and z R_J degenerates into

$$R_D(x, y, z) := R_J(x, y, z, z). \quad (73)$$

The Legendre elliptic integrals [11] can be expressed in terms of R_F , R_J and R_D :

$$\begin{aligned} F(\phi, k) &= \sin(\phi) R_F(\cos^2(\phi), 1 - k^2 \sin^2(\phi), 1), \\ E(\phi, k) &= \sin(\phi) R_F(\cos^2(\phi), 1 - k^2 \sin^2(\phi), 1) - \\ &\quad \frac{1}{3} k^2 \sin^3(\phi) R_D(\cos^2(\phi), 1 - k^2 \sin^2(\phi), 1), \\ \Pi(\phi, k, n) &= \sin(\phi) R_F(\cos^2(\phi), 1 - k^2 \sin^2(\phi), 1) - \\ &\quad \frac{n}{3} k^2 \sin^3(\phi) R_J(\cos^2(\phi), 1 - k^2 \sin^2(\phi), 1, 1 + n \sin^2(\phi)). \end{aligned}$$

Algorithms for its fast evaluation can be found in [6].

REFERENCES

- [1] Boatto, S., Koiller, J., *Vortices on Closed Surfaces*, Geometry, Mechanics and Dynamics: The Legacy of Jerry Marsden, Dong Eui Chang, Darryl D. Holm, George Patrick, Tudor Ratiu, ch. 10, New York, NY: Springer (2015) [MR3380056]
- [2] Bogomolov, V. A., *The dynamics of vorticity on a sphere. (Russian)*, Izv. Akad. Nauk SSSR Ser. Meh. Zidk. Gaza 6, 5765 (1977) [MR0475220]
- [3] Bolsinov, A. V., Fomenko A. T., *Integrable Hamiltonian systems. Geometry, topology, classification*, CRC Press, (2004) [MR2036760]
- [4] Bolsinov, A. V., Matveev, V. S., Fomenko, A. T., *Two-dimensional Riemannian metrics with integrable geodesic flows. Local and global geometry*, Sb. Math. 189:10 1441-1466 (1998)
- [5] Byrd, P. F., Friedman, M. D. *Handbook of elliptic integrals for engineers and physicists*, Berlin: Springer-Verlag (1954).
- [6] Carlson, B. C., *Computing Elliptic Integrals by Duplication*, Numerische Mathematik 33:1, 1-16 (1979) [MR0545738]
- [7] Castilho, C., Machado, H., *The N-vortex problem on a symmetric ellipsoid: a perturbation approach*, J. Math. Phys. 49: 2, 022703 (2008) [MR2392856].
- [8] Dritschel D.G., Boatto S. 2015, *The motion of point vortices on closed surfaces*, Proc. R. Soc. A 471: 20140890 [MR3325200]
- [9] Craig, T., *Orthomophic Projection of an Ellipsoid upon a sphere*, Amer. J. Math. 3:2, 114-127 (1880).
- [10] Crowdy D.G., Kropf E.H., Green C.C., Nasser M.M.S. *The Schottky-Klein prime function: a theoretical and computational tool for applications*, IMA J. Applied Math., 81, 589-628 (2016)
- [11] Gradshteyn, I. S., Ryzhik, J. M., Jeffrey, Alan, *Table of integrals, series, and products*. 4.ed. New York: Academic Press (1965).
- [12] Goes, F., Beibei L., Budninskiy, M., Tong, Y., Desbrun, M., *Discrete 2-Tensor Fields on Triangulations*, Eurographics Symposium on Geometry Processing 33:5, editors Thomas Funkhouser and Shi-Min Hu (2014).
- [13] Gromeka, I., *Sobranie socinenii (Russian) (Collected works)*, Izdat. Akad. Nauk SSSR, Moscow (1952) [MR0056525]
- [14] Hally, D., *Stability of streets of vortices on surfaces of revolution with a reflection symmetry*, J. Math. Phys. 21:1, 211-217 (1980).
- [15] Helmholtz, H., *Über Integrale der hydrodynamischen Gleichungen, welche den Wirbelbewegungen entsprechen. (German)*, J. Reine Angew. Math. 55 2555 (1858) [MR1579057]
- [16] Henon, M., *On the numerical computation of Poincaré maps*, Physica D, 5:2-3, 412-414 (1982) [MR0680575].
- [17] Jacobi, C. G. J., *Note von der geodätischen Linie auf einem Ellipsoid und den verschiedenen Anwendungen einer merkwürdigen analytischen Substitution [The geodesic on an ellipsoid and various applications of a remarkable analytical substitution]*, Jour. Crelle 19, 309313 (1839).
- [18] Jacobi, C. G. J., *Vorlesungen über Dynamik [Lectures on Dynamics]*, edited by Clebsch, Reimer, Berlin (1866); second edition edited by Weierstrass, 1884; English translation by K. Balagangadharan (Hindustan Book Agency, 2009) [MR2569315].
- [19] Lin, C.C., *On the Motion of Vortices in Two Dimensions: I. Existence of the Kirchhoff-Routh Function; II. Some Further Investigations on the Kirchhoff-Routh Function*, Proc. Natl.Acad. Sci. USA.27(12):570-577 (1941).
- [20] Karney, C.F., <https://geographiclib.sourceforge.io/html/jacobi.html>.
- [21] Kim, S.-C. *Latitudinal point vortex rings on the spheroid*, Proceedings Royal Society A, doi:10.1098/rspa.2009.0597 (2010).
- [22] Kidambi, R., Newton, P. K., *Motion of three point vortices on a sphere*, Physica D: Nonlinear Phenomena, 116: 1, 143-175 (1998) [MR1621912]
- [23] Kimura, Y., *Vortex motion on surfaces with constant curvature*, Proc. R. Soc. Lond. A 455, 245-259 (1999).
- [24] Kirchhoff, G. R., *Vorlesungen über Mathematische Physik*, Mechanic, Teubner, Leipzig (1876).
- [25] Koiller, J., Boatto, S., *Vortex pairs on surfaces*, AIP Conference Proceedings 1130, 77 (2009); doi: 10.1063/1.3146241 (Geometry and Physics: XVII International Fall Workshop, edited by F. Etayo, M. Fioravanti, and R. Santamaria).

- [26] Koiller, J., Ehlers, K., *Rubber rolling over a sphere*, Reg. Chaotic Dyn. 12:2, 127-152 (2007).[MR2350302]
- [27] Montaldi, J., Nava-Gaxiola, C., *Point vortices on the hyperbolic plane* J. Math. Phys. 55, 102702 (2014).[MR3390464]
- [28] Moser, J., *Integrable Hamiltonian systems and spectral theory.*, Lezioni Fermiane. [Fermi Lectures] Scuola Normale Superiore, Pisa, (1983) [MR0854865]
- [29] Nyrtsov, M. V., Flies, M. E. , Borisov, M. M. and Stooke, P. J., *Jacobi conformal projection of the triaxial ellipsoid: new projection for mapping of small celestial bodies*, in Cartography from Pole to Pole (Springer, 2014), pp. 235-246.
- [30] Ragazzo, C., *The motion of a vortex on a closed surface: an algorithm and its application to the Bolza surface*, Proc.Royal Soc. London A: Mathematical, Physical and Engineering Sciences, 473: 2206 (2017) [doi: 10.1098/rspa.2017.0447]
- [31] Regis, A., *Dinâmica de vórtices pontuais sobre o elipsóide triaxial (Portuguese)*, Ph.D. thesis, Departamento de Matemática, Universidade Federal de Pernambuco, Brazil (2011).
- [32] Miguel, A S. *Numerical description of the motion of a point vortex pair on ovaloids*, J. Phys. A: Math. Theor. 46 115502 (2013).
- [33] Sakajo, T., *The motion of three point vortices on a sphere*, Japan Journal of Industrial and Applied Mathematics, 16: 3, 321-347 (1999).
- [34] Schering, E., *Über die conforme abbildung des ellipsoids auf der ebene*, Gesammelte Mathematische Werke, ch. III, Mayer and Muller, Berlin (1902) (available in <http://name.umdl.umich.edu/AAT1702.0001.001>).
- [35] Steiner, J., *A geometrical mass and its extremal properties for metrics on S^2* , Duke Math. J. 129(1), 6386 (2005).[MR2153456]
- [36] Vankerschaver, J. Leok, M., *A Novel Formulation of Point Vortex Dynamics on the Sphere: Geometrical and Numerical Aspects*, J. Nonlinear Science 24:1, 137 (2014).[MR3162499]
- [37] Zermelo, E., *Hydrodynamische Untersuchungen über die Wirbelbewegungen in einer Kugelfläche*, Z. Math. Phys. 47 201237 (1902).

E-mail address: adrianoregis@ufrpe.br

E-mail address: castilho@dmate.ufpe.br

E-mail address: jairkoiller@gmail.com

Vortex Pairs on the Triaxial Ellipsoid: Axis Equilibria Stability

Jair Koiller^{1*}, César Castillo^{2**}, and Adriano Regis Rodrigues^{3***}

¹*Departamento de Matemática, Universidade Federal de Juiz de Fora
Juiz de Fora, MG, 36036-900 Brazil*

²*Departamento de Matemática, Universidade Federal de Pernambuco
Recife, PE, 50740-540 Brazil*

³*Universidade Federal Rural de Pernambuco
Recife, PE CEP, 52171-900 Brazil*

Received October 15, 2018; revised January 02, 2019; accepted January 04, 2019

Abstract—We consider a pair of opposite vortices moving on the surface of the triaxial ellipsoid $\mathbb{E}(a, b, c) : x^2/a + y^2/b + z^2/c = 1$, $a < b < c$. The equations of motion are transported to $S^2 \times S^2$ via a conformal map that combines confocal quadric coordinates for the ellipsoid and sphero-conical coordinates in the sphere. The antipodal pairs form an invariant submanifold for the dynamics. We characterize the linear stability of the equilibrium pairs at the three axis endpoints.

MSC2010 numbers: 76B99, 34C28, 37D99

DOI: 10.1134/S1560354719010039

Keywords: point vortices, Riemann surfaces

INTRODUCTION

In 1999 Yoshifumi Kimura conjectured that a pair of opposite vortices moving on a two-dimensional surface Σ , endowed with a Riemannian metric g , *when placed close together*, would stay close, bordering the geodesic path in between them [18].

In [26] we presented a numerical study to verify Kimura’s conjecture, taking the triaxial ellipsoid $\Sigma = \mathbb{E}(a, b, c) : x^2/a + y^2/b + z^2/c = 1$, $a < b < c$ as the test surface. One observes indeed that near the diagonal $D = \{(\sigma, \sigma) \in \Sigma \times \Sigma\}$ the vortex system looks like a KAM perturbation of Jacobi’s geodesic problem on the ellipsoid.

In this paper we focus on the other extreme situation, vortices *placed near an antipodal configuration*. For surfaces with antipodal symmetry, such as the triaxial ellipsoid, if a pair of opposite vortices is placed *exactly* in an antipodal configuration, the motion will remain antipodal for all time. In other words, antipodal pairs form an invariant submanifold for the dynamics. In fact, we show that the center manifold dynamics is governed by the conformal factor of a conformal map $\Sigma \rightarrow S^2$ that preserves “antipodicity”. This map is unique up to Moebius transformations of the sphere.

We present here a study on the stability of the pair configurations at the three axis endpoints. We reach the (not very surprising) conclusion that the minimum and maximum axis endpoints are of center-center type, while the middle axis is a saddle-center.

This paper is organized as follows. We review in Section 1 some results from [5]. Our new results are presented in Section 2. The formulas for the stability analysis are given in Theorem 3 in terms of the ellipsoid parameters a, b, c and associated sphero-conical parameters I_1, I_2, I_3 (that are functions

* E-mail: jairkoiller@gmail.com

** E-mail: castilho@dmat.ufpe.br

*** E-mail: regis.ufrpe@gmail.com

of a, b, c). These relations are found in Section 3. Sections 4 and 5 contain calculations leading to the proof of Theorem 3. Some final comments are presented in Section 6. For completeness, confocal quadrics and spherico-conical coordinate systems are reviewed in Appendix A. In Appendix B we present a simple proof of the main theorem (Theorem 2) from Section 1. Appendix C outlines some of the steps required for the numerical work.

The conformal map. The key is a “master equation” $K(\sqrt{1-\kappa^2})/K(\kappa) = n(a, b, c)$ in Section 3, see (3.25). The K 's are complementary complete elliptic integrals of the first kind¹. The ratio on the left-hand side comes from the spherico-conical coordinates [6, 7] for the round metric in the sphere

$$ds^2 = \frac{\mu_2 - \mu_1}{4} \left[\frac{d\mu_1^2}{(\mu_1 - I_1)(\mu_1 - I_2)(\mu_1 - I_3)} - \frac{d\mu_2^2}{(\mu_2 - I_1)(\mu_2 - I_2)(\mu_2 - I_3)} \right].$$

Likewise, the right-hand side $n(a, b, c)$ is the ratio of two complete elliptic integrals of the third kind, coming from the ellipsoid metric in confocal coordinates

$$ds^2 = \frac{\lambda_2 - \lambda_1}{4} \left[\frac{\lambda_1 d\lambda_1^2}{(\lambda_1 - a)(\lambda_1 - b)(\lambda_1 - c)} + \frac{-\lambda_2 d\lambda_2^2}{(\lambda_2 - a)(\lambda_2 - b)(\lambda_2 - c)} \right].$$

Together with (3.27), the master equation solution for κ yields the parameters I_1, I_2, I_3 of the spherico-conical coordinates in terms of the ellipsoid parameters a, b, c . This construction ensures that the four artificial singular points of the spherico-conical coordinates correspond to the four umbilical points of the ellipsoid. The coordinate lines in both systems have the same topology, going around the singular points in the same fashion. Riemann surface theory shows that the construction is well defined at these branch points upon composition to produce a conformal map from the ellipsoid to the sphere. The conformal factor is simply $h^2 = (\lambda_2 - \lambda_1)/(\mu_2 - \mu_1)$. This is the key for our analysis.

1. THE VORTEX PAIR SYSTEM

We normalize vorticities to ± 1 . The phase space for a vortex pair on a surface Σ with metric g is $\Sigma \times \Sigma - D$, the symplectic form is

$$\Omega_{\text{pair}} = \Omega(\sigma_1) - \Omega(\sigma_2), \quad (1.1)$$

where $\Omega(\sigma)$ is the area form of (Σ, g) . The Hamiltonian is

$$H = -G_g(\sigma_1, \sigma_2) + \frac{1}{2} (R_g(\sigma_1) + R_g(\sigma_2)), \quad (1.2)$$

where G_g is the *Green function* of the Laplace–Beltrami operator Δ_g on Σ , and R_g , called *Robin's function*, is its regularization at the diagonal D ,

$$R_g(\sigma_o) = \lim_{\sigma \rightarrow \sigma_o} G(\sigma, \sigma_o) - \log d(\sigma, \sigma_o)/2\pi, \quad (1.3)$$

where d is the distance function of the metric g . The Green function satisfies

$$\begin{aligned} \Delta_g G(\sigma, \sigma_o) &= -\frac{1}{\text{Area}(\Sigma)} + \delta(\sigma, \sigma_o), \\ G(\sigma, \sigma_o) - \log d(\sigma, \sigma_o)/2\pi &\text{ bounded}, \\ \int_{\Sigma} G(\sigma, \sigma_o)\Omega(\sigma) &= 0, \quad G(\sigma, \sigma_o) = G(\sigma_o, \sigma). \end{aligned} \quad (1.4)$$

More information about vortices on closed surfaces can be found in [5], building up on D. Hally's seminal work [13].

¹In elliptic function theory, the ratio of the K 's on the left-hand side is the so-called *nome function*.

1.1. Kimura’s Assertion

Let us assume Σ is a compact surface without boundary. The manifold $\Sigma \times \Sigma - D$ can be re-compactified: one glues $T^1\Sigma$ (where the geodesic motion takes place) to the diagonal, keeping track of the direction that the two points σ_1, σ_2 approach each other. This is a well-known construction (Axelrod – Singer [1] and Fulton – MacPherson [11]).

The Hamiltonian (1.2) can be rewritten as

$$H = -\frac{1}{2\pi} \log d(\sigma_1, \sigma_2) + B(\sigma_1, \sigma_2). \tag{1.5}$$

The function B , which was called *Batman’s function*, is given by

$$B(\sigma_1, \sigma_2) = \frac{1}{2}(R(\sigma_1) + R(\sigma_2)) - (G(\sigma_1, \sigma_2) - \log d(\sigma_1, \sigma_2)/2\pi). \tag{1.6}$$

It seems to be still an unexplored object in geometric function theory. Since $B = O(d(\sigma_1, \sigma_2)^2)$, near the diagonal the dominant term is $-\log d(\sigma_1, \sigma_2)$. Introduce a small parameter ϵ . Energy conservation guarantees that, if $d(s_1, s_2)$ is initially $O(\epsilon)$, it remains so for all time. A map from a neighborhood of the zero section of $T^*(\Sigma)$ to a neighborhood of the diagonal of $\Sigma \times \Sigma$ is defined by

$$\underbrace{p_\sigma \in T^*\Sigma \rightarrow v_\sigma \in T\Sigma}_{\text{Legendre transform}} \rightarrow \underbrace{w_\sigma = J(v_\sigma/2)}_{\text{rotate by } \pi/2} \rightarrow \underbrace{(\sigma_1, \sigma_2) = (\exp(-\epsilon w_\sigma), \exp(\epsilon w_\sigma))}_{\text{exponential map}}. \tag{1.7}$$

The vector v_σ is perpendicular to the geodesic between σ_1 and σ_2 at the midpoint σ . Thus, it is the direction of the proposed geodesic line.

The vortex problem in $\Sigma \times \Sigma - D$ has a symplectic form $\Omega_{\Sigma \times \Sigma}$ which is the area form in the first factor *minus* the area form in the second. $T^*\Sigma$ has a canonical 2-form $\Omega_{T^*\Sigma}$ that is intrinsically defined (no metric needed). What is the relation between them? Using local coordinates, one easily shows that the pull back of (1.7) is

$$\Omega_{\Sigma \times \Sigma} = \epsilon^2 \Omega_{T^*\Sigma} + O(\epsilon^4). \tag{1.8}$$

Moreover, to leading order, the vortex problem is governed by the Hamiltonian

$$-\ln d(s_1, s_2) = -\ln |2\epsilon v_q|. \tag{1.9}$$

Therefore, under a suitable time scale reparametrization, the geodesic system is the blow-up of the vortex pair problem at the diagonal. Obtaining the perturbation terms is in order.

1.2. Genus-0 Surfaces: Transporting the Vortex Problem to the Sphere

From now on we will confine ourselves with genus zero surfaces. One learns in basic courses that two-dimensional ideal hydrodynamics behaves nicely under conformal mappings. So we are led to consider a conformal map $\sigma \in \Sigma \rightarrow s \in S^2$. Two such maps differ by a Moebius transformation of the target sphere. A metric on the sphere S^2 is obtained by pushing forward the metric in Σ , expressed as $g = h^2(s) g_o$, where g_o denotes the constant curvature metric in S^2 . h^2 is the conformal factor. The equations for point vortices moving in Σ will be transported to corresponding virtual points moving in S^2 .

Conversely, for any arbitrarily chosen positive (C^∞ or analytic) function $h^2(s)$ one can consider the abstract metric $g = h^2(s) g_o$ in the Riemann sphere²⁾.

The symplectic form in $S^2 \times S^2$ is given by

$$\Omega_{\text{pair}} = h^2(s_1)\Omega_o(s_1) - h^2(s_2)\Omega_o(s_2), \tag{1.10}$$

²⁾Although such a general metric cannot always be realized as an embedded surface $\Sigma \subset \mathbb{R}^3$, it can be done in \mathbb{R}^5 (Gromov, [14]). For us this does not matter: in a “Platonic” perspective, ideal two-dimensional hydrodynamics takes place on an abstract Riemann surface with a Riemannian metric g .

where Ω_o is the area form of the round sphere. The Hamiltonian is given by (for the derivation of the change of Hamiltonian under a conformal map, see [5])

$$\begin{aligned} H &= -\frac{1}{2} \ln (h(s_1)h(s_2)|s_1 - s_2|^2) \\ &= -\left(\ln |s_1 - s_2| + \frac{1}{2} \ln h(s_1) + \frac{1}{2} \ln h(s_2) \right), \end{aligned} \quad (1.11)$$

where $|\cdot|$ is the Euclidian distance. The equations of motion become imbedded in $\mathbb{R}^3 \times \mathbb{R}^3$:

$$\dot{s}_1 = \frac{1}{h^2(s_1)} \left(\frac{s_1 \times s_2}{|s_1 - s_2|^2} - \frac{1}{2} s_1 \times \text{grad } h(s_1)/h(s_1) \right) \quad (1.12)$$

$$\dot{s}_2 = \frac{1}{h^2(s_2)} \left(\frac{s_1 \times s_2}{|s_1 - s_2|^2} + \frac{1}{2} s_2 \times \text{grad } h(s_2)/h(s_2) \right). \quad (1.13)$$

Studying the dynamics in the “virtual” sphere S^2 is very convenient. For instance, we can consider antipodal pairs in S^2 even if Σ does not have the antipodal (or other) symmetries.

The following facts are not hard to prove (we will present them in detail in a separate publication focused on surfaces of revolution).

- i) The system (1.12), (1.13) is well defined, meaning that it behaves invariantly under a Moebius transformation in the target sphere. This is a six-dimensional group.
- ii) Any equilibrium pair $(\sigma_1, \sigma_2) \in \Sigma \times \Sigma$, if one applies a conveniently chosen Moebius transformation, can be represented by an antipodal pair $(s, -s) \in S^2 \times S^2$.
- iii) An antipodal pair $(s, -s) \in S^2 \times S^2$ is in equilibrium if and only if the gradient of h vanishes at both s and $-s$.
- iv) When a surface Σ has the antipodal symmetry $\sigma \rightarrow -\sigma$, then there is a conformal map preserving the antipodicity, so that $\text{grad } h(-s) = -\text{grad } h(s)$, $s \in S^2$.

For such surfaces iv), a key observation is the following:

Theorem 1. *For surfaces with antipodal symmetry, the antipodal pairs (either seen in Σ or equivalently in S^2) form an invariant two-dimensional submanifold for the dynamics $S_{\text{ant}} = \{(s, -s) \in S^2 \times S^2\}$.*

Proof. The proof is very simple. In S_{ant} the first terms of the two Eqs. (1.12), (1.13) disappear. The second equation becomes

$$\begin{aligned} -\dot{s}_1 = \dot{s}_2 &= \frac{1}{2h^2(s_2)} (s_2 \times \text{grad } h(s_2)/h(s_2)) \\ &= \frac{1}{2h^2(s_1)} ((-s_1) \times [-\text{grad } h(s_1)/h(s_1)]) \end{aligned} \quad (1.14)$$

and reproduces the first equation. \square

A remark should be added to the first item i). By suitably repositioning the target sphere, any Moebius transformation can be seen as a $SO(3)$ rotation [30]. Hence we may assume, by performing a $SO(3)$ rotation, that an antipodal pair in Σ which is an equilibrium pair for the system, becomes the north-south pair $s_{1,2}^* = (0, 0, \pm 1)$.

Take for coordinate systems the tangent planes x, y at the points s_1^*, s_2^* . Then (1.12), (1.13) can be rewritten as a system of four ODEs for x_1, y_1, x_2, y_2 .

Linearization. All we need are the quadratic expansions of the conformal factors at $s_{1,2}^*$. There are five parameters: the two pairs of coefficients of the quadratic forms and the angle θ between

the principal axis of the second quadratic form and the principal axis of the first. We impose no restrictions on the parameters of the quadratic forms, since we have no special concerns about Gromov’s embedding problem. Clearly, it is possible to construct a Morse function h on the sphere with arbitrary quadratic expansions at two chosen critical points (we will provide the linearization in this general case in another publication).

Here we focus on surfaces with antipodal symmetry. The quadratic expansions at the poles are the same, of the form

$$H(x, y) = h^* + (1/2) p x^2 + (1/2) q y^2, \quad h^* > 0. \tag{1.15}$$

Theorem 2. *Denote $p' = p/h^*$, $q' = q/h^*$. The characteristic polynomial for the linearized system factors as*

$$[\lambda^2 + 4p'q'] [\lambda^2 + 4(1 - p')(1 - q')]. \tag{1.16}$$

The first factor corresponds to the invariant submanifold S_{ant} . If p', q' have the same sign, we have a center on the restriction of the system to the invariant submanifold S_{ant} . If p', q' have opposite signs, we have a saddle. For the transverse subspace: if $(1 - p')(1 - q') > 0$, we have linear stability; if $(1 - p')(1 - q') < 0$, we have a saddle.

Remark 1. Note the undefined situations when p or q are $= 0$ or 1 .

Remark 2. For surfaces of revolution in \mathbb{R}^3 with equatorial symmetry (spheroids, with $p = q$), we can also show that $-\infty < p \leq 1/2$. The case $p = q = 0$ corresponds to the sphere.

The proof of Theorem 2 is given in Appendix B.

2. MAIN RESULT: COEFFICIENTS OF THE QUADRATIC EXPANSIONS

We now present the formulae for the coefficients of the quadratic expansions (1.15) at the axis endpoints $(A, -A)$, $(B, -B)$, $(C, -C)$. Together with Theorem 2 they determine the stability of the vortex pair problem of the triaxial ellipsoid at the axis equilibria.

The quantities I_1, I_2, I_3 (we will normalize $I_1 = 0$) below are functions of a, b, c that are computed via the master Eqs. (3.25), (3.27) presented in the next section (Section 3), which gives an explicit conformal map from the ellipsoid to the sphere. The quadratic expansion is derived in Section 5 using the partial derivatives obtained in Section 4. Mixed terms in the quadratic expansion are ruled out simply by symmetry considerations.

Theorem 3. *In the notation of (1.15) we have*

$$\begin{cases} h_A^* = \sqrt{\frac{c - b}{I_3 - I_2}} \\ p_A/h_A^* = \frac{1}{I_3 - I_2} \left[\frac{b - a}{b} - (I_2 - I_1) \right] \\ q_A/h_A^* = \frac{1}{I_3 - I_2} \left[(I_3 - I_1) - \frac{c - a}{c} \right]. \end{cases} \tag{2.1}$$

$$\begin{cases} h_B^* = \sqrt{\frac{c - a}{I_3 - I_1}} \\ p_B/h_B^* = \frac{1}{I_3 - I_1} \left[(I_3 - I_2) - \frac{c - b}{c} \right] \\ q_B/h_B^* = \frac{1}{I_3 - I_1} \left[(I_2 - I_1) - \frac{b - a}{a} \right]. \end{cases} \tag{2.2}$$

$$\begin{cases} h_C^* = \sqrt{\frac{b-a}{I_2-I_1}} \\ p_C/h_C^* = \frac{1}{I_2-I_1} \left[(I_3-I_1) - \frac{c-a}{a} \right] \\ q_C/h_C^* = \frac{1}{I_2-I_1} \left[\frac{c-b}{b} - (I_3-I_2) \right]. \end{cases} \quad (2.3)$$

The results of the numerical implementation are presented in Tables 1 and 2. Without loss of generality we fix $c = 1, I_1 = 0$ so we omit them in the tables. We took a, b varying in units of 0.1. We believe to have covered a sufficient range of $a < b < 1$ values.

Observing Table 1 we reach the following conclusions.

- i) The minor axis antipodal equilibrium $(A, -A)$ is *center-center*, since

$$0 < p'_A < q'_A < 1.$$

The conformal factor has a minimum.

- ii) The middle axis antipodal equilibrium $(B, -B)$ is a *saddle* for the invariant submanifold, and a *center* in the transverse direction. We observe that

$$0 < p'_B < 1, q'_B < 0.$$

The conformal factor has a saddle at $B, -B$.

- iii) The major axis antipodal equilibrium $(C, -C)$ is a *center-center*, since

$$p'_C < q'_C < 0.$$

The conformal factor has a maximum.

Table 2 compares the values of

$$h_A^2 = \frac{c-b}{I_3-I_2}, h_B^2 = \frac{c-a}{I_3-I_1}, h_C^2 = \frac{b-a}{I_2-I_1}, h_U^2 = \frac{(b-a)(c-b)}{b(I_2-I_1)(I_3-I_2)}.$$

The last expression is derived in Section 4. As expected, all along the table $h_A < h_B < h_C$. It is interesting to compare h_B and h_U , the value at the umbilical points. We observe that the difference $h_U^2 - h_B^2$ can have both signs, meaning:

- i) When $h_U^2 < h_B^2$, then in the invariant submanifold there are two periodic orbits passing through the opposite umbilical points at which the antipodal pair orbits around the points A and $-A$.
- ii) When $h_U^2 > h_B^2$, the antipodal pair orbits around the points C and $-C$.
- iii) In the special situations where $h_U^2 = h_B^2$, the separatrix emanating from $(B, -B)$ passes through the umbilical points.

3. CONFORMAL MAP OF THE TRIAXIAL ELLIPSOID TO THE SPHERE

In his 1839 note about the integrability of the geodesic problem on the triaxial ellipsoid [16], and especially in [17], Jacobi used confocal quadrics coordinates to write the Riemannian metric in $\mathbb{E}^2(a, b, c)$, induced by the Euclidian metric in the ambient space \mathfrak{R}^3 :

$$ds_{\mathbb{E}}^2 = \frac{\lambda_2 - \lambda_1}{4} [J(\lambda_1)d\lambda_1^2 - J(\lambda_2)d\lambda_2^2] \quad (3.1)$$

with

$$J(\lambda) = \frac{\lambda}{(\lambda-a)(\lambda-b)(\lambda-c)}. \quad (3.2)$$

Table 1. Stability of axis pairs ($c = 1, I_1 = 0$).

a	b	I_2	I_3	p'_A	q'_A	p'_B	q'_B	p'_C	q'_C
0.1	0.2	0.0163	5.7206	0.0848	0.8451	0.8573	-0.1720	-200.6683	-104.2811
0.1	0.3	0.0581	4.0752	0.1515	0.7904	0.8140	-0.4765	-84.7257	-28.9658
0.2	0.3	0.0425	3.0214	0.0976	0.7457	0.7543	-0.1514	-23.0377	-15.1976
0.1	0.4	0.1257	3.0724	0.2119	0.7372	0.7638	-0.9355	-47.1513	-11.5078
0.2	0.4	0.1078	2.3748	0.1730	0.6947	0.7020	-0.3757	-15.0739	-7.1144
0.3	0.4	0.0634	1.8846	0.1024	0.6505	0.6480	-0.1432	-7.0727	-5.0615
0.1	0.5	0.2163	2.3980	0.2676	0.6866	0.7013	-1.5778	-30.5278	-5.4646
0.2	0.5	0.1922	1.9150	0.2367	0.6472	0.6385	-0.6829	-10.8461	-3.7596
0.3	0.5	0.1435	1.5535	0.1819	0.6053	0.5857	-0.3368	-5.4338	-2.8562
0.4	0.5	0.0780	1.2567	0.1035	0.5571	0.5401	-0.1369	-3.1203	-2.2917
0.1	0.6	0.3262	1.9165	0.3189	0.6392	0.6211	-2.4387	-21.7141	-2.8314
0.2	0.6	0.2923	1.5724	0.2924	0.6034	0.5597	-1.0860	-8.3037	-2.0982
0.3	0.6	0.2369	1.2996	0.2476	0.5642	0.5099	-0.5872	-4.3632	-1.6717
0.4	0.6	0.1673	1.0662	0.1847	0.5186	0.4679	-0.3120	-2.5925	-1.3876
0.5	0.6	0.0875	0.8578	0.1027	0.4645	0.4316	-0.1311	-1.6243	-1.1836
0.1	0.7	0.4522	1.5586	0.3660	0.5953	0.5174	-3.5594	-16.4552	-1.4989
0.2	0.7	0.4053	1.3090	0.3419	0.5632	0.4612	-1.6003	-6.6396	-1.1722
0.3	0.7	0.3411	1.0998	0.3036	0.5269	0.4171	-0.9023	-3.6169	-0.9680
0.4	0.7	0.2658	0.9135	0.2513	0.4840	0.3807	-0.5301	-2.2067	-0.8248
0.5	0.7	0.1826	0.7423	0.1842	0.4329	0.3498	-0.2928	-1.4111	-0.7180
0.6	0.7	0.0936	0.5816	0.1010	0.3721	0.3232	-0.1256	-0.9091	-0.6347
0.1	0.8	0.5914	1.2847	0.4091	0.5549	0.3840	-4.9883	-13.0462	-0.7497
0.2	0.8	0.5288	1.1015	0.3863	0.5264	0.3384	-2.2434	-5.4817	-0.6105
0.3	0.8	0.4539	0.9392	0.3525	0.4930	0.3037	-1.2912	-3.0711	-0.5183
0.4	0.8	0.3715	0.7890	0.3077	0.4528	0.2757	-0.7965	-1.9136	-0.4509
0.5	0.8	0.2838	0.6470	0.2512	0.4046	0.2523	-0.4888	-1.2441	-0.3989
0.6	0.8	0.1920	0.5107	0.1819	0.3473	0.2323	-0.2767	-0.8124	-0.3574
0.7	0.8	0.0972	0.3787	0.0987	0.2795	0.2151	-0.1205	-0.5132	-0.3234
0.1	0.9	0.7413	1.0705	0.4483	0.5179	0.2141	-6.7807	-10.6968	-0.2942
0.2	0.9	0.6608	0.9353	0.4262	0.4929	0.1865	-3.0357	-4.6378	-0.2471
0.3	0.9	0.5740	0.8082	0.3956	0.4621	0.1661	-1.7643	-2.6569	-0.2145
0.4	0.9	0.4833	0.6861	0.3563	0.4245	0.1498	-1.1175	-1.6841	-0.1897
0.5	0.9	0.3898	0.5673	0.3077	0.3792	0.1365	-0.7230	-1.1100	-0.1701
0.6	0.9	0.2944	0.4509	0.2488	0.3252	0.1253	-0.4560	-0.7330	-0.1541
0.7	0.9	0.1974	0.3363	0.1787	0.2614	0.1157	-0.2626	-0.4674	-0.1408
0.8	0.9	0.0992	0.2231	0.0961	0.1867	0.1073	-0.1156	-0.2708	-0.1294

Table 2. Values of the conformal factor at the distinguished points ($c = 1$, $I_1 = 0$).

a	b	I_2	I_3	h_A^2	h^2B	h_C^2	h_U^2	$h_U^2 - h_B^2$
0.1	0.2	0.0163	5.7206	0.140245078	0.157326155	6.134969325	4.301996266	4.144670111
0.1	0.3	0.0581	4.0752	0.174255506	0.220848057	3.442340792	1.999484333	1.778636276
0.2	0.3	0.0425	3.0214	0.234986069	0.264777918	2.352941176	1.84302799	1.578250072
0.1	0.4	0.1257	3.0724	0.203617606	0.292930608	2.386634845	1.214902185	0.921971577
0.2	0.4	0.1078	2.3748	0.264666961	0.336870473	1.85528757	1.227583306	0.890712833
0.3	0.4	0.0634	1.8846	0.329453108	0.371431604	1.577287066	1.299105315	0.927673711
0.1	0.5	0.2163	2.398	0.229179081	0.375312761	1.849283403	0.84763414	0.472321379
0.2	0.5	0.1922	1.915	0.290225215	0.417754569	1.560874089	0.906010036	0.488255467
0.3	0.5	0.1435	1.5535	0.354609929	0.45059543	1.282051282	1.087682432	0.537864303
0.4	0.5	0.078	1.2567	0.424196148	0.477440917	1.282051282	1.087682432	0.610241515
0.1	0.6	0.3262	1.9165	0.25152487	0.469606053	1.532801962	0.642563022	0.17295697
0.2	0.6	0.2923	1.5724	0.312475588	0.508776393	1.368457065	0.712682376	0.203905983
0.3	0.6	0.2369	1.2996	0.376399737	0.53862727	1.266357113	0.794427473	0.255800203
0.4	0.6	0.1673	1.0662	0.444988319	0.562746201	1.195457262	0.88660753	0.323861328
0.5	0.6	0.0875	0.8578	0.519278203	0.582886454	1.142857143	0.98910134	0.406214886
0.1	0.7	0.4522	1.5586	0.271149675	0.577441293	1.326846528	0.513962863	-0.06347843
0.2	0.7	0.4053	1.309	0.331968574	0.611153552	1.233654083	0.585049123	-0.026104429
0.3	0.7	0.3411	1.0998	0.395413207	0.63647936	1.172676634	0.662416898	0.025937538
0.4	0.7	0.2658	0.9135	0.463177397	0.65681445	1.128668172	0.746819408	0.090004958
0.5	0.7	0.1826	0.7423	0.536001429	0.67358211	1.095290252	0.838681629	0.16509952
0.6	0.7	0.0936	0.5816	0.614754098	0.687757909	1.068376068	0.938269381	0.250511472
0.1	0.8	0.5914	1.2847	0.288475407	0.700552658	1.18363206	0.426810926	-0.273741732
0.2	0.8	0.5288	1.1015	0.349222979	0.726282342	1.134644478	0.495304906	-0.230977437
0.3	0.8	0.4539	0.9392	0.412116217	0.745315162	1.101564221	0.567465599	-0.177849563
0.4	0.8	0.3715	0.789	0.479041916	0.760456274	1.076716016	0.644740129	-0.115716144
0.5	0.8	0.2838	0.647	0.550660793	0.772797527	1.057082452	0.727617327	-0.0451802
0.6	0.8	0.192	0.5107	0.62754942	0.783238692	1.041666667	0.81712164	0.033882948
0.7	0.8	0.0972	0.3787	0.710479574	0.792183787	1.028806584	0.913682579	0.121498793
0.1	0.9	0.7413	1.0705	0.303766707	0.840728631	1.079185215	0.364245044	-0.476483588
0.2	0.9	0.6608	0.9353	0.364298725	0.855340532	1.059322034	0.428788518	-0.426552014
0.3	0.9	0.574	0.8082	0.426985482	0.866122247	1.045296167	0.495918098	-0.370204149
0.4	0.9	0.4833	0.6861	0.493096647	0.874508089	1.034554107	0.566816846	-0.307691243
0.5	0.9	0.3898	0.5673	0.563380282	0.881367883	1.026167265	0.642358226	-0.239009657
0.6	0.9	0.2944	0.4509	0.638977636	0.88711466	1.019021739	0.723480113	-0.163634547
0.7	0.9	0.1974	0.3363	0.719942405	0.89206066	1.013171226	0.810472143	-0.081588517
0.8	0.9	0.0992	0.2231	0.807102502	0.896458987	1.008064516	0.904012659	0.007553672

Jacobi also mentioned that these coordinates can be used to produce a conformal map of the ellipsoid to the plane, the conformal factor becoming singular at the umbilical points. The umbilical points are branch points from the complex analysis viewpoint.

Can one produce a map from the sphere to the plane having the same singular behavior? Upon composition, the divergences would “cancel each other”. We claim that this can be achieved by writing the standard Euclidian metric in the sphere in sphero-conical coordinates (see [6, 7])

$$ds_{S^2}^2 = \frac{\mu_2 - \mu_1}{4} [I(\mu_1) d\mu_1^2 - I(\mu_2) d\mu_2^2] \tag{3.3}$$

with

$$I(\mu) = \frac{1}{(\mu - I_1)(\mu - I_2)(\mu - I_3)}. \tag{3.4}$$

We now give some details on the conformal map, following our previous work [26].

3.1. Matching the Coordinate Lines

One can combine the two systems of coordinates in order to produce a conformal map between the two surfaces. Both metrics can be put in Liouville form [6] and the topologies of the coordinate lines correspond (for the triaxial ellipsoid the coordinate lines are given explicitly in [2]).

Theorem 4. *The conformal map from the triaxial ellipsoid to the unit sphere is defined by two independent functions that relate separately the coordinate lines, $\mu_i = \mu_i(\lambda_i)$, $i = 1, 2$. Each one is constructed by combining one real incomplete elliptic integral of the third kind on λ_i followed by a real Jacobi sn (inversion on an elliptic integral of the first kind on μ_i). The parameters I_1, I_2, I_3 are chosen so that the ellipsoid umbilical points ($\lambda_1 = \lambda_2 = b$) map to the singular points of the sphero-conical coordinates ($\mu_1 = \mu_2 = I_2$). Thus, the two systems of coordinate lines on the surfaces correspond. The conformal factor between the ellipsoid and the sphere is*

$$h^2 = \frac{\lambda_2 - \lambda_1}{\mu_2 - \mu_1}. \tag{3.5}$$

The master equation (Theorem 5) shows how to obtain I_1, I_2, I_3 as functions of a, b, c .

Technical details. We consider $a \neq 0$. We will consider elsewhere the case $a = 0$ (double faced elliptical region) for which the expression (3.2) simplifies. Let F be the incomplete Legendre elliptic integral of the first kind

$$F(\phi, k) = \int_0^\phi \frac{d\theta}{\sqrt{1 - k^2 \sin^2 \theta}} = \int_0^t \frac{dt}{\sqrt{1 - t^2} \sqrt{1 - k^2 t^2}}, \tag{3.6}$$

where $t = \sin \phi$ and Π is the incomplete elliptical integral of the third kind

$$\Pi(\phi, \ell, n) = \int_0^\phi \frac{d\theta}{(1 + n \sin^2 \theta) \sqrt{1 - \ell^2 \sin^2 \theta}}. \tag{3.7}$$

The relations between λ_i and μ_i , $i = 1, 2$ are given by

$$\boxed{P(\lambda_1) = S(\mu_1), Q(\lambda_2) = T(\mu_2)} \tag{3.8}$$

where P, Q, S, T are defined by

(i)

$$P(\lambda_1) = \int_a^{\lambda_1} \sqrt{\frac{t}{(t-a)(t-b)(t-c)}} dt = \frac{2a}{\sqrt{b(c-a)}} \Pi(\phi_1, \ell_1, n_1) \quad (3.9)$$

with

$$\phi_1 = \arcsin \sqrt{\frac{b(\lambda_1 - a)}{\lambda_1(b-a)}}, \quad (3.10)$$

$$\ell_1 = \sqrt{\frac{1 - (a/b)}{1 - (a/c)}} \quad (0 < \ell_1 < 1) \quad \text{and} \quad -1 < n_1 = -1 + a/b < 0. \quad (3.11)$$

(ii)

$$Q(\lambda_2) = \int_{\lambda_2}^c \sqrt{\frac{-t}{(t-a)(t-b)(t-c)}} dt = \frac{2c}{\sqrt{b(c-a)}} \Pi(\phi_2, \ell_2, n_2) \quad (3.12)$$

with

$$\phi_2 = \arcsin \sqrt{\frac{b(c - \lambda_2)}{\lambda_2(c-b)}} \quad (3.13)$$

$$\ell_2 = \sqrt{\frac{(c/b) - 1}{(c/a) - 1}} \quad (0 < \ell_2 < 1) \quad \text{and} \quad n_2 = c/b - 1 > 0. \quad (3.14)$$

(iii)

$$S(\mu_1) = \int_{I_1}^{\mu_1} \sqrt{\frac{1}{(t-I_1)(t-I_2)(t-I_3)}} dt = \frac{2}{\sqrt{I_3 - I_1}} F(\phi_1, k_1) \quad (3.15)$$

$$\phi_1 = \arcsin \sqrt{\frac{\mu_1 - I_1}{I_2 - I_1}}, \quad k_1 = \sqrt{\frac{I_2 - I_1}{I_3 - I_1}}; \quad (3.16)$$

(iv)

$$T(\mu_2) = \int_{\mu_2}^{I_3} \sqrt{\frac{-1}{(t-I_1)(t-I_2)(t-I_3)}} dt = \frac{2}{\sqrt{I_3 - I_1}} F(\phi_2, k_2), \quad (3.17)$$

$$\phi_2 = \arcsin \sqrt{\frac{I_3 - \mu_2}{I_3 - I_2}}, \quad k_2 = \sqrt{\frac{I_3 - I_2}{I_3 - I_1}} \quad (3.18)$$

It is important to note that both k_1, k_2 and ℓ_1, ℓ_2 are complementary:

$$k_1^2 + k_2^2 = 1, \quad \ell_1^2 + \ell_2^2 = 1. \quad (3.19)$$

3.2. Master Equation: the Relation Between (a, b, c) and (I_1, I_2, I_3)

We denote, as it is traditional, by

$$K(k) = F\left(\frac{\pi}{2}, k\right) = \int_0^{\pi/2} \frac{d\theta}{\sqrt{1 - k^2 \sin^2 \theta}}, \quad 0 \leq k \leq 1 \quad (3.20)$$

the complete elliptic integral of the first type. $K(k)$ is an increasing function of k with $K(0) = \pi/2$, $K(1) = \infty$ diverging logarithmically.

We now enforce the requirement that the umbilical points of the ellipsoid do correspond to the artificial singular points in the sphere. This insures that the correspondence between $\mathbb{E}^2(a, b, c)$ and S^2 is well defined. As we showed in [26], this amounts to the equalities

$$K(k_1) = \frac{\sqrt{I_3 - I_1}}{2} P(b), \quad K(k_2) = \frac{\sqrt{I_3 - I_1}}{2} Q(b), \tag{3.21}$$

where we have the complete integrals of the third kind

$$P(b) = \frac{2a}{\sqrt{b(c-a)}} \Pi(\pi/2, \ell_1, n_1) \tag{3.22}$$

$$Q(b) = \frac{2c}{\sqrt{b(c-a)}} \Pi(\pi/2, \ell_2, n_2), \tag{3.23}$$

where we changed the notation for (3.7) to

$$\Pi(x, \ell, n) = \int_0^x \frac{dt}{(1 + nt^2)\sqrt{(1-t^2)(1-\ell^2 t^2)}}, \quad x = \sin \phi. \tag{3.24}$$

Observing that k_1 and k_2 are complementary, i. e., $k_1^2 + k_2^2 = 1$, we get

Theorem 5 (Master Equation). *The modulus k_1 is the solution of*

$$\frac{K(\sqrt{1-k_1^2})}{K(k_1)} = n(a, b, c), \tag{3.25}$$

where

$$n = \frac{Q(b)}{P(b)} = \frac{c}{a} \frac{\Pi(\pi/2, \ell_2, n_2)}{\Pi(\pi/2, \ell_1, n_1)}. \tag{3.26}$$

After getting k_1 , the parameters I_1 , I_2 and I_3 are obtained from

$$I_3 - I_1 = 4 \left(\frac{K(k_1)}{P(b)} \right)^2 \quad \left[= 4 \left(\frac{K(k_2)}{Q(b)} \right)^2 \right] \tag{3.27}$$

$$I_2 - I_1 = (I_3 - I_1) k_1^2, \quad (I_3 - I_2 = (I_3 - I_1) k_2^2 \text{ is redundant}).$$

No harm is done by setting $I_1 = 0$ for simplicity.

The left-hand side of (3.25) decreases from ∞ to 0 as k_1 runs from 0 to 1. Thus, there is an unique solution to this equation.

Remark 3. Interestingly, the “fake” singular points in the sphere corresponding to the umbilics of the ellipsoid are

$$(\pm k_1, 0, \pm k_2).$$

3.3. About the Equation $K(\sqrt{1-k^2})/K(k) = \sqrt{r}$

The solution $k = \Lambda(r)$ of this equation is called the *elliptic lambda function* ([28, Section 4]), and can be obtained via Jacobi theta functions (see, e. g., [27, Sections 7.8–7.10]).

$$k = \left[\frac{\theta_2(0, q_r)}{\theta_3(0, q_r)} \right]^2 \tag{3.28}$$

where $q_r = \exp(-\pi/\sqrt{r})$ is called the *nome* and the theta functions are

$$\theta_2(0, q) = \sum_{m=-\infty}^{\infty} q^{(m+1/2)^2}, \quad \theta_3(0, q) = \sum_{m=-\infty}^{\infty} q^{m^2}. \tag{3.29}$$

4. PRELIMINARY CALCULATIONS FOR THE MAIN THEOREM

It is immediate that

$$\begin{cases} h^2(A) = \frac{c-b}{I_3-I_2} \\ h^2(B) = \frac{c-a}{I_3-I_1} \\ h^2(C) = \frac{b-a}{I_2-I_1} \end{cases} \quad (4.1)$$

We now show that

$$h^2(U) = \frac{(b-a)(c-b)}{b(I_2-I_1)(I_3-I_2)}. \quad (4.2)$$

and derive the coefficients of the quadratic expansion of h at A , B , C in the next section.

First we compute the partial derivatives $d\lambda_2/d\mu_2$, $d\lambda_1/d\mu_1$ at the special values I_1, I_2, I_3 . By the chain rule we get

$$d\lambda_1/d\mu_1 = \left[\frac{(\lambda_1-a)(b-\lambda_1)(c-\lambda_1)}{\lambda_1(\mu_1-I_1)(I_2-\mu_1)(I_3-\mu_1)} \right]^{1/2}, \quad (4.3)$$

$$d\lambda_2/d\mu_2 = \left[\frac{(\lambda_2-a)(\lambda_2-b)(c-\lambda_2)}{\lambda_2(\mu_2-I_1)(\mu_2-I_2)(I_3-\mu_2)} \right]^{1/2}. \quad (4.4)$$

We presented the following trick in [26]:

$$\begin{aligned} \frac{d\lambda_1}{d\mu_1}(I_1) &= \lim_{\mu_1 \rightarrow I_1} \left[\frac{(\lambda_1-a)(b-a)(c-a)}{a(\mu_1-I_1)(I_2-I_1)(I_3-I_1)} \right]^{1/2} \\ &= \left[\frac{(b-a)(c-a)}{(I_2-I_1)(I_3-I_1)} \right]^{1/2} \lim_{\mu_1 \rightarrow I_1} \left[\frac{\lambda_1-a}{\mu_1-I_1} \right]^{1/2} \\ &= \left[\frac{(b-a)(c-a)}{a(I_2-I_1)(I_3-I_1)} \right]^{1/2} \times \left[\frac{d\lambda_1}{d\mu_1}(I_1) \right]^{1/2}, \end{aligned} \quad (4.5)$$

hence

$$\frac{d\lambda_1}{d\mu_1}(I_1) = \frac{(b-a)(c-a)}{a(I_2-I_1)(I_3-I_1)}. \quad (4.6)$$

In a similar fashion we get

$$\frac{d\lambda_2}{d\mu_2}(I_3) = \frac{(c-a)(c-b)}{c(I_3-I_1)(I_3-I_2)}, \quad (4.7)$$

and moreover,

$$\frac{d\lambda_1}{d\mu_1}(I_2) = \frac{d\lambda_2}{d\mu_2}(I_2) = \frac{(b-a)(c-b)}{b(I_2-I_1)(I_3-I_2)}. \quad (4.8)$$

It follows that

$$\begin{aligned} h^2(U) &= \lim_{\mu_2 \searrow I_2} \frac{\lambda_2-b}{\mu_2-I_2} = d\lambda_2/d\mu_2(I_2) \\ &= \lim_{\mu_1 \nearrow I_2} \frac{b-\lambda_1}{I_2-\mu_1} = d\lambda_1/d\mu_2(I_2) \\ &= \frac{(b-a)(c-b)}{b(I_2-I_1)(I_3-I_2)}. \end{aligned} \quad (4.9)$$

Remark 4. One may wonder if the gradient of h could vanish at U for some special values of a, b, c , but our tables and further theoretical calculations indicate that it does not happen.

5. PROOF OF THE MAIN THEOREM 3

We want to obtain the quadratic expansion of h at the axis endpoints A, B, C . It is more convenient to expand h^2 instead of h ,

$$h^2 = \left[h_* + \frac{p}{2} x^2 + \frac{q}{2} y^2 + \dots \right]^2 = h_*^2 + ph_* x^2 + qh_* y^2 + \dots \tag{5.1}$$

We now show that

$$p_A h_A^* = \frac{c-b}{(I_3 - I_2)^2} \left[\frac{b-a}{b} - (I_2 - I_1) \right] \tag{5.2}$$

$$q_A h_A^* = \frac{c-b}{(I_3 - I_2)^2} \left[(I_3 - I_1) - \frac{c-a}{c} \right].$$

$$p_B h_B^* = \frac{c-a}{(I_3 - I_1)^2} \left[(I_3 - I_2) - \frac{c-b}{c} \right] \tag{5.3}$$

$$q_B h_B^* = \frac{c-a}{(I_3 - I_1)^2} \left[(I_2 - I_1) - \frac{b-a}{a} \right].$$

$$p_C h_C^* = \frac{b-a}{(I_2 - I_1)^2} \left[(I_3 - I_1) - \frac{c-a}{a} \right] \tag{5.4}$$

$$q_C h_C^* = \frac{b-a}{(I_2 - I_1)^2} \left[\frac{c-b}{b} - (I_3 - I_2) \right].$$

Proof. The derivations use the partial derivatives in the previous section (Section 4). We present only the calculation for point C . The formulas for A and B are obtained in a similar fashion.

i) Moving from C towards A in the x_1 direction (see Appendix A) we have

$$\mu_2 \equiv I_2, \quad \mu_1 = I_1 + x_1^2(I_3 - I_1),$$

therefore

$$\begin{aligned} h_C^2(x_1, 0) &= \frac{b - \lambda_1(I_1 + x_1^2(I_3 - I_1))}{I_2 - (I_1 + x_1^2(I_3 - I_1))} \\ &= \frac{1}{I_2 - I_1} \frac{b - (a + x_1^2(I_3 - I_1) d\lambda_1/d\mu_1(I_1) + \dots)}{1 - x_1^2(I_3 - I_1)/(I_2 - I_1)} = \\ &= \frac{b-a}{I_2 - I_1} \left[1 - x_1^2 \frac{I_3 - I_1}{b-a} d\lambda_1/d\mu_1(I_1) + \dots \right] \\ &\quad \times \left[1 + x_1^2(I_3 - I_1)/(I_2 - I_1) + \dots \right] \\ &= \frac{b-a}{I_2 - I_1} \left[1 - x_1^2 \frac{I_3 - I_1}{b-a} \frac{(b-a)(c-a)}{a(I_2 - I_1)(I_3 - I_1)} + \dots \right] \\ &\quad \times \left[1 + x_1^2(I_3 - I_1)/(I_2 - I_1) + \dots \right] \\ &= \frac{b-a}{I_2 - I_1} \left[1 + x_1^2 \frac{1}{I_2 - I_1} \left(I_3 - I_1 - \frac{c-a}{a} \right) + \dots \right] \end{aligned} \tag{5.5}$$

ii) From C moving towards B in the x_2 direction we have

$$\mu_1 \equiv I_1, \quad \mu_2 = I_2 + x_2^2(I_3 - I_2),$$

therefore,

$$\begin{aligned} h^2(0, x_2) &= \frac{\lambda_2(I_2 + x_2^2(I_3 - I_2)) - a}{I_2 + x_2^2(I_3 - I_2) - I_1} \\ &= \frac{1}{I_2 - I_1} \frac{b - a + x_2^2(I_3 - I_2) d\lambda_2/d\mu_2(I_2) + \dots}{1 + x_2^2(I_3 - I_2)/(I_2 - I_1)} \end{aligned}$$

$$\begin{aligned}
&= \frac{b-a}{I_2-I_1} \left(1 + x_2^2 \frac{I_3-I_2}{b-a} d\lambda_2/d\mu_2(I_2) + \dots \right) \\
&\quad \times (1 - x_2^2(I_3-I_2)/(I_2-I_1)) \\
&= \frac{b-a}{I_2-I_1} \left(1 + x_2^2 \frac{I_3-I_2}{b-a} \frac{(b-a)(c-b)}{b(I_2-I_1)(I_3-I_2)} + \dots \right) \\
&\quad \times (1 - x_2^2(I_3-I_2)/(I_2-I_1)) \\
&= \frac{b-a}{I_2-I_1} \left[1 + x_2^2 \frac{1}{I_2-I_1} \left(\frac{c-b}{b} - I_3 + I_2 \right) + \dots \right]. \tag{5.6}
\end{aligned}$$

□

6. FINAL COMMENTS

6.1. Historical Notes

- i) Jacobi and Riemann were the first to study iK'/K . According to [27], Riemann regarded this ratio as a complex function of κ^2 with branch points $0, 1, \infty$, and “as early as 1828, Jacobi was aware that κ^2 was a modular function of iK'/K with respect to the subgroup $\Gamma(2)$ of the full modular group”. The study was pursued further by Dedekind, Hermite, Schwarz, Picard and other contemporaries.
- ii) Triaxial ellipsoids are emblematic. The theory of integrable Hamiltonian systems got started at Königsberg, on Wednesday, December 26, 1838. In a letter to Bessel, dated two days later, Jacobi wrote:

“Ich habe vorgestern die geodätische Linie für ein *Ellipsoid mit drei ungleichen Achsen* auf Quadraturen zurückgeführt. Es sind die einfachsten Formeln von der Welt, Abelsche Integrale, die sich in die bekannten elliptischen verwandeln, wenn man 2 Achsen gleich setzt” ([15], p. 385)³⁾.

6.2. Some Directions for Further Research

- i) As regards Section 1.1, it would be interesting to obtain the next order term in the deformation of the canonical symplectic form in $T^*\Sigma$ and of the perturbation of the Hamiltonian geodesic system, both arising from the pullback of the vortex pair problem near the diagonal to a neighborhood of the zero section of $T^*\Sigma$.
- ii) Floquet analysis of the periodic orbits that fill the invariant submanifold S_{ant} given by Theorem 1. For that purpose several symplectic integrators on products of spheres are available, such as [21–23, 31]. Appendix C outlines some steps of the procedure.
- iii) There is a sizeable amount of literature about center-saddle equilibria [3, 12, 19, 20, 24, 25]. It would be interesting to apply it around $(B, -B)$ as a first step to understand the transversal structure to the global center manifold S_{ant} .
- iv) Hamiltonians in products of spheres also appear in spin systems, so it is interesting to find integrable Hamiltonians in $(S^2)^N$ with weighted symplectic forms (positive or negative). In the case of vortex pairs with opposite vorticities, we believe that, unfortunately, there are no integrable cases, except surfaces of revolution. This is because (in view of Kimura’s assertion) the candidates can only be the surfaces whose metrics yield integrable geodesic systems. Those are classified (see, e. g., [6–8, 29]). It would be the matter of numerically simulating them to exhibit chaotic behavior as we did in [26], or to apply some of the traditional theoretical methods (Melnikov, Ziglin, Morales – Ramis, etc.).

³⁾The day before yesterday, I reduced to quadrature the problem of geodesic lines on an ellipsoid with three unequal axes. They are the simplest formulas in the world, Abelian integrals, which become the well-known elliptic integrals if 2 axes are set equal. (Translation in https://en.wikipedia.org/wiki/Geodesics_on_an_ellipsoid.)

v) In the opposite direction are surfaces with negative curvature. Their geodesics play a key role in the interplay of differential geometry and other branches of pure mathematics. Trace formulas relate the distribution of eigenvalues of the Laplacian to the distribution of lengths of closed geodesics. Those techniques are one of the tools used in studies related to the Riemann hypothesis [4]. Could vortex pairs be used as well?

APPENDIX A. COORDINATES ON THE ELLIPSOID AND ON THE SPHERE

Confocal Quadrics Coordinates (λ_1, λ_2)

The ellipsoid

$$\mathbb{E}^2(a, b, c) : \frac{x^2}{a} + \frac{y^2}{b} + \frac{z^2}{c} = 1, \quad a < b < c \tag{A.1}$$

corresponds to the root $\lambda_o = 0$ of the cubic equation

$$\frac{x^2}{a - \lambda} + \frac{y^2}{b - \lambda} + \frac{z^2}{c - \lambda} = 1.$$

The other two roots

$$\lambda_o = 0, \quad a < \lambda_1 < b < \lambda_2 < c$$

define two confocal hyperboloids (of one and two sheets) forming a triorthogonal family. These coordinates $(\lambda_1, \lambda_2) \in [a, b] \times [b, c]$ parametrize each octant of the ellipsoid by

$$\begin{aligned} x^2 &= \frac{a(a - \lambda_1)(a - \lambda_2)}{(a - b)(a - c)}, \\ y^2 &= \frac{b(b - \lambda_1)(b - \lambda_2)}{(b - a)(b - c)}, \\ z^2 &= \frac{c(c - \lambda_1)(c - \lambda_2)}{(c - a)(c - b)}. \end{aligned} \tag{A.2}$$

Sphero-conical Coordinates (μ_1, μ_2)

Similarly, each octant of the sphere

$$S^2 : x_1^2 + x_2^2 + x_3^2 = 1 \tag{A.3}$$

is parametrized by $(\mu_1, \mu_2) \in [I_1, I_2] \times [I_2, I_3]$ via

$$\begin{aligned} x_1^2 &= \frac{(I_1 - \mu_1)(I_1 - \mu_2)}{(I_1 - I_2)(I_1 - I_3)}, \\ x_2^2 &= \frac{(I_2 - \mu_1)(I_2 - \mu_2)}{(I_2 - I_1)(I_2 - I_3)}, \\ x_3^2 &= \frac{(I_3 - \mu_1)(I_3 - \mu_2)}{(I_3 - I_1)(I_3 - I_2)}. \end{aligned} \tag{A.4}$$

The sphero-conical coordinates are defined by a triorthogonal system of cones and spheres, with parameters $I_1 < I_2 < I_3$:

$$\frac{X_1^2}{I_1 - \mu} + \frac{X_2^2}{I_2 - \mu} + \frac{X_3^2}{I_3 - \mu} = 0, \quad X_1^2 + X_2^2 + X_3^2 = r^2. \tag{A.5}$$

Equations (A.4) for the $x_i = X_i/r$ solve the matrix system

$$\begin{bmatrix} 1 & 1 & 1 \\ 1/(I_1 - \mu_1) & 1/(I_2 - \mu_1) & 1/(I_3 - \mu_1) \\ 1/(I_1 - \mu_2) & 1/(I_2 - \mu_2) & 1/(I_3 - \mu_2) \end{bmatrix} \begin{bmatrix} x_1^2 \\ x_2^2 \\ x_3^2 \end{bmatrix} = \begin{bmatrix} 1 \\ 0 \\ 0 \end{bmatrix}. \tag{A.6}$$

Given $(x_1, x_2, x_3) \in S^2$, the sphero-conical coordinates $I_1 \leq \mu_1 \leq I_2 < \mu_2 \leq I_3$ satisfy the quadratic equation

$$\begin{aligned} \mu^2 - [(x_1^2(I_2 + I_3) + x_2^2(I_1 + I_3) + x_3^2(I_1 + I_2))] \mu \\ + (x_1^2 I_2 I_3 + x_2^2 I_1 I_3 + x_3^2 I_1 I_2) = 0. \end{aligned} \quad (\text{A.7})$$

The coordinates are the same on all concentric spheres, and we can make $r = 1$.

Ten Special Points

The semiaxis endpoints of the ellipsoid correspond to

$$\begin{aligned} (A, -A) : \lambda_1 = b, \lambda_2 = c &\Rightarrow (\pm\sqrt{a}, 0, 0), \\ (B, -B) : \lambda_1 = a, \lambda_2 = c &\Rightarrow (0, \pm\sqrt{b}, 0), \\ (C, -C) : \lambda_1 = a, \lambda_2 = b &\Rightarrow (0, 0, \pm\sqrt{c}). \end{aligned} \quad (\text{A.8})$$

The four umbilical points, with $\lambda_1 = \lambda_2 = b$, are located in the middle ellipse:

$$(U_{++}, U_{+-}, U_{-+}, U_{--}) : \left(\pm\sqrt{\frac{a(b-a)}{c-a}}, 0, \pm\sqrt{\frac{c(c-b)}{c-a}} \right). \quad (\text{A.9})$$

We have the corresponding points on the main equators of the sphere

$$\begin{aligned} \mu_1 = I_2, \mu_2 = I_3 &\Rightarrow (\pm 1, 0, 0), \\ \mu_1 = I_1, \mu_2 = I_3 &\Rightarrow (0, \pm 1, 0), \\ \mu_1 = I_1, \mu_2 = I_2 &\Rightarrow (0, 0, \pm 1). \end{aligned} \quad (\text{A.10})$$

There are four special points located in the equator ($x_2 = 0$) with

$$(V_{++}, V_{+-}, V_{-+}, V_{--}) : (\pm k_1, 0, \pm k_2), \quad k_1 = \sqrt{\frac{I_2 - I_1}{I_3 - I_1}}, \quad k_2 = \sqrt{\frac{I_3 - I_2}{I_3 - I_1}}. \quad (\text{A.11})$$

As $a \rightarrow b$, the triaxial ellipsoid tends to a prolate ellipsoid of revolution around the z -axis. The umbilical points U_{++}, U_{-+} merge with C , U_{+-}, U_{--} with $-C$. In the image sphere we have $k_1 \rightarrow 0$. Likewise, when $b \rightarrow c$, the triaxial ellipsoid tends to an oblate ellipsoid of revolution around the x -axis, with $k_1 \rightarrow 1$. As $a \rightarrow 0$, the triaxial ellipsoid tends to a double faced planar elliptical region.

Formulas for the Sphero-conical Coordinates Along the Main Equators

The expressions for μ_1, μ_2 in terms of (x_1, x_2, x_3) are very simple along the principal great circles, with a slight twist on $x_2 \equiv 0$. From (A.7),

i) Equator $x_3 \equiv 0$. Here $\mu_2 \equiv I_3$. The other solution is given by

$$\mu_1 = x_1^2 I_2 + x_2^2 I_1, \quad x_1^2 + x_2^2 = 1. \quad (\text{A.12})$$

ii) Equator $x_1 \equiv 0$. Here $\mu_1 \equiv I_1$. The other solution is given by

$$\mu_2 = x_3^2 I_2 + x_2^2 I_3, \quad x_2^2 + x_3^2 = 1. \quad (\text{A.13})$$

iii) The equator $x_2 = 0$ (corresponding to the middle ellipse $y = 0$) is especially important. $\mu = I_2$ is likewise one solution, and the other is

$$\mu^* = x_1^2 I_3 + x_3^2 I_1, \quad x_1^2 + x_3^2 = 1. \quad (\text{A.14})$$

But here from $(1, 0, 0)$ to V_{++} we have $\mu_1 \equiv I_2, \mu_2 = \mu^*$, and from V_{++} to $(0, 0, 1)$ we have $\mu_2 = I_2, \mu_1 = \mu^*$. Recall that $\mu_1 = \mu_2 = I_2$ at the V 's.

APPENDIX B. PROOF OF THEOREM 2

For surfaces with antipodal symmetry, since S_{ant} is invariant under the flow, we know that the linearization matrix at an antipodal pair in equilibrium (we may assume at the north and south poles of the sphere) will have an invariant subspace $W_1 \subset \mathbb{R}^4$ generated by $v_1 = (1, 0, -1, 0)$, $v_2 = (0, 1, 0, -1)$. A quick computation shows that the linearization matrix A is given by

$$A = \begin{bmatrix} 0 & \gamma & 0 & -1 \\ \delta & 0 & 1 & 0 \\ 0 & -1 & 0 & \gamma \\ 1 & 0 & \delta & 0 \end{bmatrix} \tag{B.1}$$

where

$$\gamma = -1 + 2q/h, \quad \delta = 1 - 2p/h. \tag{B.2}$$

where the conformal factor expands as (1.15)

$$H(x, y) = h + (1/2)p x^2 + (1/2)q y^2, \quad h > 0.$$

Matrix A has indeed two invariant subspaces of dimension 2:

i) V spanned by $v_1 = (1, 0, -1, 0)$, $v_2 = (0, 1, 0, -1)$. We have

$$Av_1 = (\delta - 1)v_2 = (-2p/h)v_2, \quad Av_2 = (1 + \gamma)v_1 = (2q/h)v_1; \tag{B.3}$$

ii) W spanned by $w_1 = (1, 0, 1, 0)$, $w_2 = (0, 1, 0, 1)$. We have

$$Aw_1 = (\delta + 1)w_2, \quad Aw_2 = (\gamma - 1)w_1. \tag{B.4}$$

The first subspace V is tangent to the center manifold ($s_1 = -s_2$), while W is transverse to it. On the subspace $V = \text{span}\{v_1, v_2\}$, the eigenvalues satisfy

$$\lambda^2 = (\delta - 1)(1 + \gamma) = -4pq/h^2, \tag{B.5}$$

and on the subspace $W = \text{span}\{w_1, w_2\}$, the eigenvalues satisfy

$$\lambda^2 = (\gamma - 1)(\delta + 1) = -4(1 - p/h)(1 - q/h). \tag{B.6}$$

APPENDIX C. OUTLINE FOR NUMERICAL SIMULATIONS

One first solves the master equation to obtain I_1, I_2, I_3 in terms of a, b, c . At each time step of the symplectic integrator for (1.12), (1.13), one applies the following sequence of mappings to compute the conformal factor.

- 1) Solve the quadratic equation (A.7) obtaining μ_1, μ_2 in terms of x_1, x_2, x_3 . This is a bit of a nuisance algebraically because of the \pm outside the square roots, but numerically it is nice and easy: the discriminant is always positive. μ_2 receives the + square root.
- 2) Compute the functions $\lambda_i(\mu_i)$, $i = 1, 2$, each given by one elliptic integral and one inversion. Fast and reliable codes are available for that purpose [9, 10].
- 3) In order to solve the EDOS (1.12), (1.13) in $S^2 \times S^2$, only the conformal factor given by $h = \sqrt{(\lambda_2 - \lambda_1)/(\mu_2 - \mu_1)}$ is needed. The sphere representation provides the octants where the two vortices are located.
- 4) If one desires to plot the curves in the “physical ellipsoid” $\mathbb{E}(a, b, c)$, then one computes (x, y, z) via the parametrization (A.2), keeping track of the octant one is traversing in the representing sphere S^2 (signs of the corresponding coordinates are the same).

ACKNOWLEDGMENTS

(JK) wants to thank the Organizing Committee of the The Seventh International Conference “Geometry, Dynamics, Integrable Systems — GDIS 2018”, 5–9 June, 2018, for their kind invitation, and specially to Prof. Sergey Sokolov for the hospitality in Moscow. His work was supported by a visiting fellowship from the Universidade Federal de Juiz de Fora, Brazil.

REFERENCES

1. Axelrod, S. and Singer, I. M., Chern – Simons Perturbation Theory: 2, *J. Differential Geom.*, 1994, vol. 39, no. 1, pp. 173–213.
2. Bărbat, C.Ş., The Liouville Parametrization of a Triaxial Ellipsoid, arXiv:1409.7783v2 (2014).
3. Bernard, P., Grotta Ragazzo, C., and Salomão, P., Homoclinic Orbits near Saddle-Center Fixed Points of Hamiltonian Systems with Two Degrees of Freedom, in *Geometric Methods in Dynamics: Vol. 1. Papers from the Internat. Conf. on Dynamical Systems (Rio de Janeiro, July 2000)*, W. de Melo, M. Viana, J.-Ch. Yoccoz (Eds.), Astérisque, vol. 286, Paris: Soc. Math. France, 2003, pp. 151–165.
4. Berry, M. V. and Keating, J. P., The Riemann Zeros and Eigenvalue Asymptotics, *SIAM Rev.*, 1999, vol. 41, no. 2, pp. 236–266.
5. Boatto, S. and Koiller, J., Vortices on Closed Surfaces, in *Geometry, Mechanics, and Dynamics: The Legacy of Jerry Marsden*, D. E. Chang, D. D. Holm, G. Patrick, T. Ratiu (Eds.), Fields Inst. Commun., vol. 73, New York: Springer, 2015, pp. 185–237.
6. Bolsinov, A. V. and Fomenko, A. T., *Integrable Hamiltonian Systems: Geometry, Topology, Classification*, Boca Raton, Fla.: Chapman & Hall/CRC, 2004.
7. Bolsinov, A. V., Matveev, V. S., and Fomenko, A. T., Two-Dimensional Riemannian Metrics with an Integrable Geodesic Flow: Local and Global Geometries, *Sb. Math.*, 1998, vol. 189, nos. 9–10, pp. 1441–1466; see also: *Mat. Sb.*, 1998, vol. 189, no. 10, pp. 5–32.
8. Bolsinov, A. V. and Jovanović, B., Integrable Geodesic Flows on Riemannian Manifolds: Construction and Obstructions, in *Contemporary Geometry and Related Topics*, N. Bokan, M. Djorić, Z. Rakić, A. T. Fomenko, J. Wess (Eds.), River Edge, N.J.: World Sci., 2004, pp. 57–103.
9. Carlson, B. C., Computing Elliptic Integrals by Duplication, *Numer. Math.*, 1979, vol. 33, no. 1, pp. 1–16.
10. Fukushima, T., Fast Computation of Complete Elliptic Integrals and Jacobian Elliptic Functions, *Celestial Mech. Dynam. Astronom.*, 2009, vol. 105, no. 4, pp. 305–328.
11. Fulton, W. and MacPherson, R., A Compactification of Configuration Spaces, *Ann. of Math. (2)*, 1994, vol. 139, no. 1, pp. 183–225.
12. Giles, W., Lamb, J. S. W., and Turaev, D., On Homoclinic Orbits to Center Manifolds of Elliptic-Hyperbolic Equilibria in Hamiltonian Systems, *Nonlinearity*, 2016, vol. 29, no. 10, pp. 3148–3173.
13. Hally, D., Stability of Streets of Vortices on Surfaces of Revolution with a Reflection Symmetry, *J. Math. Phys.*, 1980, vol. 21, no. 1, pp. 211–217.
14. Gromov, M., *Partial Differential Relations*, *Ergeb. Math. Grenzgeb. (3)*, vol. 9, Berlin: Springer, 1986.
15. Jacobi, C. G. J., *Gesammelte Werke: Vol. 7*, Berlin: Reimer, 1878.
16. Jacobi, C. G. J., Note von der geodätischen Linie auf einem Ellipsoid und den verschiedenen Anwendungen einer merkwürdigen analytischen Substitution, *J. Reine Angew. Math.*, 1839, vol. 19, pp. 309–313.
17. Jacobi, C. G. J., *Vorlesungen über Dynamik*, 2nd ed., Berlin: Reimer, 1884.
18. Kimura, Y., Vortex Motion on Surfaces with Constant Curvature, *Proc. R. Soc. Lond. Ser. A Math. Phys. Eng. Sci.*, 1999, vol. 455, no. 1981, pp. 245–259.
19. Koltsova, O., Lerman, L., Delshams, A., and Gutiérrez, P., Homoclinic Orbits to Invariant Tori near a Homoclinic Orbit to Center-Center-Saddle Equilibrium, *Phys. D*, 2005, vol. 201, nos. 3–4, pp. 268–290.
20. Lerman, L. M., Hamiltonian Systems with Loops of a Separatrix of a Saddle-Center, *Selecta Math. Soviet.*, 1991, vol. 10, pp. 297–306.
21. Lewis, D. and Nigam, N., Geometric Integration on Spheres and Some Interesting Applications, *J. Comput. Appl. Math.*, 2003, vol. 151, no. 1, pp. 141–170.
22. Mclachlan, R., Modin, K., and Verdier, O., A Minimal-Coordinate Symplectic Integrator on Spheres, *Math. Comput.*, 2017, vol. 86, pp. 2325–2344.
23. Marsden, J., Pekarsky, S., and Shkoller, S., Stability of Relative Equilibria of Point Vortices on a Sphere and Symplectic Integrators, *Il Nuovo Cimento C*, 1999, vol. 22, no. 6, pp. 793–802.
24. Grotta Ragazzo, C., Irregular Dynamics and Homoclinic Orbits to Hamiltonian Saddle Centers, *Comm. Pure Appl. Math.*, 1997, vol. 50, no. 2, pp. 105–147.
25. Grotta-Ragazzo, C. and Salomão, P. A. S., The Conley–Zehnder Index and the Saddle-Center Equilibrium, *J. Differential Equations*, 2006, vol. 220, no. 1, pp. 259–278.

26. Rodrigues, A.R., Castilho, C., and Koiller, J., Vortex Pairs on a Triaxial Ellipsoid and Kimura's Conjecture, *J. Geom. Mech.*, 2018, vol. 10, no. 2, pp. 189–208.
27. Roy, R., *Elliptic and Modular Functions from Gauss to Dedekind to Hecke*, Cambridge: Cambridge Univ. Press, 2017.
28. Scarpello, G. and Ritelli, D., Legendre Hyperelliptic Integrals, π New Formulae and Lauricella Functions through the Elliptic Singular Moduli, *J. Number Theory*, 2014, vol. 135, pp. 335–352.
29. Selivanova, E.N., Classification of Geodesic Flows of Liouville Metrics on a Two-Dimensional Torus up to Topological Equivalence, *Sb. Math.*, 1993, vol. 75, no. 2, pp. 491–505; see also: *Mat. Sb.*, 1992, vol. 183, no. 4, pp. 69–86.
30. Siliciano, R., Constructing Möbius Transformations with Spheres, *Rose-Hulman Undergrad. Math. J.*, 2012, vol. 13, no. 2, pp. 115–124.
31. Vankerschaver, J. and Leok, M., A Novel Formulation of Point Vortex Dynamics on the Sphere: Geometrical and Numerical Aspects, *J. Nonlinear Sci.*, 2014, vol. 24, no. 1, pp. 1–37.

On the stability of vortex pairs moving on Riemann surfaces of genus zero

Adriano Regis Rodrigues*, César Castillo[†] and Jair Koiller[‡]

Abstract

This paper is a continuation of [7], that focused on vortex pairs motion on surfaces with antipodal symmetry such as the triaxial ellipsoid. We present the (linear) stability analysis of an equilibrium for an arbitrary genus zero surface. In particular, we present an easy way to compute on the pair of poles on a surface of revolution of genus zero (an ovoid). It is expected that this pair is linearly stable - however, we observe that two of the eigenvalues can vanish exceptionally. Calculations for the double faced elliptical region are also presented, a limit case of the triaxial ellipsoid.

Key words: Point vortices, Symplectic Geometry, Hamiltonian systems.
MSC2020: Primary: 76B47, 76M60; Secondary: 34C23, 37E35.

*Departamento de Matemática, Universidade Federal Rural de Pernambuco, Recife, PE, Brazil 52171-900. (email: regis.ufrpe@gmail.com)

[†]Departamento de Matemática, Universidade Federal de Pernambuco, Recife, PE, Brazil 50740-540 . (email: castilho@dmate.ufpe.br)

[‡]Departamento de Matemática, Universidade Federal de Juiz de Fora, Juiz de Fora, MG, Brazil 36036-900. (email: jairkoiller@gmail.com)

Contents

1	Introduction	3
1.1	Equations of motion	3
1.2	Invariance under Moebius transformations	4
2	Linearization of Equilibria.	5
2.1	The linearized Hamiltonian system	7
2.2	Surfaces with antipodal symmetry	12
3	Surfaces of revolution	14
3.1	Eigenvalues of the pair at the poles	14
3.2	Example: the circular vortex billiard	15
3.3	Conformal expansion at the poles	19
4	Examples	28
4.1	Matryoshkas	28
4.2	Ellipsoid of revolution	30
4.3	Mr. Bean surfaces	32
4.4	The elliptic vortex billiard	34
5	Conclusion	37

1 Introduction

Motivation for the study of point vortices on curved surfaces comes mainly from two dimensional condensed matter physics: liquid crystals, superfluids, Bose Einstein condensates and soft materials. Soon it may be experimentally possible to produce fluids of cold atoms on a prescribed surface [1], [2].

Vortex pairs, with opposite vorticities have been observed experimentally in BE condensates since at least 2010 [3]. Their dissociation are manifestations of the Berezinskii-Kosterlitz-Thouless (BKT) phase transition¹. For a mathematician the interest on vortex pairs on a surface Σ with metric g comes from the fact that a closeby pair shadows the geodesic perpendicular to the midpoint. This was predicted by [4], and verified numerically for the catenoid and the triaxial-ellipsoid [5], [6].

This is a sequel of our previous paper [7] about the motion of vortex pairs on surfaces with antipodal symmetry. A special feature of those surfaces is that the antipodal pairs form an invariant submanifold $\Sigma_{ant} = \{(\sigma, -\sigma)\}$. We analyzed the stability of equilibria of the pairs in the three symmetry axis of the triaxial ellipsoid.

Here we present some additional examples and also discuss other aspects, including surfaces of revolution. For those, we show that the pair at the poles is always linearly stable, except for the possibility of a degenerate case when one of the frequencies vanishes.

1.1 Equations of motion

We developed in [7] the idea of representing a genus zero surface Σ with metric g conformally over the sphere $S^2 \subset \mathbf{R}^3$ with constant curvature metric g_o , so that $h = h^2(s) g_o$, $s \in S^2$ where h is the conformal factor. While the ‘true’ physical object is Σ , transporting the dynamics to the ‘virtual’ sphere S^2 proves to be very convenient. The Hamiltonian description goes as follows. Let $||$ the euclidian distance between $s_1, s_2 \in S^2 \subset \mathbf{R}^3$.

Proposition 1. *The symplectic form in $S^2 \times S^2$ is given by*

$$\Omega_{\text{pair}} = h^2(s_1)\Omega_o(s_1) - h^2(s_2)\Omega_o(s_2) \quad (1)$$

where Ω_o is the area form of the round sphere, and the Hamiltonian is

$$H = -\ln\left(\sqrt{h(s_1)h(s_2)}|s_1 - s_2|\right). \quad (2)$$

¹Kosterlitz was one of the 2016 Physics Nobel prize laureates.

The equations of motion are therefore

$$\begin{aligned}\dot{s}_1 &= \frac{1}{h^2(s_1)} \left(\frac{s_1 \times s_2}{|s_1 - s_2|^2} - \frac{1}{2h(s_1)} s_1 \times \text{grad } h(s_1) \right) \\ \dot{s}_2 &= \frac{1}{h^2(s_2)} \left(\frac{s_1 \times s_2}{|s_1 - s_2|^2} + \frac{1}{2h(s_2)} s_2 \times \text{grad } h(s_2) \right) .\end{aligned}\tag{3}$$

All the required information is contained in the conformal factor h .

The sphere ($h \equiv 1$) is highly degenerate in the sense that all antipodal pairs are in equilibrium. In [8] it was shown that for generic h there are finitely many equilibria and infinitely many periodic orbits. Together with $|s_1| = |s_2| = 1$, the equilibrium configurations will satisfy six equations for s_1, s_2, α, β

$$\frac{s_2}{|s_1 - s_2|^2} - \frac{\text{grad } h(s_1)}{2h(s_1)} = \alpha s_1 \quad , \quad -\frac{s_1}{|s_1 - s_2|^2} + \frac{\text{grad } h(s_2)}{2h(s_2)} = \beta s_2 .\tag{4}$$

1.2 Invariance under Moebius transformations

In [7] we mentioned the following basic properties:

Proposition 2.

- i) The EDOs (3) transform invariantly under Moebius transformations on the extended complex plane $\mathbf{C} \cup \infty \equiv S^2$.*
- ii) An antipodal pair $(s, -s)$ is an equilibrium if and only if the gradient of the conformal factor vanishes at both s and $-s$.*
- iii) For the purpose of linearization, under a Moebius transformation, any pair at equilibrium can be represented by the poles $(0, 0, \pm 1)$. Moreover the Moebius transformation can be chosen to produce equal conformal factors at the poles.*

Point i) reflects the fact that Proposition 1 must be intrinsic. Two conformal maps from Σ to S^2 (extended complex plane $\mathbf{C} \cup \infty$) differ by a Moebius transformation. One can avoid doing the algebra by a geometric reasoning. Moebius transformations correspond to a $SO(3)$ rotation on a suitably translated sphere $S^2 \subset \mathfrak{R}^3$, composed with one stereographic transformations and one inverses [9]. Points ii) and iii) clearly show the usefulness of the representation (3).

In [7] we explored the following observation:

Proposition 3. *For conformal metrics whose factor $h(s)$ has the antipodal symmetry, the set of antipodal points $S_{ant} = \{(s, -s) | s \in S^2\}$ form an invariant submanifold, governed by*

$$\dot{s}_1 = -\frac{1}{h^3(s_1)} s_1 \times \text{grad } h(s_1) = -\frac{1}{h^2(s_1)} s_1 \times \text{grad } \log h(s_1) \quad (s_2 = -s_1) \quad (5)$$

Trajectories of s_1 are on the level curves of h . Equilibria coincide with the critical points of h .

2 Linearization of Equilibria.

We just saw that for genus zero surfaces, with the help of the conformal factor, we can represent the dynamics in the sphere S^2 . Moreover, in making general reasonings about stability, we may assume that a given equilibrium solution pair for the system (4) is antipodal, and we will in fact take them as the north and south poles.

Note that the original surface Σ may not have symmetries at all!

We will now discuss the linear stability of an antipodal equilibrium in terms of the quadratic expansions of the conformal factors. Finding h^2 is a global problem, but interestingly, for surfaces of revolution, the equilibrium of the pair at the poles is *always* linearly stable, except for a degenerate case when one of the frequencies vanishes.

The study will extend the one we presented in [7]. As we did there, we start by taking for the antipodal pair in S^2 the poles

$$s_{1,2}^* = (0, 0, \pm 1).$$

We take for coordinate systems the corresponding tangent planes. Then eliminating the z coordinates, (3) yields a system of four ODEs on the cartesian coordinates x_1, y_1, x_2, y_2 . All we will need for the linear analysis are the quadratic expansions H of the conformal factor

$$h(x, y, z), \quad \text{with } z = \pm(1 - x^2 - y^2)^{1/2}$$

at $s_{1,2}^*$. In general there will be two (different) pairs of quadratic coefficients and a rotation of an angle θ of the principal axis of the second quadratic form with respect to the principal axis of the first. This is encoded in:

Data needed for the linearization

$$H_1(x_1, y_1) = h_1 + \frac{1}{2} (p_1 x_1^2 + q_1 y_1^2) \quad (6)$$

$$H_2(x_2, y_2) = h_2 + \frac{1}{2} (p_2 (x_2')^2 + q_2 (y_2')^2) \quad (7)$$

with $h_1, h_2 > 0$ and where

$$\begin{aligned} x_2' &= x_2 \cos \theta - y_2 \sin \theta \\ y_2' &= x_2 \sin \theta + y_2 \cos \theta . \end{aligned} \quad (8)$$

We stress emphatically that there are *global informations* hidden in these local expansions. They must be interdependent.

For instance, on a surface of revolution, choose a parallel γ , and let D_γ the cap surrounding the south pole bounded by γ . Due to the rotational symmetry, there is a unique conformal map from D_γ to the unit disk D in the complex plane sending meridians to rays.

It extends to a unique global conformal map from Σ to the extended complex plane $\mathbf{R} \cup \infty \equiv S^2$. So the expansion at $z = \infty$ is tied to the expansion at $z = 0$.

We will see shortly that a Moebius transformation on the sphere preserving the poles can be chosen so that the conformal factors h_1 and h_2 can be made equal.

For a general surface Σ without symmetries, imagine a domain D_γ bounded by a simple closed curve $\gamma \subset \Sigma$. Let D_r the geodesic disk of radius r , around say, the south pole of the sphere. There is a conformal map from D_γ to D_r , providing a local expansion like (6). But that conformal map will not extend (except for a stroke of luck) to a global map from Σ to S^2 .

2.1 The linearized Hamiltonian system

Theorem 1. *When we substitute in (3)*

$$s_1 = \left(x_1, y_1, \sqrt{1 - x_1^2 - y_1^2} \right)$$

$$s_2 = \left(x_2, y_2, -\sqrt{1 - x_2^2 - y_2^2} \right)$$

and retain only the linear terms we get the Hamiltonian

$$H = \frac{1}{8} [(x_1 + x_2)^2 + (y_1 + y_2)^2] - \frac{1}{4h_1} H_1(x_1, y_1) - \frac{1}{4h_2} H_2(x_2, y_2) \quad (9)$$

and symplectic form

$$\Omega = h_1^2 dx_1 \wedge dy_1 + h_2^2 dx_2 \wedge dy_2 \quad (10)$$

where the quadratic expansions H_1, H_2 are given by (6, 7).

The linearized system is therefore

$$4h_1^2 (\dot{x}_1, \dot{y}_1) = (-y_1 - y_2, x_1 + x_2) + \frac{2}{h_1} (\partial H_1 / \partial y_1, -\partial H_1 / \partial x_1) \quad (11)$$

$$4h_2^2 (\dot{x}_2, \dot{y}_2) = (-y_1 - y_2, x_1 + x_2) + \frac{2}{h_2} (\partial H_2 / \partial y_2, -\partial H_2 / \partial x_2)$$

Note that the *plus* sign in the symplectic form even though the vortices are opposite. This is due to the fact that the expansions are done in antipodals $(0, 0, \pm 1)$. The factor 4 results from the distance between the poles being 2.

We will show that we may assume $h_1 = h_2 = h$ in (6, 7). Then the linearized system (11) will be written in matrix form as

$$4h^2 \dot{X} = A X, \quad X = (x_1, y_1, x_2, y_2)^\dagger. \quad (12)$$

The factor $4h^2$ is irrelevant for the analysis. It can be made equal to one by a linear change of time scale. From now on we will neglect this factor on the eigenvalue formulas.

Theorem 2.

Assuming $h_1 = h_2 = h$ the matrix of the system is

$$A = \begin{bmatrix} 0 & \gamma_1 & 0 & -1 \\ \delta_1 & 0 & 1 & 0 \\ 0 & -1 & a & b \\ 1 & 0 & c & -a \end{bmatrix} \quad (13)$$

whose characteristic polynomial is (as expected) a biquadratic,

$$p(\lambda) = \lambda^4 - 2\rho\lambda^2 + \kappa \quad (14)$$

$$\rho = \frac{1}{2} (a^2 + bc + \gamma_1\delta_1) - 1 \quad (15)$$

$$\kappa = 1 + (a^2 + bc)\gamma_1\delta_1 - \gamma_1b - c\delta_1 . \quad (16)$$

The coefficients (depending on the data $h, p_1, q_1, p_2, q_2, \theta$) are:

$$\begin{aligned} \gamma_1 &= -1 + 2(q_1/h) \\ \delta_1 &= 1 - 2(p_1/h) \\ a &= 2 \sin \theta \cos \theta [(q_2/h) - (p_2/h)] \\ b &= -1 + 2 [(q_2/h) \cos^2 \theta + (p_2/h) \sin^2 \theta] \\ c &= 1 - 2 [(p_2/h) \cos^2 \theta + (q_2/h) \sin^2 \theta] \end{aligned} \quad (17)$$

One verifies a simplification valid for arbitrary θ :

$$a^2 + bc = \gamma_2\delta_2 \quad (18)$$

where

$$\gamma_2 = -1 + 2(q_2/h) , \quad (19)$$

$$\delta_2 = +1 - 2(p_2/h) . \quad (20)$$

Example. When there is no twist between the principal axis, ie., $\theta = 0$ the characteristic polynomial has a more symmetric form

$$p(\lambda) = \lambda^4 + (2 - \delta_1\gamma_1 - \delta_2\gamma_2)\lambda^2 + (1 - \delta_1\delta_2)(1 - \gamma_1\gamma_2) \quad (21)$$

The discriminant of this biquadratic is

$$\Delta = (\delta_1\gamma_1 - \delta_2\gamma_2)^2 + 4(\delta_1 - \gamma_2)(\delta_2 - \gamma_1) . \quad (22)$$

For instance, with these (more or less randomly chosen) values

$$p_1 = 0.1, q_1 = 11/30, p_2 = 0.6, q_2 = 0.2$$

we get *loxodromic* eigenvalues, since $\Delta = -(3.2)(14/15) < 0$.

In the conclusions we present some questions related to the ranges of (15, 16) in (14).

The following Lemma shows that without loss of generality we could (as we did) assume $h_1 = h_2 = h$ in Theorem 2.

Lemma 1. *The conformal factor can be adjusted in order to make*

$$h(0, 0, -1) = h(0, 0, 1) . \quad (23)$$

More precisely, we can replace h_1, h_2 by a common factor h given by

$$h = h_1\beta = h_2/\beta, \quad \beta = (h_2/h_1)^{1/2} . \quad (24)$$

and replace the parameters in (13) via

$$\begin{aligned} \gamma_1^{new} &= \beta^2 \gamma_1 \\ \delta_1^{new} &= \beta^2 \delta_1 \\ \gamma_2^{new} &= (1/\beta^2) \gamma_2 \\ \delta_2^{new} &= (1/\beta^2) \delta_2 \end{aligned} \quad (25)$$

where

$$\gamma_i = -1 + 2q_i/h_i, \quad \delta_i = 1 - 2p_i/h_i .$$

The proof of Lemma 1 will be done next.

The adjustment parameter β

Consider the conformal map from the unit sphere to itself

$$g_\beta : (x, y, z) \rightarrow (\tilde{x}, \tilde{y}, \tilde{z})$$

that fixes the poles, but shifts parallels up or down, corresponding to a homothety in the *equatorial* complex plane \mathbf{C} , given by

$$r = \beta \tilde{r}.$$

A short calculation yields

$$z = \frac{\beta^2(1 + \tilde{z}) - (1 - \tilde{z})}{\beta^2(1 + \tilde{z}) + (1 - \tilde{z})} \quad (26)$$

where $z = \sin \phi$, $\tilde{z} = \sin \tilde{\phi}$ are the heights of the corresponding parallels given by $\phi, \tilde{\phi}$. The conformal factor from the (x, y, z) sphere (called ‘old’ for short) to the $(\tilde{x}, \tilde{y}, \tilde{z})$ sphere (called ‘new’) is

$$h_{old/new} = \frac{\cos \phi}{\cos \tilde{\phi}} = \frac{\sqrt{1 - z^2}}{\sqrt{1 - \tilde{z}^2}} = \frac{2\beta}{(\beta^2 - 1)\tilde{z} + (\beta^2 + 1)} \quad (27)$$

Substituting $\tilde{z} = \pm 1$ gives

$$h_{old/new}(-1) = \beta, \quad h_{old/new}(1) = 1/\beta \quad (28)$$

which in hindsight is what one should expect.

Since conformal factors multiply composition, we can choose a suitable β so that, upon composition of the original map from Σ to S^2 with $g_\beta : S^2 \rightarrow S^2$, the conformal factors at the poles become equal. In fact, the common factor h satisfies

$$h = h_1\beta = h_2/\beta, \quad \beta = (h_2/h_1)^{1/2}. \quad (29)$$

We call β the *adjustment parameter*.

Recalculating the local expansions via β

Initially (6, 7) were given, with $h_1 \neq h_2$ in general. Concomitantly to their equalization, in order to write down the matrix (13), we must recalculate the coefficients of the quadratic forms. Substituting in (27)

$$z = \pm \sqrt{1 - x^2 - y^2} \sim \pm \left(1 - \frac{x^2 + y^2}{2} \right),$$

we get, after a short calculation, the local expansions of g_β

$$\begin{aligned} h_{(south)} &= \beta \left(1 - \frac{\beta^2 - 1}{4} (x^2 + y^2) \right) \\ h_{(north)} &= \frac{1}{\beta} \left(1 - \frac{\beta^2 - 1}{4\beta^2} (x^2 + y^2) \right). \end{aligned} \tag{30}$$

Hence

$$\begin{aligned} H_1^{new} &= \beta [h_1 + (1/2) p_1 x_1^2 + (1/2) q_1 y_1^2] \left[1 - \frac{\beta^2 - 1}{4} (x_1^2 + y_1^2) \right] \\ H_2^{new} &= \frac{1}{\beta} [h_2 + (1/2) p_2 x_2^2 + (1/2) q_2 y_2^2] \left[1 - \frac{\beta^2 - 1}{4\beta^2} (x_2^2 + y_2^2) \right] \end{aligned} \tag{31}$$

The new p 's and q 's follow by collecting terms. The end result is nice:

$$\begin{aligned} \delta_1^{new} &:= +1 - 2 p_1^{new}/h = \beta^2 (+1 - 2 p_1/h_1) \quad (= \beta^2 \delta_1) \\ \gamma_1^{new} &:= -1 + 2 q_1^{new}/h = \beta^2 (-1 + 2 q_1/h_1) \quad (= \beta^2 \gamma_1) \\ \delta_2^{new} &:= +1 - 2 p_2^{new}/h = (1/\beta^2) (+1 - 2 p_2/h_2) \quad (= \delta_2/\beta^2) \\ \gamma_2^{new} &:= -1 + 2 q_2^{new}/h = (1/\beta^2) (-1 + 2 q_2/h_2) \quad (= \gamma_2/\beta^2) \end{aligned}$$

This concludes the proof of Lemma 1. □

We now revisit some derivations from [7], for the case of surfaces with antipodal symmetry.

2.2 Surfaces with antipodal symmetry

In this case

$$p_1 = p_2 = p, \quad q_1 = q_2 = q, \quad (32)$$

and matrix A simplifies to

$$A = \begin{bmatrix} 0 & \gamma & 0 & -1 \\ \delta & 0 & 1 & 0 \\ 0 & -1 & 0 & \gamma \\ 1 & 0 & \delta & 0 \end{bmatrix}. \quad (33)$$

where

$$\gamma = -1 + 2q/h, \quad \delta = +1 - 2p/h. \quad (34)$$

Matrix A has two invariant subspaces of dimension 2:

- V spanned by $v_1 = (1, 0, -1, 0)$, $v_2 = (0, 1, 0, -1)$. We have

$$Av_1 = (\delta - 1)v_2 = -2\frac{p}{h}v_2, \quad Av_2 = (1 + \gamma)v_1 = 2\frac{q}{h}v_1 \quad (35)$$

- W spanned by $w_1 = (1, 0, 1, 0)$, $w_2 = (0, 1, 0, 1)$. We have

$$Aw_1 = (\delta + 1)w_2, \quad Aw_2 = (\gamma - 1)w_1 \quad (36)$$

The first subspace V is tangent to the center manifold ($s_1 = -s_2$) while W is transverse to it.

Theorem 3. (*Surfaces with antipodal symmetry [7]*)

On the subspace $V = \text{span}\{v_1, v_2\}$, the eigenvalues satisfy

$$\lambda^2 = (\delta - 1)(1 + \gamma) = -4pq/h^2. \quad (37)$$

and on the subspace $W = \text{span}\{w_1, w_2\}$, the eigenvalues satisfy

$$\lambda^2 = (\gamma - 1)(\delta + 1) = -4(1 - p/h)(1 - q/h). \quad (38)$$

Conclusions for surfaces with antipodal symmetry:

i) On the system restricted to the invariant submanifold S_{ant} , if p, q have the same (resp. opposite) sign, then one has a center (resp. saddle.) The eigenvalues satisfy

$$\lambda^2 + 4pq/h^2 = 0.$$

ii) For the transverse subspace: if $(1 - p/h)(1 - q/h)$ is positive (resp. negative) one has a center (resp. saddle). The eigenvalues satisfy

$$\lambda^2 + 4(1 - p/h)(1 - q/h) = 0.$$

iii) The loxodromic case is ruled out.

Undefined situations occur when p or q are equal to 0 or to h .

Remark 1. *When $p = q$ the pair is always linearly stable, except for the undefined situations above. Nonetheless, we will show that for embedded spheroids in \mathbf{R}^3 then $p/h \leq 1/2$, so the only undefined case is when $p = 0$.*

Remark 2. *Along the invariant submanifold S_{ant} the result is consistent with that one expects from quadratic hamiltonians in a two dimensional phase space. In the transverse plane W spanned by w_1, w_2 both stable or unstable behavior can also happen.*

3 Surfaces of revolution

Here we have

$$p_1 = q_1, p_2 = q_2. \quad (39)$$

so the (interconnected) local expansions will be of the form

$$H_1 = h_1 + \frac{p_1}{2}(x_1^2 + y_1^2) \quad , \quad H_2 = h_2 + \frac{p_2}{2}(x_2^2 + y_2^2). \quad (40)$$

We will see in Proposition 6 how these coefficients can be related to the local profiles at the poles, and just one global information, simplifying substantially the work. When the surface is convex with

$$p_1/h_1 \neq p_2/h_2$$

it is called an *ovoid*, like the Matryoshka dolls². When $p_1/h = p_2/h$ we called it an *spheroid*.

3.1 Eigenvalues of the pair at the poles

Theorem 4. (*Surfaces of revolution: the poles are always center-center*)

Assume that the adjustments on the quadratic expansions at the poles were done, so $h_1 = h_2 = h$. Let

$$\gamma_1 = -\delta_1 = -1 + 2 p_1/h \quad , \quad \gamma_2 = -\delta_2 = -1 + 2 p_2/h. \quad (41)$$

The eigenvalues are $\pm i\omega_+$, $\pm i\omega_-$, with frequencies

$$\omega_{\pm} = \left[\left(1 + \frac{\gamma_1^2 + \gamma_2^2}{2} \right) \pm \left(\frac{(\gamma_1^2 - \gamma_2^2)^2}{4} + (\gamma_1 + \gamma_2)^2 \right)^{1/2} \right]^{1/2} \quad (42)$$

The expression inside the [] is always non-negative.

NOTA BENE: degenerate situations may occur. The sphere is the simplest example, where $\gamma = -1$, so one frequency is $\omega = 2$ and the other vanishes.

²A Marylin Monroe Matryoshka should not be convex.

Proof. Put $\gamma_1 = -\delta_1$, $\gamma_2 = -\delta_2$ in (21). The characteristic polynomial is

$$p = \lambda^4 + 2\rho\lambda^2 + \kappa \quad (43)$$

with

$$\rho = 1 + \frac{\gamma_1^2 + \gamma_2^2}{2} \geq 0, \quad \kappa = (1 - \gamma_1\gamma_2)^2 \geq 0.$$

We have

$$\lambda^2 = -\rho \pm \sqrt{\rho^2 - \kappa}, \quad \rho \geq 0. \quad (44)$$

A short calculation gives the discriminant

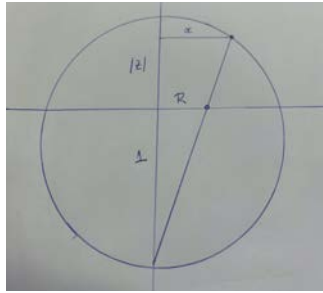
$$\Delta_{rev} = \rho^2 - \kappa = \frac{(\gamma_1^2 - \gamma_2^2)^2}{4} + (\gamma_1 + \gamma_2)^2 \geq 0. \quad (45)$$

so we see that λ^2 is nonpositive for both signs in the right hand side of (44). \square

3.2 Example: the circular vortex billiard

The double faced unit disk is the limit of an oblate ellipsoid of revolution when the minor axis shrinks to zero. One should not confuse vortex motion in this boundaryless surface with the well known vortex motion inside a planar circular domain.

In order to apply our methodology, we map this surface over the round sphere. This is done via the inverses of the stereographic projections from the north and south poles. In this way we “inflate” the double face unit disk to the sphere S^2 . A point in the top side of the disk is sent to a point in the northern hemisphere by a ray emanating from the south pole. Likewise, a point in the bottom side of the disk is sent to a point in the southern hemisphere by a ray emanating from the north pole.



Let (r, θ) , $r \leq 1$, polar coordinates in the unit disk, and let (ϕ, θ) be respectively the latitude (measured from the equator $z = 0$) and longitude in the unit sphere in (X, Y, Z) space. It is readily seen

$$r = \frac{\cos \phi}{1 + |\sin \phi|} = \sqrt{\frac{1 - |Z|}{1 + |Z|}}, \quad -\pi/2 \leq \phi \leq \pi/2. \quad (46)$$

The conformal factor from the planar (euclidian) metric to the sphere (round) metric at a point $(X, Y, Z) \in S^2$ is

$$h(X, Y, Z) = \frac{1}{1 + |Z|} \quad (47)$$

It is maximum along the equator (with $h = 1$) and minimum at the poles (with $h = 1/2$). If $\phi > 0$, the corresponding vortex is in the *down* face of the disk, and when $\phi < 0$ it is in the *up* face. This loss of differentiability of the double disk metric at the turning edge (the equator $z = 0$ of the sphere) corresponds to the fact that the curvature is concentrated there.

Note the lack of differentiability when $Z = 0$. For simulations of (3) in the representing $S^2 \times S^2$, with

$$\text{grad } h = \frac{-\text{sign}(Z)}{(1 + |Z|)^2} \hat{k}, \quad \hat{k} = (0, 0, 1),$$

it is useful to use a symplectic integrator. The event discontinuities at $z = 0$ can be handled with specialized ODEs codes [10], [11], [12]. It would be interesting to have them adapted to symplectic integrators.

Expansion of h at the center of the disk

The centers of faces of the double disk correspond to $Z = \pm 1$.

Proposition 4. *The expansion of the conformal factor h from the doubled disk $P : (r, \theta)$ to the sphere S^2 at the poles $Z = \pm 1$, corresponding the center of the (doubled) disk, is given by*

$$h_{D/S^2}(X, Y, Z) = \frac{1}{2} + \frac{1}{8}(X^2 + Y^2) + \dots \quad (48)$$

Proof. From (9) then

$$h = \frac{1}{1 + \sqrt{1 - (X^2 + Y^2)}} = \frac{1}{1 + 1 - (X^2 + Y^2)/2}$$

where X, Y are moved from the plane $Z = 0$ to the tangent planes at the poles $Z = \pm 1$. In the notation of (6),

$$h = \frac{1}{2}, \quad p = q = \frac{1}{4}. \quad (49)$$

We obtain without need to do further computations:

Proposition 5. *The linearization of the vortex pair system of the double edged unit disk at the pair located at $x = y = 0, z = \pm 1$ is of center-center kind, with eigenvalues $\pm i$ both along the tangent space of the center manifold, and in the transverse subspace. The frequencies are in 1:1 resonance.*

Proof. We can either use Proposition 3 or Proposition 4. In the former, we compute $4pq/h^2 = 4(1 - p/h)(1 - q/h) = 1$. In the latter, we see that $\gamma_1 = \gamma_2 = 0$, so (41) yields again the quadruplet $\pm i, \pm i$. Both ways coincide. \square

We will show in section 4.4 that the frequencies stay in 1:1 relation for all elliptic vortex billiards.

Reduction of the S^1 symmetry

We outline the reduction procedure. This seemingly peaceful problem becomes quite involved, actually. Using spherical coordinates as above with longitude θ and latitude ϕ , measured from the equator, so $z = \sin \phi$,

$$h(\phi) = 1/(1 + |\sin \phi|),$$

$$\Omega_{pair} = \frac{\cos \phi_1}{1 + |\sin \phi_1|} d\phi_1 \wedge d\theta_1 - \frac{\cos \phi_2}{1 + |\sin \phi_2|} d\phi_2 \wedge d\theta_2$$

and the Hamiltonian is $H = -\log F$ where

$$F = 2 \frac{1 - \cos \phi_1 \cos \phi_2 \cos(\theta_1 - \theta_2) - \sin \phi_1 \sin \phi_2}{[(1 + |\sin \phi_1|)(1 + |\sin \phi_2|)]^{1/2}}. \quad (50)$$

The momentum map for the Hamiltonian action of S^1 on $(S^2 \times S^2, \Omega_{pair})$ (which is the translation along parallels in simultaneous fashion) is

$$J = m(\phi_1) - m(\phi_2) \quad (51)$$

where

$$m(\phi) = \begin{cases} +\log(1 + \sin \phi), & 0 \leq \phi \leq \pi/2 \\ -\log(1 - \sin \phi), & -\pi/2 \leq \phi < 0 \end{cases}. \quad (52)$$

Note that the maximum and minimum values of J occur when

$$J = \pm 2 \log 2.$$

It corresponds to the vortices being at the center of the disk in opposite faces. $J = 0$ corresponds to vortices having opposite (in general varying) values of ϕ . To implement the reduction, one fixes the hypersurface $\theta_2 \equiv 0$, so the reduced symplectic form is

$$\Omega_{red} = \frac{\cos \phi_1}{1 + |\sin \phi_1|} d\phi_1 d\theta_1.$$

The reduced Hamiltonian is $H_{red} = -\log F_{red}$ where

$$F_{red} = F_{red}(\phi_1, \theta_1; J)$$

is obtained replacing $\sin \phi_2$ and $\cos \phi_2$ in (50) by solving for ϕ_2 (see (51)),

$$m(\phi_2) = m(\phi_1) - J.$$

Due to the switching in (52) at $\phi = 0$, two cases occur: either the vortices on the same or opposite faces. At the transition at least one of the vortices, say s_1 , is at the rim. The product $s_1 \times \hat{k}$ is tangent to the equator at s_1 .

So if there is a switching, the velocity \dot{s}_1 gets an instantaneous push along the rim. Let us look at the other contribution to \dot{s}_1 , coming from the term with $s_1 \times s_2$. We can take without loss of generality, $s_1 = (1, 0, 0)$, and an arbitrary $s_2 = (x_2, y_2, z_2)$. This other contribution is $y_2 \hat{k} - z_2 \hat{j}$. Hence, depending on the sign of y_2 , vortex s_1 will move either to the upper or lower hemispheres, irrespective of whichever of the hemispheres s_2 .

We stop the study here with this task: depict the level curves

$$H_{red}(\phi_1, \theta_1; J) = h = \text{const}$$

in the allowed region (ϕ_1, θ_1) inside S^2 , for various choices of J , in order to obtain a qualitative understanding. Quantitatively, one finds the time dependence $\theta_1(t), \phi_1(t)$ on the motion of the first vortex by solving

$$\frac{\cos \phi_1}{1 + \sin \phi_1} \dot{\phi}_1 = -\partial H_{red} / \partial \theta_1, \quad \frac{\cos \phi_1}{1 + \sin \phi_1} \dot{\theta}_1 = \partial H_{red} / \partial \phi_1$$

Reconstructing the motion of the second vortex comes from substituting $\phi_1(t)$ in (51) to obtain $\phi_2(t)$ and a quadrature of the ODE for $\dot{\theta}_2$ after inserting $\phi_1(t), \theta_1(t), \phi_2(t)$. Clearly, this is easier to say than to do.

ADRIANO: NUMERICAL EXPERIMENTS?

3.3 Conformal expansion at the poles

In this section we present a rather simple method to compute the quadratic expansions H of the conformal factors at the poles. It depends only on the local profiles of the surface of revolutions and just a single integral along the meridian. This allows to readily compute the frequencies.

We visualize the surface of revolution Σ sitting vertically over the (physical) x, y plane P with the south pole at the origin. We assume that the profile of the surface at one each of the poles is quadratic. Say, at the south pole, the meridian $y = 0$ is

$$z = \frac{1}{2\alpha} x^2 + \dots \quad (53)$$

We will also consider *another* plane Π with polar coordinates r, θ superposed over P , where r accounts for stretchings/compressions along the meridians $\theta = \text{const.}$ so that the map $\Sigma \rightarrow \Pi$ is conformal. Our task is to relate the arc length $s \in [0, L]$ along the meridian with the radial coordinate r on Π . For this purpose, it is convenient to describe the profile of the meridian $y = 0$ of Σ by a function $x = x(s)$, such that

$$x(0) = x(L) = 0, \text{ and } x(s) > 0, \quad |dx/ds| \leq 1, \quad s \in (0, L) \quad (a).$$

We do not require $x(s)$ to have just one critical value, the surface does not need to be convex. The other coordinate $z(s)$ of the meridian can be recovered from the arc length condition $(dx/ds)^2 + (dz/ds)^2 = 1$.

We assume that the surface is smooth at the poles, and (53) is equivalent to

$$(dx/ds)^2 = 1 \text{ for } s = 0 \text{ and } s = L \quad (b).$$

Then for small x for which $x(s)$ is monotone, (53) yields

$$s(x) = \int_0^x \sqrt{1 + (dz/dx)^2} dx \sim x + \frac{1}{6\alpha^2} x^3 + \dots \quad (54)$$

Gauss already called the attention that a conformal map to the plane obeys a very nice separable ODE

$$\frac{ds}{x(s)} = \frac{dr}{r} \quad (\text{with } ds/dr = x/r = h) \quad (55)$$

Local conformal map: an indeterminate ρ combines with α

Recall, we are assuming that the profile of the surface Σ in x, y, z space at one of the poles, say, the south pole, is of the form $z = (1/2\alpha)x^2 + \dots$ so that for small x

$$s(x) = \int_0^x \sqrt{1 + (dy/dx)^2} dx \sim x + \frac{1}{6\alpha^2}x^3 + \dots$$

Lemma 2.

$$r(x) = \rho x (1 + x^2/4\alpha^2 + O(x^4)). \quad (56)$$

(the undetermined ρ corresponds to homotheties in the plane.)

Proof. Insert (56) in the ODE (55). The left hand side of

$$ds/dr = x/r \quad (= h_{\Sigma/\Pi})$$

gives

$$h_{\Sigma/\Pi} = \frac{ds}{dr} = \frac{ds/dx}{dr/dx} = \frac{1 + x^2/2\alpha^2}{\rho(1 + 3x^2/4\alpha^2)} = \frac{1}{\rho} (1 - x^2/4\alpha^2).$$

The right hand side is

$$h_{\Sigma/\Pi} = \frac{x}{r} \sim \frac{1}{\rho(1 + x^2/4\alpha^2)} \sim \frac{1}{\rho} (1 - x^2/4\alpha^2). \quad (57)$$

□

We summarize:

Proposition 6. *Let*

$$z = (1/2\alpha)x^2 + \dots \quad (58)$$

be the profile of a surface of revolution at one of the poles.

The conformal factor of $\Sigma \rightarrow \Pi$ at that pole expands as

$$h_{\Sigma/\Pi} = \frac{1}{\rho} (1 - \frac{r^2}{4\rho^2\alpha^2} + \dots) \quad (59)$$

where r is the radial parameter in the plane Π . It is related to x (or s) via

$$\begin{aligned} r(x) &= \rho x (1 + x^2/4\alpha^2 + O(x^4)) = \rho s (1 + s^2/4\alpha^2 + O(s^4)) \\ s(x) &= x + x^3/6\alpha^2 + O(x^5). \end{aligned} \quad (60)$$

Proposition 7. *The conformal factor of the map $\Sigma \rightarrow S^2$ from the surface Σ to the unit sphere $X^2 + Y^2 + Z^2 = 1$ expands at the corresponding pole ($Z = \pm 1$) as*

$$h_{\Sigma/S^2} = h \left[1 + \frac{1}{4} \left(1 - \frac{h^2}{\alpha^2} \right) (X^2 + Y^2) \right], \quad h = \frac{1}{2\rho} \quad (61)$$

where X, Y are transported to the tangent plane of S^2 at the pole.

Important: the choice of ρ on one pole determines forcibly the value of the corresponding at the other pole.

Proofs. For the plane we insert $x \sim r/\rho$ from (56) in (57). For the sphere, we may fix the meridian $\theta = 0$. We need to multiply the conformal factor

$$\frac{1}{\rho} \left(1 - \frac{r^2}{4\rho^2\alpha^2} \right)$$

from the surface to the plane Π by the conformal factor

$$\frac{1}{2} + \frac{1}{8} X^2$$

from the plane Π to the sphere given in (48). For this, we need to relate r with X . We claim that to first order

$$r \sim X/2,$$

so the result for the sphere will follow by this substitution and the above mentioned multiplication. This claim that $r \sim X/2$ is proved now.

Lemma 3. *The point in the equatorial plane Π with radial coordinate r corresponds to the point $(X, 0, Z) \in S^2$ via the stereographic projection from the north pole, with Z near -1, satisfies $r \sim X/2$. (Moreover around $Z = -1$ the infinitesimal ratio of areas from the projection in the equatorial plane to the corresponding spherical region is $1/4$, hence the factor $h = 1/2$).*

Proof. The stereographic projection from the north pole $(0, 0, 1)$ to the equatorial plane is given by

$$r^2 = \frac{1+Z}{1-Z}$$

For $X \ll 1$, then near the south pole,

$$Z = -\sqrt{1-X^2} \sim -1 + \frac{X^2}{2}.$$

Hence

$$r^2 \sim \frac{1 + (-1 + X^2/2)}{1 + 1 - X^2/2} \sim X^2/4 \quad \text{for } |X| \ll 1.$$

Also using spherical coordinates, $Z = \sin \phi$, then

$$r^2 = \frac{1 + \sin \phi}{1 - \sin \phi} \Rightarrow r dr = \frac{\cos \phi}{(1 - \sin \phi)^2} d\phi, \quad \frac{A_{\Pi}}{A_{S^2}} = \frac{r dr}{\cos \phi d\phi} = \frac{1}{(1 - \sin \phi)^2} \quad (62)$$

which gives $1/4$ when $\phi = -\pi/2$. \square

Spheroids. Here $p_1 = p_2 = q_1 = q_2 (= p)$ and there will be just one parameter in matrix (13), namely $\gamma = -1 + 2p/h$. From (42), the frequencies are

$$\omega_{\pm} = |1 \pm \gamma| = \begin{cases} 2|p|/h & \text{(relative to invariant submanifold)} \\ 2|1 - p/h| & \text{(transverse subspace)} \end{cases} \quad (63)$$

Moreover, the local expansion above (see (61)) gives

$$\gamma = -\frac{h^2}{\alpha^2} \leq 0, \quad h = \frac{1}{2\rho}$$

$$2(1 - p/h) = 1 + \frac{h^2}{\alpha^2} \geq 1.$$

where α comes from the local profile, but ρ is still unknown, and needs to be determined from global considerations. A simple procedure for this will be presented in the next section.

It is important to notice that an indefinite case occurs in the invariant subspace, when $\gamma = -1$, i.e, when

$$2\rho\alpha = 1. \quad (64)$$

Ellipsoids of revolution (preview)

$$\mathcal{E}(1, 1, c): \quad x^2 + y^2 + z^2/c^2 = 1.$$

The profile meridian of a for small $|x|$ is $z = c\sqrt{1 - x^2} \sim c(1 - x^2/2)$, hence the parameter α in $z \sim x^2/(2\alpha)$ is

$$\alpha = 1/c. \quad (65)$$

For the sphere, $c = 1$, so $\alpha = 1$. Moreover, in view of (61), the value of ρ must be

$$\rho = \frac{1}{2},$$

since the conformal factor is constant. This is coherent with $\gamma = -1$, $p = 0$. Note that formula (61) gives $h \equiv 1/4$, instead of $1/2$. This is merely an innocuous artifact, coming from the fact that the original sphere is on top of plane P while the representative unit sphere has its equator in the plane Π , justifying this extra $1/2$ factor.

For $c = 1/\alpha \neq 1$, we need to compute $\rho = \rho(c)$ in order to get the parameter $\gamma = \gamma(c)$ explicitly. We will do it in section 4.2. We expect that when $\alpha \rightarrow \infty$ (i.e, $c = 0$, the double faced disk), we will still get $\rho\alpha \rightarrow \infty$, so that $p/h \rightarrow 1/4$ as we saw in (48).

Global conformal maps

Let us now explore more fully the EDO (55), governing the conformal map from the surface to the plane sending meridians to rays.

$$\frac{ds}{x(s)} = \frac{dr}{r} \quad (\text{with } ds/dr = x/r = h)$$

Likewise, conformality of the surface Σ to a sphere S preserving meridians means in spherical coordinates that

$$ds^2 + x(s)^2 d\theta^2 = h^2(s) (d\phi^2 + \cos^2 \phi d\theta^2)$$

so that a separable ODE relating s and ϕ results,

$$\frac{ds}{x(s)} = \frac{d\phi}{\cos \phi} \quad (\text{with } ds/d\phi = h) . \quad (66)$$

Proposition 8.

i) Let the parallel corresponding to a value s_o map over the circle of radius r_o in the plane. Then we have from (55)

$$r(s) = r_o \exp \left(\int_{s_o}^s \frac{ds}{x(s)} \right), \quad s \in [0, L]. \quad (67)$$

ii) We have $r = 0$ at the south pole and $r = \infty$ at the north pole. Moreover, $r = r(s)$ monotone in $s \in [0, L]$.

iii) Take the unit sphere with its equator on plane Π . If the parallel $s = s_o$ in the surface is made to correspond to the parallel $\phi = \phi_o$ in the sphere, then

$$\sec \phi + \tan \phi = \kappa \exp \left(\int_{s_o}^s \frac{ds}{x(s)} \right), \quad \kappa = \sec \phi_o + \tan \phi_o. \quad (68)$$

iv) The left hand side $r = \sec \phi + \tan \phi$ in (68) is the stereographic projection from the north pole of the sphere to the equatorial plane.

Proof. Our assumptions (a) and (b) imply logarithmical divergence of the improper integral at $s = 0$ and $s = L$. Indeed, at these points $x(s) \sim s$. In fact, near the poles we can write

$$\frac{ds}{x} = \frac{\sqrt{1 + (dz/dx)^2} dx}{x} = \frac{dx}{x} + \frac{\sqrt{1 + (dz/dx)^2} - 1}{x} dx.$$

The first integrand takes care of the logarithmic divergences. The second term, that we call $m(x)$, can be rationalized:

$$\begin{aligned} m(x) &= \frac{\sqrt{1 + (dz/dx)^2} - 1}{x} = \\ &= \frac{(\sqrt{1 + (dz/dx)^2} - 1)(\sqrt{1 + (dz/dx)^2} + 1)}{x(\sqrt{1 + (dz/dx)^2} + 1)} = \\ &= \frac{(dz/dx)^2/x}{\sqrt{1 + (dz/dx)^2} + 1} \end{aligned} \quad (69)$$

Now we assumed that the surface is smooth at the poles, meaning that at $s = 0$ and $s = L$, where $x = 0$, we have $z = O(x^2)$. Thus $(dz/dx)^2/x = O(x)$.

For the proof of iii) and iv) is obvious, just recall the stereographic projection formula

$$r = \frac{\cos \phi}{1 - \sin \phi} = \frac{1 + \sin \phi}{\cos \phi} = \sec \phi + \tan \phi.$$

□

Let us assume in addition to (a), (b) in section 3.3 that $x(s)$ increases from $x = 0$ in the south pole to a maximum parallel with radius $x(c)$, for $s \in [0, c]$ and then decreases to 0 at the north pole for $s \in (c, L]$. We do not require, however, the surface to be convex. It can ‘wiggle’ in the z -direction.

This assumption is just for clarity. If the surface wiggles in the x -direction, it will become clear from the computations below that more switches in (71) would be done, at the end of each monotone interval.

In order to add some more flexibility, we use any parameter $t \in [a, b]$, with $t = a$ corresponding to the south pole, $t = b$ to the north pole, and $t = t_o$ corresponding to $s = c$. The circle with radius $r_o = 1$ in the target plane Π , will correspond to the parallel $t = t_o$ in the surface Σ , with radius $x_o = x(t_o)$:

$$r(t) = r_o \exp \left(\int_{t_o}^t \frac{\sqrt{\dot{x}^2 + \dot{z}^2}}{x(t)} dt \right)$$

This function $r(t)$ is increasing, with $r(a) = 0$, $r(b) = \infty$. We split the integrand into two parts as

$$\frac{\sqrt{\dot{x}^2 + \dot{z}^2}}{x} = \frac{|\dot{x}|}{x} + \left(\frac{\sqrt{\dot{x}^2 + \dot{z}^2} - |\dot{x}|}{x} \right).$$

We change variables in (69), now denoting the second term by $m(t)$.

$$m(t) = \frac{\sqrt{\dot{x}^2 + \dot{z}^2} - |\dot{x}|}{x} (= \frac{\dot{z}^2/x}{\sqrt{\dot{x}^2 + \dot{z}^2} + |\dot{x}|}) \geq 0 \quad (70)$$

Note that $\dot{x} > 0$ in (a, t_o) and it is < 0 in (t_o, b) and this reflects in the combination of exp and log integration of the first term. The result is

Proposition 9. *(Conformal map to the plane)*

$$r(t) = \begin{cases} \frac{x(t)}{x_o} A(t), & a \leq t \leq t_o \\ \frac{x_o}{x(t)} B(t), & t_o \leq t < b. \end{cases} \quad (71)$$

$$A(t) = \exp \left(- \int_t^{t_o} m(t) dt \right), \quad B(t) = \exp \left(\int_{t_o}^t m(t) dt \right) \quad (72)$$

$A(t)$ increases from A_o to 1 in $[a, t_o]$; $B(t)$ increases from 1 to B_o in $[t_o, b]$. Since $A(t_o) = B(t_o) = 1$ then $r_o = 1$.

Theorem 5. (*Conformal expansion at the poles*)

i) When the parallel corresponding to $t = t_o$ is sent to the equator of S^2 then

$$h_{\Sigma/S^2}(\text{south}) = \frac{x_o}{2A_o} \quad , \quad h_{\Sigma/S^2}(\text{north}) = \frac{x_o B_o}{2}$$

where

$$A_o = A(a) = \exp\left(-\int_a^{t_o} m(t) dt\right) < 1 \quad , \quad B_o = B(b) = \exp\left(\int_{t_o}^b m(t) dt\right) > 1$$

ii) The adjustment β is

$$\beta^2 = h_{\Sigma/S^2}(N)/h_{\Sigma/S^2}(S) = B_o A_o = \exp\left[\int_{t_o}^b m(t) dt - \int_a^{t_o} m(t) dt\right]$$

iii) The adjusted quadratic expansions of the conformal factors at the poles have coefficients (see Proposition 4)

$$\begin{aligned} \gamma_S &= (-1 + 2p_S/h) = -\frac{h^2}{\alpha_S^2}, \\ \gamma_N &= (-1 + 2p_N/h) = -\frac{h^2}{\alpha_N^2} \\ h^2 &= \frac{x_o^2}{4} e^M \quad , \quad M = \int_a^b m(t) dt \end{aligned} \tag{73}$$

Proof. i) Near the poles,

$$r \sim \frac{A}{x_o} \cdot x \quad (\text{south}), \quad r \sim \frac{Bx_o}{x} \quad (\text{north}) .$$

The conformal factor from the surface to the plane is $h_{\Sigma/\Pi} = x(t)/r(t)$, so

$$h_{\Sigma/\Pi}(\text{south}) = \rho_{\text{south}} = \frac{x_o}{A} \quad , \quad h_{\Sigma/\Pi}(\text{north}) = \rho_{\text{north}} \sim \frac{x_o B}{r^2} .$$

We then compose with the inverse of the stereographic projection of the unit sphere $X^2 + Y^2 + Z^2 = 1$ to its equatorial plane $Z = 0$, from the north pole. Along $Y \equiv 0$ this map is given by

$$|X| = \frac{2r}{1+r^2}$$

so the conformal factor from the plane to the sphere is

$$h_{\Pi/S^2} = \frac{r}{|X|} = \frac{1+r^2}{2} .$$

Just multiply, and compute at $r = 0$ and $r = \infty$.

ii) We apply Lemma 1: $\beta^2 = h_{\Sigma/S^2}(\text{north})/h_{\Sigma/S^2}(\text{south})$.

iii) B/A gives the exp of the total integral. □

Summary: the procedure to obtain the frequencies

- From the surface equation, find the coefficients $\alpha_{\text{south}}, \alpha_{\text{north}}$ of the local profiles $z \sim x^2/2\alpha$.
- Find the belt size x_o .
- Compute $M = \int_a^b m(t)dt$ and exponentiate.
- Insert in (73)
- Apply Proposition 4, using (42) to compute the frequencies.

A nice feature is that this bypasses computing the adjustment parameter β .

4 Examples

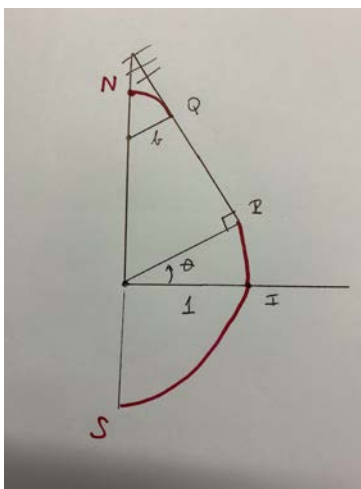
4.1 Matryoshkas

Our idealized matryoshka has two parameters b and θ , with $0 < \theta < \pi/2$. The largest cap is the south, and without loss of generality we may assume its radius $a = 1$; the north cap has radius $b < 1$. Here θ is the angle between the generating line of the conical part and the axis of symmetry.

The meridian profile is formed by three parts. In the first, take the arc $-\pi/2 \leq t \leq \theta$ in the circle $(\cos t, \sin t)$, starting in the south pole $S = (0, -a)$ with $t = -\pi/2$, to the point $P = (\cos \theta, \sin \theta)$ corresponding to $t = \theta$.

The transition from $\dot{x} > 0$ to $\dot{x} < 0$ occurs at $t_o = 0$, at the intermediate point $I = (1, 0)$. The second stretch is a segment of length $\ell = (1 - b) \cot \theta$. The third is the north cap, with opening $\pi/2 - \theta$ from the vertical. We add the possibility of $b = 1$, ℓ arbitrary, where the surface becomes a spheroid.

We simply ignore the issue that the profile is only C^1 .



Let us compute the integral $M = M(b, \theta)$. It will have three pieces $(x(t), z(t))$ for the integrand $(\sqrt{\dot{x}^2 + \dot{z}^2} - |\dot{x}|)/x$

- i) $(\cos t, \sin t)$, $t \in [-\pi/2, \theta]$
- ii) $(\cos \theta, \sin \theta) + t \ell$, $\ell = (1 - b) \cot \theta (-\sin \theta, \cos \theta)$, $t \in [0, 1]$
- iii) $(b \cos t, b \sin t)$, $t \in [\theta, \pi/2]$ + vert

The vertical translation in the third piece is irrelevant. The corresponding integrands are

- $$\frac{1 - |\sin t|}{\cos t}, t \in [-\pi/2, \theta]$$
- $$(1 - b) \frac{1 - \sin \theta}{\sin \theta} \frac{1}{(1 - t(1 - b))}, t \in [0, 1]$$
- $$\frac{1 - |\sin t|}{\cos t}, t \in [-\pi/2 + \theta, \pi/2 - \theta]$$

Interestingly, the parameter b appears both numerator and denominator of the third integrand, so their integrals merge into the same,

$$\int_{-\pi/2}^{\pi/2} \frac{1 - \sin |t|}{\cos t} dt = 2 \int_0^{\pi/2} \frac{1 - \sin t}{\cos t} dt = 2 \int_0^{\pi/2} \frac{\cos t}{1 + \sin t} dt = 2 \log 2$$

The integral in the middle

$$\int_0^1 \frac{1}{(1 - t(1 - b))} dt = \frac{-\log b}{1 - b}$$

so

$$M = 2 \log 2 - \log b \frac{1 - \sin \theta}{\sin \theta}, \quad h^2 = b^{(1 - \sin \theta) / \sin \theta} < 1$$

Now, the profile coefficients are

$$\alpha_S = 1, \quad \alpha_N = b$$

Proposition 10.

i) The coefficients in (42) to compute the Matryoshka frequencies are

$$\gamma_S = -b^{(1 - \sin \theta) / \sin \theta}, \quad \gamma_N = -\frac{b^{(1 - \sin \theta) / \sin \theta}}{b^2} \quad (74)$$

ii) One of the Matryoshka frequencies vanishes when $\theta = \pi/6$, independently of the parameter b .

iii) We also add the exceptional case $b = 1$, ℓ arbitrary, where formally $\gamma_S = \gamma_N = 1$.

Proof. Apply (73) with

$$\alpha_S = 1, \quad \alpha_N = b.$$

An interesting case is when a pair of eigenvalues vanishes; we saw that this happens when $\gamma_S \gamma_N = 1$. Applying (74) we must have

$$(1 - \sin \theta) / \sin \theta = 1.$$

□

Remark 3. *One can use this methodology for smooth oval profiles of one's preference. However, we think that the Matryoshka example captures the phenomenon that we were looking for, exceptional cases where one of the eigenvalue pairs vanish³.*

4.2 Ellipsoid of revolution

For the ellipsoid $x^2 + y^2 + z^2/c^2 = 1$, the profiles are $z \sim x^2/2\alpha + \dots$ so

$$\alpha_{S,N} = 1/c$$

(see (65)) and the width is $x_o = 1$. With the usual parametrization

$$x = \cos t, \quad z = c \sin t, \quad t \in [-\pi/2, \pi/2],$$

the procedure gives

$$\gamma_N = \gamma_S = \gamma(c) = -\frac{c^4}{4} \exp \left(2 \int_0^{\pi/2} \frac{\cos t}{\sqrt{\sin^2 t + c^2 \cos^2 t + \sin t}} dt \right) \quad (75)$$

which we may insert in (63).

Although the integral can be obtained by elementary methods, the end result split in the two cases $c \gg 1$, and the formulas are a bit cumbersome.

³The reader can amuse himself or herself by looking at these web pages:
<https://mathcurve.com/surfaces.gb/ovoid/ovoid.shtml>
<http://www.mathematische-basteleien.de/eggcurves.htm>
http://nyjp07.com/index_egg_E.html
https://en.wikipedia.org/wiki/Cassini_oval
https://en.wikipedia.org/wiki/Matryoshka_doll
<https://www.faberge.com/the-world-of-faberge/the-imperial-eggs>

Proposition 11. *The graph of the ratio of the two frequencies*

$$f(c) = \left| \frac{1 + \gamma(c)}{1 - \gamma(c)} \right|, \quad c > 0.$$

is *DESCRIBE + FIGURE*. Here the numerator is the frequency in the invariant submanifold space, and the denominator the frequency in the transverse space.

Note as a check that for $c = 1$ (sphere), the integral gives $\ln 2$, so $\gamma = -1$ as we already know. For $c \rightarrow 0$, it is readily seen that $\gamma \rightarrow 0$, so the ratio of frequencies is 1, as we also have seen. Moreover, for $c \rightarrow \infty$, $\gamma \rightarrow \infty$, and the ratio of frequencies also tends to 1.

Adriano, poderia fazer esse grafico? pode integrar numericamente, variando $c = 0.1$ ate' digamos $c = 5$.

4.3 Mr. Bean surfaces

The “bean” family of surfaces of revolution was considered in [15]. The meridian is given by

$$z = \frac{1}{2} b \cos^2 \phi + c \sin \phi, \quad x = \cos \phi, \quad \phi \in [-\pi/2, \pi/2]. \quad (76)$$

The surface develops a depression in the north pole when $b > c$, but this does not matter for us: the x -coordinate has only one maximum $x_o = 1$.

For $b = 0$ the family reduces to the ellipsoids of revolution $\mathcal{E}(1, 1, c)$ that we just considered.

Eliminating ϕ , the meridian profile is

$$z = (b/2)x^2 \pm c \sqrt{1 - x^2} \quad (77)$$

where the bottom sign is for the southern region $\phi \in [0, -\pi/2]$, the upper sign for the northern region $\phi \in [0, \pi/2]$. At the poles the local profile is

$$z \sim \pm c + \left(\frac{b}{2} \mp \frac{c}{2}\right) x^2$$

so we get immediately

$$\alpha_S = \frac{1}{b + c} \quad (78)$$

$$\alpha_N = \frac{1}{|b - c|} \quad (79)$$

The required definite integral is

$$M = M(b, c) = \int_{-\pi/2}^{\pi/2} m(t) dt$$

with

$$m(t) = \frac{\cos \phi (b \sin \phi - c)^2}{\sqrt{\cos^2 \phi (b \sin \phi - c)^2 + \sin^2 \phi + |\sin \phi|}}$$

Note that $M(b, c)$ is an incomplete elliptic integral, computable in closed form.

Since the belt radius is $x_o = 1$ we have

Proposition 12. *(Mr. Bean surfaces) For the surfaces given by (76)*

$$\gamma_S = -\frac{1}{4}(b+c)^2 e^{M(b,c)} \quad , \quad \gamma_N = -\frac{1}{4}(b-c)^2 e^{M(b,c)}$$

Since $x(\phi)$ has only one maximum (does not matter that Mr. Bean is not convex), we can use formula (73) in Proposition 9. We use (42) in Proposition 4 to compute the frequencies. The ratio ω_-/ω_+ is depicted in figure FAZER E REFERENCIAR.

ADRIANO: de novo, poderia graficar a razao? aqui voce usa a formula para as frequencias dadas por (42). Sugiro escolher um valor de b e variar c e/ou vice versa. Produzir figura e tabela de valores...

4.4 The elliptic vortex billiard

In 1869 H.A. Schwarz gave the conformal map from the unit disk D in the complex plane ω to the interior of an ellipse $R = R_r$ in the ξ -plane ([16], [17]; see also [18], [19]):

$$\omega \mapsto \xi = \sin \left[\frac{\pi}{2K(r)} F\left(\frac{\omega}{\sqrt{r}}; r\right) \right]$$

where F is the incomplete elliptic integral of the first kind

$$F(w; r) = \int_0^w \frac{dt}{\sqrt{(1-t^2)(1-r^2 t^2)}} .$$

Let $\tau = \tau(r)$ be defined via the “master equation”

$$\frac{K\left(\sqrt{1-r^2}\right)}{K(r)} = \frac{4\tau}{\pi} , \quad r \in (0, 1), \quad \tau \in (0, \infty)$$

where $K(r) = F(1, r)$ is the complete (real) elliptic integral.

We can use either $r \in (0, 1)$ or $\tau \in (0, \infty)$ to define the ellipse parameters: the ellipse semiaxis are

$$c = \cosh \tau > b = \sinh \tau$$

so the foci are at ± 1 in the ξ -plane. As $r \rightarrow 1$ the numerator in the master equation becomes $K(0) = \pi/2$ and the denominator $K(1) = \infty$, so $\tau \rightarrow 0$ (the segment). As $r \rightarrow 0$, then $\tau \rightarrow \infty$ (a very large disk).

We proceed as before, in the example of the circular vortex billiard. The south pole of the unit sphere in the (X, Y, Z) space is sent to the origin of ω -plane by stereographic projection to the equatorial plane from $(0, 0, 1)$.

We denote by $h(X, Y, Z)$ the conformal factor of the composition

$$s = (X, Y, Z) \xrightarrow{\text{stereographic}} \omega \text{ (disk)} \xrightarrow{\text{Schwarz}} \xi \text{ (ellipse)} .$$

The reader should bare with us the following calculations. First, we expand the integrand of the incomplete $F(\cdot, r)$

$$1/\sqrt{(1-t^2)(1-r^2 t^2)} \sim 1 + \frac{1}{2}(1+r^2)t^2$$

Hence

$$F\left(\frac{w}{\sqrt{r}}; r\right) \sim \frac{w}{\sqrt{r}} + \frac{1}{6}(1+r^2) \frac{w^3}{r\sqrt{r}} \quad (80)$$

Denote for short, $K = K(r)$. Inserting in the sine series we get up to third order,

$$\xi = \frac{\pi}{2K} \left[\frac{w}{\sqrt{r}} + \frac{1}{6}(1+r^2) \frac{w^3}{r\sqrt{r}} \right] - \frac{1}{6} \left(\frac{\pi}{2K} \right)^3 \frac{w^3}{r\sqrt{r}}$$

Collecting the cubic terms, we get the local expansion

$$\xi = \frac{\pi}{2K(r)\sqrt{r}} \left(w + \frac{1}{3} M w^3 \right) + \dots \quad (81)$$

where

$$M = M(r) = \frac{1}{2r} \left(1 + r^2 - \frac{\pi^2/4}{K^2(r)} \right). \quad (82)$$

Lemma 4. $M(r)$ increases from 0 to 1 in the interval $0 \leq r \leq 1$.

Proof. Since $K(0) = \pi/2$, in the limit $r \rightarrow 0$ (circle) we get $M \rightarrow 0$. Likewise, in the limit $r \rightarrow 1$, we get $M \rightarrow 1$. \square

See the table below for intermediate values.

r	K(r)	M(r)
0.1	1.574745562	0.07504711
0.2	1.586867847	0.1503827
0.3	1.60804862	0.22632604
0.4	1.639999866	0.30326745
0.5	1.685750355	0.38173312
0.6	1.750753803	0.46250971
0.7	1.845693998	0.54692635
0.8	1.995302778	0.63765125
0.9	2.280549138	0.74199017
0.95	2.590011231	0.80772582
0.99	3.356600523	0.88944538
0.995	3.696875082	0.90928962
0.999	4.495596396	0.9388965
0.9995	4.841257367	0.94733652
0.9999	5.645148217	0.96128293
1	11.40135369	0.99050933

We now compute the conformal factor. We have

$$h_{R_r/D}^2 = \frac{d\xi}{dw} \cdot \frac{\overline{d\xi}}{d\bar{w}} \sim \left(\frac{\pi/2}{K\sqrt{r}} \right)^2 [1 + M(w^2 + \bar{w}^2)]$$

Write

$$D : w = u + iv, \quad u^2 + v^2 \leq 1.$$

Then

$$h_{R_r/D}^2 \sim \left(\frac{\pi/2}{K\sqrt{r}} \right)^2 [1 + M(w^2 + \bar{w}^2)] = \left(\frac{\pi/2}{K\sqrt{r}} \right)^2 [1 + 2M(u^2 - v^2)]$$

Therefore

$$h_{R_r/S^2} = \frac{\pi}{2K\sqrt{r}} [1 + M(u^2 - v^2)] \cdot \frac{1}{2} \left(1 + \frac{1}{4}(X^2 + Y^2) \right)$$

Near the south pole $(0, 0, -1)$, we have as before $u \sim X/2$, $v \sim Y/2$ so that

$$h_{R_r/S^2} = \frac{\pi}{2K\sqrt{r}} \left[1 + \frac{M}{4}(X^2 - Y^2) \right] \cdot \frac{1}{2} \left(1 + \frac{1}{4}(X^2 + Y^2) \right)$$

Collecting terms we are lead to

Proposition 13.

i) The conformal map from the double faced ellipse to the unit sphere expands at the poles (corresponding to the center of the faces) as

$$h_{R_r/S^2} = \frac{\pi}{4K\sqrt{r}} \left[1 + \frac{p'}{2}X^2 + \frac{q'}{2}Y^2 \right]. \quad (83)$$

$$p' = \frac{1+M}{2}, \quad q' = \frac{1-M}{2} \quad (84)$$

$$M = \frac{1}{2r} \left(1 + r^2 - \frac{\pi^2/4}{K^2(r)} \right) \quad (85)$$

ii) Therefore we have always the center-center case with equal frequencies

$$\omega_1 = \omega_2 = \sqrt{1 - M^2}$$

(when $r \rightarrow 0$ (circle), $M = 0$, $p' = q' = 1/2$, and in the limit $r \rightarrow 1$, $M = 1$ so $p' = 1$, $q' = 0$.)

Proof.

$$4p'q' = 4(1-p')(1-q') = 1 - M^2. \quad (86)$$

□

5 Conclusion

In this work we continued our previous paper [7], presenting here the general linear analysis of an equilibrium pair, based on the quadratic expansions of the conformal factor h . We provided some more examples for surfaces with antipodal symmetries and for surfaces of revolution. We end with some questions, hoping to attract interest to the theme.

- i) In the characteristic polynomial of the main Theorem, can all (ρ, κ) be attained when the parameters vary? If not, what is the range?
- ii) Nonlinear analysis of equilibria via Hamiltonian normal form methods, from higher order expansions of h .
- iii) Inverse shape problems (the objectives must be thought about).
- iv) Study of systems of more than two vortices, with total vorticity arbitrary. In particular the stability of vortex rings.
- v) Immersion/embedding of genus zero Riemann surfaces (Σ, g) in \mathbf{R}^3 , with prescribed conditions on the conformal factor at a pair of points.

Let us briefly comment on items i) and v).

There are five parameters $p_1/h, q_1/h, p_2/h, q_2/h, \theta$, There are no restrictions on them since Morse functions $h(s)$ on the sphere can be constructed with arbitrary quadratic expansions at two chosen critical points. Classifying all the eigenvalue cases is in order. In particular we would like to have a concrete surface in \mathbf{R}^3 with a loxodromic equilibrium.

Gromov showed that $(\Sigma, h^2 g_o)$ can be isometrically embedded in R^5 (see [20], p. 298)⁴. It is to be expected that p/h is not arbitrary in a “physical” surface of revolution. For surfaces in \mathbf{R}^3 , the arc length along a meridian starting at a pole satisfies $s > x(s)$, for $s > 0$. An abstract S^1 equivariant metric in S^2 can violate this condition. Consider the family of metrics on the sphere with coordinates (ϕ, θ) given by $ds^2 = \alpha^2 d\phi^2 + \cos^2 \phi d\theta^2$ with $0 < \alpha < 1$. Then along the meridians $s = \alpha\phi < \phi$. This is a simple example, but already illustrates the depth of Gromov C^∞ embedding results. Does the added request about the quadratic expansions matter?

⁴See also the discussion in

<https://mathoverflow.net/questions/37708/nash-embedding-theorem-for-2d-manifolds>

Acknowledgements.

We thank bla ... This research was supported by

References

- [1] A.M.Turner, V. Vitelli and D.R.Nelson, Vortices on Curved Surfaces, *Rev. Mod. Phys.* 82 1301–1348 (2010).
- [2] Mark Keil, Omer Amit, Shuyu Zhou, David Groswasser, Yonathan Japha, Ron Folman, Fifteen years of cold matter on the atom chip: promise, realizations, and prospects, *Journal of Modern Optics*, 63:18, 1840-1885 (2016).
- [3] T. W. Neely, E. C. Samson, A. S. Bradley, M. J. Davis, and B. P. Anderson, Observation of Vortex Dipoles in an Oblate Bose-Einstein Condensate *Phys. Rev. Lett.* 104, 160401 (2010).
- [4] Y. Kimura, Vortex Motion on Surfaces with Constant Curvature, *Proc. R. Soc. Lond. Ser. A Math. Phys. Eng. Sci.*, 455: 1981, 245-259 (1999).
- [5] S. Boatto and J. Koiller, Vortices on Closed Surfaces, in *Geometry, Mechanics, and Dynamics: The Legacy of Jerry Marsden*, D.E. Chang, D. D. Holm, G. Patrick, T. Ratiu (Eds.), *Fields Inst. Commun.*, vol. 73, New York: Springer, 2015, pp. 185-237.
- [6] A. R. Rodrigues, C. Castilho, and J. Koiller, Vortex Pairs on a Triaxial Ellipsoid and Kimuras Conjecture, *J. Geom. Mech.*, 10:2, 189-208 (2018).
- [7] J. Koiller, C. Castilho and A. R. Rodrigues Vortex Pairs on the Triaxial Ellipsoid: Axis Equilibria Stability, *Regular and Chaotic Dynamics* 24, 61-79(2019)
- [8] Q. Wang, The N-vortex Problem on a Riemann Sphere, *Commun. Math. Phys.* (2021) <https://doi.org/10.1007/s00220-021-04044-8> (arXiv:2003.05299)
- [9] R. Siciliano, Constructing Möbius Transformations with Spheres, *Rose-Hulman Undergraduate Mathematics Journal*, 13:2, 115-124 (2012)
- [10] C. W. Gear, O. Osterby, Solving Ordinary Differential Equations with Discontinuities, *ACM Transactions on Mathematical Software*, Association for Computing Machinery 10 (1), pp.23-44 (1984)

- [11] G. Mao, L. R. Petzold, Efficient Integration over Discontinuities for Differential-Algebraic Systems, *Computers and Mathematics with Applications*, 43, 65-79 (2002).
- [12] L. Dieci and L.Lopez, A survey of numerical methods for IVPs of ODEs with discontinuous right-hand side, *Journal of Computational and Applied Mathematics*, 236: 16, 3967-3991 (2012).
- [13] J. Vankerschaver and M. Leok, A Novel Formulation of Point Vortex Dynamics on the Sphere: Geometrical and Numerical Aspects, *J. Non-linear Sci.* 24, 1-37(2014).
- [14] R. McLachlan, K. Modin, O. Verdier, A minimal-variable symplectic integrator on spheres, *Math. Comp.* 86, 2325-2344 (2017).
- [15] D.G. Dritschel and S. Boatto, The motion of point vortices on closed surfaces. *Proc. R. Soc. A* 471: 20140890 (2015).
- [16] H. A. Schwarz, Ueber einige Abbildungsaufgaben, *Journal für die reine und angewandte Mathematik* 70 (1869), pgs. 105-120. available also in *Gesammelte Mathematische Abhandlungen*, vol. 2, Julius Springer, pgs. 65–82.
- [17] H. A. Schwarz, Notizia sulla rappresentazione conforme di un' are ellittica sopra un' area circolare, *Annali di Matematica pura ed applicata*, II serie, tomo III, pg. 166–170, 1869 (*Gesammelte Mathematische Abhandlungen*, vol. 2, pg. 102-107)
- [18] Szego, G., Conformal Mapping of the Interior of an Ellipse onto a Circle, *The American Mathematical Monthly*, 57: 7, 474–478 (1950)
- [19] Kanas, S., Sugawa, T., On conformal representations of the interior of an ellipse, *Annales Academiæ Scientiarum Fennicæ Mathematica* 31, 329- 348 (2006)
- [20] M. Gromov, *Partial Differential Relations*, Springer, 1986.

Project:

The vortex pair on Bolza's surface: an experimental investigation

"In mathematics and in life it is not okay to give up on a problem
or a cause just because the struggle is difficult."

(Chandler Davis)¹

Contents

1	Introduction	2
2	A vortex pair system is never chaotic	2
3	Theoretical questions.	3
4	Constructing Poincaré sections	4
5	Robin function of Bolza's surface (C. Ragazzo)	5
6	Bolza's Green function and its derivatives.	7
7	Weierstrass points (see Ragazzo's paper)	8
8	Implementation: mapping $\mathcal{F}_{\text{Bolza}}$ to the unit disk?	12
A	Eigenfunctions of Bolza's: a poor man's way	15
B	The unit disk or hemisphere to represent $\mathcal{F}_{\text{Bolza}}$	17
C	Mapping curvilinear triangles to upper half plane	19

¹<https://link.springer.com/article/10.1007/s00283-013-9419-z>
See also: <https://www.ams.org/publicoutreach/math-history/hmath1-davis30.pdf>

1 Introduction

We discuss some of the numerical challenges for the study the vortex pair system on a compact surface

$$z \in X = \mathbb{H}/G,$$

where $\Gamma \subset \mathrm{PSL}_2(\mathbb{R})$ is a cocompact Fuchsian subgroup acting on the upper half plane \mathbb{H} , via Moebius transformations. As X is compact, Γ does not have elliptic or parabolic elements. We also use the Poincaré disk $w \in \mathbb{D}$, for which the hyperbolic metric is $2/(1 - |w|^2)|dw|$.

Bolza's² is a Riemann surface for which many results are known. It will be the object of the experimental investigation.

We want to produce pictures and quantitative results. But of what kind? What would be the purpose? What theoretical questions could emerge from the investigation?

2 A vortex pair system is never chaotic

Recall Anosov's famous result: on a compact manifold of constant negative curvature the geodesic flow is chaotic³. Anosov flows are not only mixing, but even Bernoullian⁴. Poincaré section never show KAM tori⁵.

This is not what happens for the vortex pair system, for a very simple reason. Denote G_X the Green function and $R(z) = \lim_{w \rightarrow z} G_X(w, z) - \log d_{\mathrm{hyp}}(w, z)$ the Robin function. The rescaled Hamiltonian

$$F(x_1, y_1; x_2, y_2) = \frac{\exp G_X(z_1, z_2)}{\sqrt{\exp R(z_1)} \sqrt{\exp R(z_2)}} \quad (1)$$

is symmetric in z_1, z_2 and $F \sim d_{\mathrm{hyp}}$ near the diagonal.

²https://en.wikipedia.org/wiki/Bolza_surface

³D. V. Anosov, Proc. Steklov Math. Inst. 90, 1 (1967)

⁴Ornstein, D., Weiss, B. Geodesic flows are Bernoullian. Israel J. Math. 14, 184–198 (1973) <https://doi.org/10.1007/BF02762673>

⁵A. N. Kolmogorov, Dokl. Akad. Nauk. SSSR, 98, 527 (1954); V. I. Arnold, Soviet Math. Dokl., 2, 501 (1961); J. Moser, Nachr. Akad. Wiss. Göttingen, Math. Phys. Kl, p.1 (1962)

Since X is compact,

$$\max F = M < \infty \quad (2)$$

(the *hydrodynamical diameter*). Even without special discrete symmetries, critical points appear on a pair of pairs, (z_1^*, z_2^*) and (z_2^*, z_1^*) .

For energy levels a lit bit smaller than M , KAM behavior is expected to be observed, as the equilibrium point (z_1^*, z_2^*) is of elliptic type. The vortex pair symplectic form is the difference of the pullbacks of the area form

$$\Omega_{pair} = \pi_1^* \omega - \pi_2^* \omega, \quad \omega = 4dx \wedge dy / (1 - |z|^2)^2, \quad z \in \mathbb{D} \quad (3)$$

It is trivial to adapt a symplectic integrator.

3 Theoretical questions.

A good many theoretical questions could be asked to go in pair with the experimental investigation. Here's a just a few.

1. Can the hydrodynamical diameter M be estimated? Is it related to the spectrum? Or the length spectrum?
2. What can be discovered about the location of this pair (z_1^*, z_2^*) in the fundamental domain \mathcal{F}_X ? How does the pair change as the metric varies in the fixed conformal class of (x, g_o) ? How about moving along the Teichmüller space?
3. The two frequencies of the linearization around these (z_1^*, z_2^*) that gives $F = M$ encode some geometrical information? Can one get normal forms? Do resonances appear in special values of the $3g - 3$, $g \geq 2$ complex parameters as one changes the complex structure?
4. How about the other equilibrium points? How many and the corresponding indices? (numerical study is in order).
5. Is F a Morse function in $X \times X - \text{diagonal}$ for the constant curvature metric? Is it generically Morse when a conformal factor is introduced, as it was shown for genus zero⁶ ?

⁶<https://link.springer.com/article/10.1007/s00220-021-04044-8>,
<https://link.springer.com/article/10.1007/s00205-018-1300-y>

6. F vanishes on the diagonal. The relative cohomology of $H^*(X \times X/\text{diagonal})$ can be easily determined. What does this topological information entail about the number and type of equilibrium points?
7. For $F = 0$ the system is the geodesic flow in the unit tangent bundle. Continuation of closed geodesics to periodic solutions in $F = c$ for small values of $c > 0$.
8. Can symplectic geometry tools like SFT be employed in this setting?

4 Constructing Poincaré sections

Fixed some $z^* \in \mathbb{H}$, all the calculations should be done inside the *Dirichlet fundamental domain* \mathcal{F}_{X,z^*} centered around z^* , which is defined as

$$\mathcal{F}_{X,z^*} := \{w \in \mathbb{H} \mid d_{\text{hyp}}(z^*, w) < d_{\text{hyp}}(z^*, \gamma w), \text{ for all } \gamma \in \Gamma \setminus \{\text{id}\}\} \quad (4)$$

Usually one takes $z^* = i$ in the \mathbb{H} representation and $z^* = 0$ in the \mathbb{D} representation, and omit the label z^* , so it will be denoted \mathcal{F}_X .

When the fundamental domain is crossed, bringing the points back should not bring excessive numerical error. It would be important to have a nice way to visualize on a convenient model. Determining/estimating the sources of error for long time integration is a challenge to the numerical analyst. We hope that the hard work to produce Poincaré sections would be worthwhile. This effort *obiter dictum* could produce some new insights on Green, and Batman functions.

At the level $F = 0$ the vortex pair system becomes the geodesic system in the unit tangent bundle $U(X)$. Therefore Poincaré sections will exhibit total chaotic behavior.

On the other extreme, $F = M$, for a level c slightly less than M one should observe typical KAM behavior near an elliptic equilibrium - when the frequencies have resonances there is a plethora of possibilities.

Surfaces of section at intermediate values should exhibit a complicated mix of both chaos and invariant curves. For intermediate values, what insights could Poincaré sections provide us ?

The values of Green and Robin functions would be computed (and stored) for a representative number of points in the fundamental domain \mathcal{F}_X . Can Delaunay triangulations be helpful?⁷

Numerical differentiation could be done using the tabulated values of G and R , but ideally one would like to devise a direct computational method for partial derivatives up to a desired order (see section 6 below).

5 Robin function of Bolza's surface (C. Ragazzo)

The reference is the paper by C. Ragazzo on Robin's function for Bolza's surface⁸. Here's a short account (by himself). In principle, for any surface X , its Green function G_X can be obtained integrating the heat kernel of X for $t \in (0, \infty)$. Two standard representations exist⁹.

In the first, one starts with the well known formula for the heat kernel of the universal cover \mathbb{H} . To produce the heat kernel on X , one takes all the replicas of the Dirac delta as an initial condition.

For short times this representation provides good service, because as the solution originating from each delta decays in space like a Gaussian, so a small number of deltas is sufficient to describe well the heat kernel restricted to a fundamental domain of the surface.

However, as time goes on the Gaussians start to widen in space and the number of Gaussians to be used in the description becomes prohibitive.

So one uses the second representation which is the spectral one summing $\exp(-\lambda_i t)$ times the products $\phi_i(z)\phi_i(w)$ of L^2 normalized eigenfunctions.

This is good for long times, since the time decay in each mode is exponential, with rate equal to the Laplacian's eigenvalue. In the end of the day, just a few modes are enough to approximate the the heat kernel.

⁷<https://hal.inria.fr/hal-01568002>

⁸<https://royalsocietypublishing.org/doi/10.1098/rspa.2017.0447>

⁹See eg. Jorgenson, J., Kramer, J. (2006). Bounds on canonical Green's functions. *Compositio Mathematica*, 142(3), 679-700 doi:10.1112/S0010437X06001990.

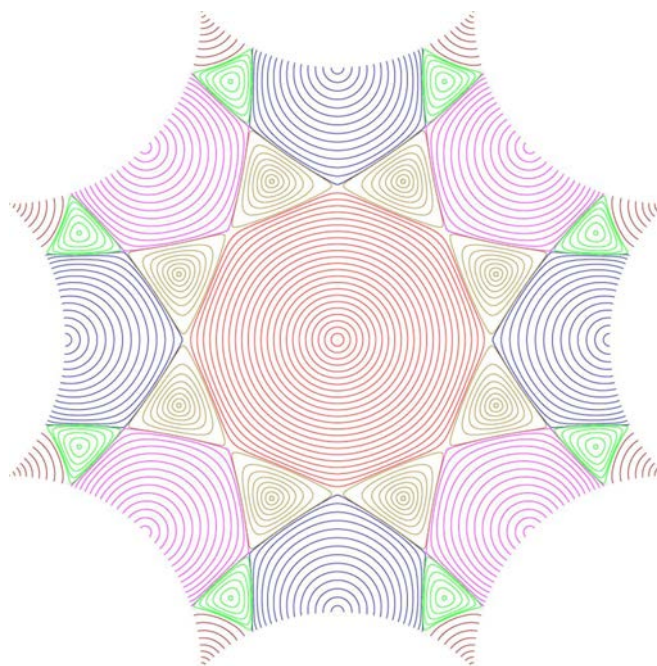
The difficulty is how to paste the two representations for intermediate times. It was necessary to invent several numerical tricks.

For the Robin function these tricks avoid calculating the eigenfunctions, only the eigenvalues are needed.

Clodoaldo: explain this? What are the locations/values of F at equilibria? Compare with Anil's estimates: we know r_X and λ_1 for Bolza's.

For Bolza's surface, the eigenvalues ≤ 1000 are available from Alexander Strohmaier's web page, with high precision¹⁰.

The picture below is from C. Ragazzo:



Robin function for Bolza's surface.

Check the Euler characteristic with the indices of the equilibria. For their location (and much more informations) see C. Ragazzo's paper.

¹⁰<http://www1.maths.leeds.ac.uk/~pmtast/publications/eigdata/datafile.html>

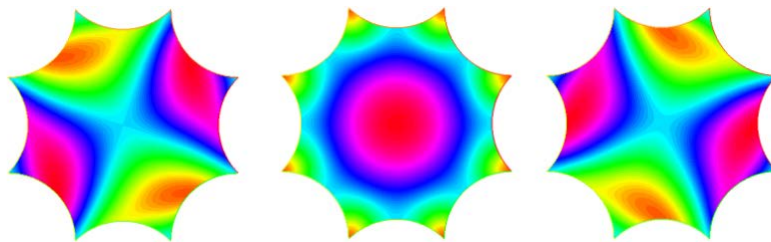
6 Bolza's Green function and its derivatives.

How much more difficult would it be to numerically calculate the Green function as compared with Robin's? For one thing, the domain has now two slots, but to store values to the square is not a big deal.

The logarithmic divergence on the diagonal should not be much of a problem; to study the dynamics outside a neighborhood of the diagonal, we would compute and store the values of G on a compact subset of $X \times X$ such that z_1, z_2 have hyperbolic distance $d_{\text{hyp}}(\cdot, \cdot)$ greater or equal than a conveniently chosen small value.

The basic idea would be the same as for Robin's function: for short times we start with the heat kernel in \mathbb{H} as before; for long times *it seems that there will be no escape from using eigenfunctions*, but still only a few may be required, for the same reason, the exponential decay in time.

The same procedures could be done for the partial derivatives (gradient, Hessians, and so on). Derivation increases the decay in the covering space which helps in the sum of the group replicas. Experts should be consulted for codes (or "home delivery") of the required quantity of eigenfunctions.



The first eigenspace of Bolza's has dimension 3. Source: wikipedia

The appendices present a poor's man approach to numerically compute the eigenfunctions of Bolza's surface.

Clodoaldo: do you have references or people to ask for files containing the eigenfunctions tabulated data?

7 Weierstrass points (see Ragazzo's paper)

In what follows S a closed Riemann surface of genus $g \geq 2$.

The set of Weierstrass points on X consists of all points s such that S admits a meromorphic function with a single pole of order less than $g + 1$ at s .

The surface S is called hyperelliptic if it has precisely $2g + 2$ Weierstrass points. Any closed Riemann surface of genus two is hyperelliptic.

Proposition 3.3¹¹. S is hyperelliptic if and only if there exists a conformal involution J (the hyperelliptic involution) that fixes exactly $2g + 2$ points; these fixed points are the Weierstrass points, and J is the unique conformal involution with exactly $2g + 2$ fixed points.

Theorem 3.2. (a) Let σ be an involutive orientation-preserving symmetry of S that is not the identity. Suppose that σ has a fixed point s . Then s is a singularity of the vortex velocity field. (b) Let σ_1 and σ_2 be two different orientation-reversing symmetries of S . Suppose that s is a fixed point of both. Then s is a singularity of the vortex velocity field.

Theorem 3.4. Every Weierstrass point of S is an equilibrium of the equations of motion of a single vortex on S .

Bolza's surface has several discrete symmetries and involutions, described with details in Ragazzo's paper.

These are obvious: the eight rotations

$$z \rightarrow e^{i\kappa\pi/4}z, \kappa = 1, \dots, 8,$$

that are orientation-preserving symmetries and the eight reflections that are orientation-reversing symmetries,

$$z \rightarrow e^{i\kappa\pi/4}\bar{z}, \kappa = 1, \dots, 8.$$

These are non-obvious: the involutions β_1, β_2 defined in eq. (4.1). Figs. 2 and 3 depict them. Fig. 4 explains the 96 symmetries of Bolza's surface.

Clodoaldo: are these 96 symmetries relevant for the vortex system?

¹¹Farkas HM, Kra I. 1980, Riemann surfaces, III. 7.9 .

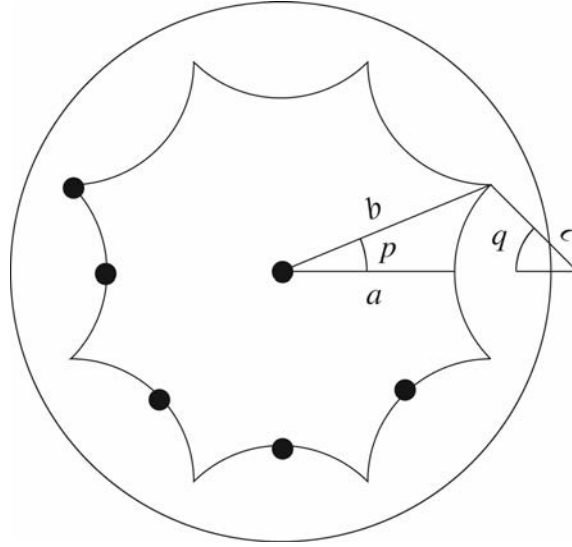


Figure 1 from Ragazzo. The eight vertices of the octagon represent the same point and opposite sides represent the same geodesic arc. \mathcal{F}_X and the hyperbolic metric are invariant under: eight rotations in multiples by $\pi/4$ and eight reflections across eight axes of symmetry (four of them connecting opposite vertices and four of them bisecting opposite sides). The geodesic triangle shown in the figure (with sides a, b , and half of a side of the octagon) is a fundamental domain in \mathcal{F}_X for this group of 16 symmetries. The angles in the figure are $p = \pi/8$ and $q = \pi/4$. The Euclidean lengths of the segments a, b and c are $E(a) = \sqrt{\sqrt{2} - 1}$, $E(b) = 2^{-1/4}$ and $E(c) = \sqrt{(\sqrt{2} - 1)/2}$ respectively. The hyperbolic lengths of the segments a and b , which are geodesic arcs, are $\ell(a) = 2 \operatorname{arctanh} E(a)$ and $\ell(b) = 2 \operatorname{arctanh} E(b)$. The conformal involution $z \rightarrow -z$ fixes the six points represented by small balls, that correspond to the six Weierstrass points of Bolza's surface.

Figures 2-4, next, depict two further involutions β_1, β_2 .

The geodesic triangle T

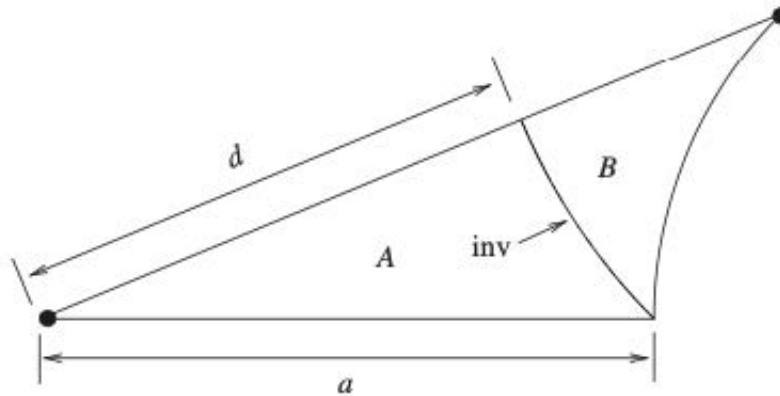


Figure 2. A detail of the geodesic triangle in figure 1. The arc of the Euclidean circle indicated as 'inv' is invariant under the symmetry β_1 . 'inv' divides the original triangle into two others: A and B . β_1 maps A onto B and maps the two points represented by small balls into each other. The Euclidean lengths of the segments a and d are $E(a) = (\sqrt{2} - 1)^{1/2}$ and $E(d) = 2^{1/4} - (\sqrt{2} - 1)^{1/2}$.

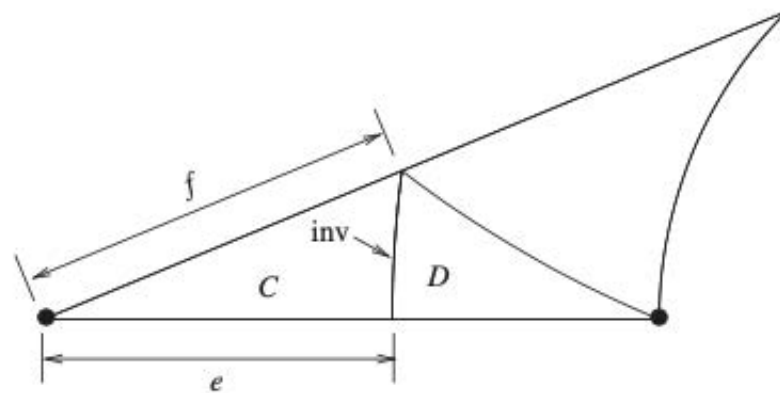


Figure 3. A detail of the geodesic triangle in figure 1. The arc of the Euclidean circle indicated as 'inv' is invariant under the symmetry β_2 . The two triangles indicated by C and D are contained in triangle A in figure 2. β_2 maps C onto D and maps the two points represented by small balls into each other. The Euclidean lengths of the segments e and f are $E(e) = (\sqrt{2} + 1)^{1/2} - 2^{1/4}$ and $E(f) = (1 + 3/\sqrt{8})^{1/2} - (3/\sqrt{8})^{1/2}$.

96 symmetries

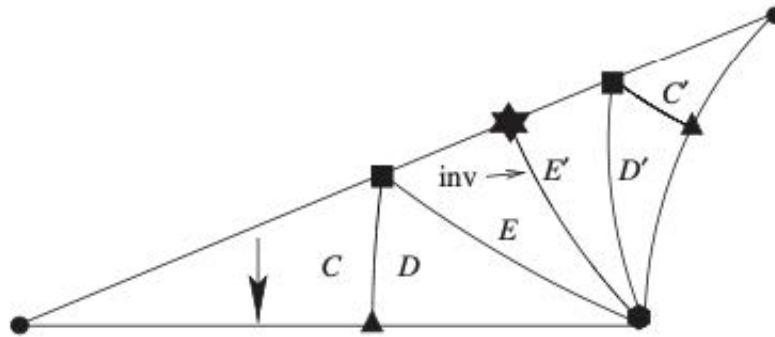


Figure 4. A detail of the geodesic triangle in figure 1. As in figure 2, the arc indicated as 'inv' is invariant under the symmetry β_1 . The three triangles marked with C , D and E are contained in triangle A in figure 2; they are mapped by β_1 onto C' , D' and E' , respectively. Each one of the six triangles in the figure is a fundamental domain of the full group of 96 symmetries of S . β_2 maps the triangle C onto D , as in figure 3, and an orientation-preserving symmetry σ_1 maps C onto E (σ_1 maps the point in C marked with a ball (triangle) to the point in E marked with a hexagon (star) and leaves invariant the point marked with a square). β_1 maps the two points represented by balls (triangles, squares) into each other and leaves invariant the points marked with a hexagon and a star. The coordinates of all points marked in the figure can be obtained using the information in figures 1, 2 and 3 and the expression for β_1 in equation (4.1).

8 Implementation: mapping $\mathcal{F}_{\text{Bolza}}$ to the unit disk?

We propose to compute and depict trajectories and Poincaré sections using as coordinates a complex variable w in the unit disk, that is conformally mapped to $\mathcal{F}_{\text{Bolza}}$:

$$z = z(w), \quad |w| \leq 1, \quad z \in \mathcal{F}_{\text{Bolza}}. \quad (5)$$

The vertices z_k of the octagon $\mathcal{F}_{\text{Bolza}}$ are mapped uniformly in the unit circle $|w| = 1$. This approach may please a numerical analyst: the $\pi/4$ kinks in the fundamental domain are smoothed, and one can use refined meshes near the corresponding w_κ .

This map can be constructed explicitly. Using the symmetries of Bolza's surface, the conformal map (5) can be reduced to triangular maps. This is done in appendix C. The same method can be applied to all generalized Bolza surfaces, of genus $\kappa \geq 2$. They correspond to regular 4κ -gons¹².

It remains to be seen if conformal maps of an irregular fundamental domain could be constructed for an arbitrary fuchsian group. Perhaps this could be of interest to a Teichmüller theorist, all information about the moduli is encoded in the conformal map.

The “onion”. We add another possibility for visualization, that could be aesthetically appealing : map via stereographic projection from the south pole the northern hemisphere of $S^2 \subset \mathbb{R}^3$ to the unit disk $|w| \leq 1$.

What is the point about mapping to the northern hemisphere? All replicas of $\mathcal{F}_{\text{Bolza}}$ will correspond either the south or the north hemispheres¹³. This is due to the old and honorable reflection principle for complex functions.

The philosophical point is this: in the (Escher like) tessellation of the Poincaré disk via replicas of $\mathcal{F}_{\text{Bolza}}$, their areas, as measured in Euclidian eyes, shrink fast as one approaches the unit circle.

¹²<https://hal.archives-ouvertes.fr/LORIA/hal-03080125v1>

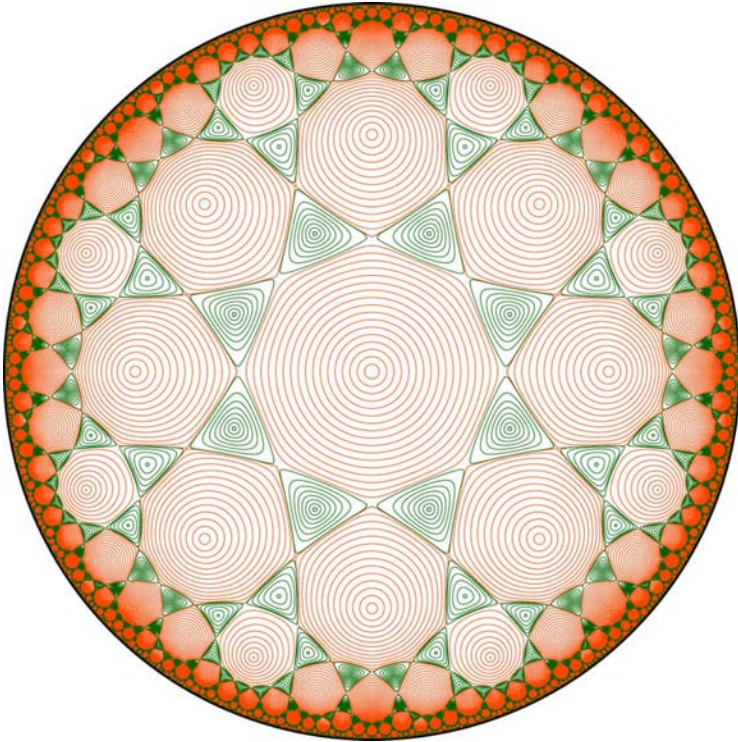
<https://arxiv.org/abs/2103.05960>, <https://hal.inria.fr/hal-01276386>

¹³This is like scissoring a polyhedrall surface to planify it. To track layers of this self covering object is the task for group or graph theorists, choosing arbitrary paths from the origin to a given point in the Poincaré disk.

This tessellation of Poincaré disk is replaced by a ‘hollow onion’, where the hemispherical replicas *are all congruent in the Euclidian sense*.

Somehow this may bring us a feeling of justice. We kind of everted curvature -1 to curvature +1.

Proving the pudding would show if the idea is useful numerically. Since the maximum area distortion from the disk to the hemisphere is 2, we will just work the conformal map from $\mathcal{F}_{\text{Bolza}}$ to the unit disk.



The replicas shrink fast in Euclidian eyes

Final comments

Should we start from scratch and try to compute the spectrum (eigenvalues + eigenfunctions) of Bolza's surface? From this data obtained by first principle we could derive the Green and Robin functions.

In the Appendix we suggest a numerical method based upon the conformal mapping approach. We wonder if will be competitive with methods currently in use by experts¹⁴.

As a first step, we propose a compromise. We would take advantage from using the already known eigenvalues ≤ 1000 given in the aforementioned web site of A. Strohmaier. So the task would be solely of finding the kernel of large linear systems.

We suggest applying finite differences in polar coordinates (rather than using finite elements or using trigonometric base functions). Near the vertices, to provide more precision, it is trivial to refine the polar coordinates grid.

To study the vortex pair system near the diagonal, one would like also to get hold of Batman's function B . A numerical method is in order to compute the leading term m_2 of its expansion near the diagonal, and the directional derivatives $dm_2.V_i$.

Ideally one wants a code to compute R, G, B, m_2 and their derivatives, allowing the fuchsian group to vary. With an algebraic description of the group generators of Γ , the above method should work the same way, once one could produce numerically a representative number of eigenvalues and eigenfunctions.

¹⁴<https://arxiv.org/pdf/1110.2150.pdf>

Appendices

A Eigenfunctions of Bolza's: a poor man's way

We now suggest a procedure that probably has not been implemented yet. One of us (JK) has outlined the idea in a short note (circa 1983?) at the Seminario Brasileiro de Análise. It is a long shot, and we may shot our own foot. But if it is doable it may have some interest to the experts.

The idea is use the the conformal mappings that we described in the previous section so that the spectral problem in Bolza's surface (represented as the fundamental octogon $z \in \mathcal{F}_{\text{Bolza}}$) becomes an equivalent spectral problem. Conceptually we should do it in the hemisphere, but as we mentioned, we think it will be just as numerically efficient to do it in the unit disk of the $w = u + iv$ -plane.

The spectral problem will be

$$L_\lambda \phi = 0 \quad , \quad L_\lambda = \Delta - \lambda m(r, \theta) \mathbb{I} \quad (6)$$

where

$$\Delta = \frac{\partial^2}{\partial r^2} + \frac{1}{r} \frac{\partial}{\partial r} + \frac{1}{r^2} \frac{\partial^2}{\partial \theta^2}$$

is the usual Laplacian operator in polar coordinates. Eigenfuntions are the same: just compose back with the map from $w = r \exp(i\theta)$ to z .

Boundary conditions on the eight arcs of the equator correspond uniformly, the same conditions that in $z \in \mathcal{F}_{\text{Bolza}}$.

Let us explain how the “mass” term $m(r, \theta)$ is computed.

Recall that in an isothermal chart $z = x + iy$ on a surface S with metric g , the metric writes locally as $ds^2 = h(z, \bar{z}) |dz|^2$. The the Laplace-Beltrami operator is

$$\Delta = (1/h)(\partial^2/\partial x^2 + \partial^2/\partial y^2).$$

For the hyperbolic metric in Poincaré disk, $h = 4/(1 - |z|^2)^2$, and hyperbolic Laplacian in $\mathcal{F}_{\text{Bolza}} \subset \mathbb{D}$ is therefore

$$\Delta_{\mathbb{D}} = \frac{(1 - |z|^2)^2}{4} (\partial^2/\partial x^2 + \partial^2/\partial y^2).$$

Let us interpret the $w = u + iv$ as coordinates in X , parametrizing the fundamental domain $\mathcal{F}_{\text{Bolza}}$. In these, the metric becomes

$$ds_{\mathbb{H}}^2 = \frac{4}{(1 - |z(w)|^2)^2} \left| \frac{dz}{dw} \right|^2 |dw|^2 \quad (7)$$

so that the Laplacian is

$$\Delta_{\mathbb{H}} = \frac{(1 - |z(w)|^2)^2}{4 \left| \frac{dz}{dw} \right|^2} (\partial^2/\partial u^2 + \partial^2/\partial v^2) \quad , \quad |w| \leq 1.$$

The spectral problem will have the above form (6), with

$$m = \frac{4 |dz/dw|^2}{(1 - |z(w)|^2)^2} \quad , \quad w = r e^{i\theta} \quad , \quad 0 \leq r \leq 1 \quad (8)$$

The denominator in m does not vanish: its minimum value occurs at the vertices

$$z_{\kappa} = \frac{1}{2^{1/4}} w_{\kappa} \quad , \quad 0 \leq \kappa \leq 7.$$

corresponding to

$$w_{\kappa} = e^{i(\frac{\pi}{8} + \kappa \frac{\pi}{4})}.$$

The numerator will be computed using the intermediary ξ -half plane,

$$|dz/dw| = |dz/d\xi d\xi/dw| = |dz/d\xi| |dw/d\xi|. \quad (9)$$

It turns out that it suffices to know $z = z(\xi)$ and $w = w(\xi)$ in the triangles T and P . The vertices of the triangles will correspond to $\xi = 0$ (mapped to the origin), $\xi = 1$ (mapped to points in the positive real axis), $\xi = \infty$ (mapped to points in the $\pi/8$ -ray).

In the quotient (9) the singularities corresponding to $\xi = 0$ and $\xi = 1$ disappear. But not at $\xi = \infty$.

It seems that the numerical challenge is to expand and match the expansions $z = z(\xi)$ and $w = w(\xi)$ near $\xi = \infty$, in order find a good approximation for $z = z(w)$ near the z_{κ} . What we already know is that the map $w \rightarrow z$ from the unit circle to the fundamental domain will have singularities only at vertices w_{κ} :

$$z - z_{\kappa} \sim (w - w_{\kappa})^{1/4}.$$

Whatever might be the bad behavior the solution in the (r, θ) coordinates, it should be neutralized when returning to the original z -coordinates in \mathbb{H} . If this behavior is theoretically understood, one could factor it out and apply a numerical method to compute the regular part.

B The unit disk or hemisphere to represent $\mathcal{F}_{\text{Bolza}}$

The fundamental domain $\mathcal{F}_{\text{Bolza}}$ inside the unit Poincaré disk is a regular octagon with circular arcs as sides. The vertices are at radius $2^{-1/4}$ and the arcs making a $\pi/4$ angle. Using the distance formula, the diameter is easily found to be (I guess) $4 \tanh^{-1}(2^{-1/4}) = 4.8969\dots$, and the systole is (see wikipedia page [show it, is it where I think?](#) $2 \cosh^{-1}(1+\sqrt{2}) = 3.05784\dots$

The Schwarz-Christoffel technique to conformally map rectilinear polygons to a half plane can be generalized to polygons with circular arcs¹⁵.

We now show how to construct in closed form a conformal mapping F of the unit disk in the w plane to the fundamental domain $z \in \mathcal{F}_{\text{Bolza}}$. This map has singularities like $(w - w_\kappa)^{1/4}$, $w_\kappa = e^{i(\pi/8 + \kappa\pi/4)}$.

Taking into account the discrete symmetry, it suffices to find a mapping

$$F : w \in P \rightarrow z \in T$$

from the the ‘pizza’ triangle P with angles $\pi/8, \pi/2, \pi/2$, which is $1/16$ of in the unit w -disc, to the triangular region $T \subset \mathcal{F}_{\text{Bolza}}$, joining the origin to consecutive vertices (which is $1/16$ of the fundamental domain having the concave arc, the corresponding angles being $\pi/8, \pi/2, \pi/8$). Such triangular maps are given explicitly via hypergeometric functions¹⁶. By the reflection principle applied 16 times this map F extends to w in the unit disk to the whole of $\mathcal{F}_{\text{Bolza}}$.

Let an upper half plane be $\xi = u + iv$, $v \leq 0$ be used as intermediary. Then F will be constructed as the composition $F = F_2 \circ F_1^{-1} : w \rightarrow \xi \rightarrow z$ where F_1, F_2 are conformal maps of the ξ -half plane to the triangles $w \in P$ and $z \in T$ respectively.

¹⁵See Nehari, Conformal mapping, V.7, p. 198-209 on, and

[https://doi.org/10.1016/0377-0427\(93\)90284-I](https://doi.org/10.1016/0377-0427(93)90284-I), [//doi.org/10.1137/0908003](https://doi.org/10.1137/0908003)

¹⁶I found the construction on a short technical report M. Harmer and G. Martin that also suggests the idea to transform the Laplace-Beltrami operator

<https://www.math.auckland.ac.nz/Research/Reports/Series/499.pdf>

Summarizing the derivations leading to the mass function m

We have (8):

$$m = \frac{4|dz/dw|^2}{(1 - |z(w)|^2)^2}, \quad w = r e^{i\theta}, \quad 0 \leq r \leq 1.$$

The denominator does not vanish. $\max |z(w)| = 2^{-1/4}$ and $z(w)$ is continuous at the boundary $|w| = 1$ (but not differentiable at the w_κ).

The factor $|dz/dw|$ simplifies as

$$|dz/dw| = \frac{\gamma_T |F_2^P|^2}{\gamma_P |F_2^T|^2} \quad (10)$$

and it will be the matter of computing the ratio near infinity of two hypergeometric functions, with $\alpha_1 = 1/8$ in both, $\alpha_3 = 1/2$ in both, and only differing in

$$\alpha_2^T = 1/8, \quad \alpha_2^P = 1/2.$$

This is because the two wronskians (25) are the same so they cancel out.

The numerical factors γ_T, γ_P are given below in (19), (24).

The F_2 's are hypergeometric functions with parameters a, b, c given by:

For triangle T : $\alpha_1 = 1/8, \alpha_3 = 1/2, \alpha_2 = 1/8$

$$a =$$

$$b =$$

$$c =$$

For triangle P : $\alpha_1 = 1/8, \alpha_3 = 1/2, \alpha_2 = 1/2$

$$a =$$

$$b =$$

$$c =$$

The hypergeometric functions have poles

C Mapping curvilinear triangles to upper half plane

7. Domains Bounded by Circular Arcs. In this section we shall consider the conformal mapping of domains which are bounded by a finite number of circular arcs. For greater brevity, such a domain will be referred to as a *curvilinear polygon* (Fig. 20).

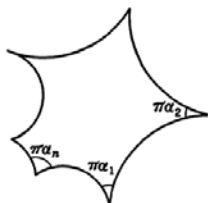


FIG. 20.

Our aim is to find the function $w = f(z)$ which maps the upper half-plane $\text{Re } \{z\} > 0$ onto the interior of this figure. In the similar problem of the preceding section, the crucial step was the introduction of the differential operator w'/w' which is not affected if the function w is replaced by $aw + b$, where a and b are arbitrary constants. To put it differently, this operator is invariant under a

linear substitution which transforms any straight line into any other straight line. In the present problem, the domain in question is not bounded by linear segments but by circular arcs, and it may therefore be expected that a fundamental role will be played by a differential operator which is not susceptible to transformations carrying circles into circles, i.e., general linear transformations.

Consider a polygon in the z -plane with circular arcs whose sides make angles $\pi\alpha_i$ at the vertices A_i , $i = 1, \dots, n$. We want it to be the conformal image

$$z = f(\xi), \quad \xi \text{ in the upper half plane.} \quad (11)$$

The vertices will correspond to points a_i on the real axis. Near the a_i , $f(\xi) = (\xi - a_i)^{\alpha_i}$ times a regular function, due to the angle conditions.

Using the Schwarzian derivative

$$\{f, z\} = (f''/f')' - (1/2)(f''/f')^2$$

and the Liouville boundedness theorem trick (used to show that a function is constant), it turns out that

$$\{f, z\} = \frac{1}{2} \sum_{\kappa=1}^n \frac{1 - \alpha_{\kappa}^2}{(\xi - a_{\kappa})^2} + \sum_{\kappa=1}^n \frac{\beta_{\kappa}}{\xi - a_{\kappa}}$$

with the accessory parameters β_{κ} , a third order ODE. The β 's satisfy three compatibility conditions¹⁷. Making $f = F_1/F_2$ one reduces to a second order linear ODE such that F_1, F_2 are linearly independent solutions¹⁸.

For triangles, the linear ODE turns out to be the hypergeometric¹⁹.

¹⁷Nehari, Conformal mapping, chapter 7, specially eqs (56, 58, 59).

¹⁸Details can be seen in Nehari, Conformal mapping, chapter 7, pg. 198-209, especially equations (56,58,59).

¹⁹Nehari, formulas (61-65, 72).

Triangle T in Poincaré z -disk²⁰.

Let T be a geodesic triangle in the Poincaré disk $|z| \leq 1$, where the sides meet at angles $\pi\alpha_1, \pi\alpha_2, \pi\alpha_3$ at the vertices A_1, A_2, A_3 . We take A_1 at the origin, A_3 in the positive real axis, and A_2 on the ray $e^{\pi\alpha_1}$.

We want the sides A_1A_2, A_1A_3 to be rectilinear, while A_2A_3 is the arc of a (concave) circle, whose extension meets the unit circle at right angles. These conditions give an uniquely defined geodesic triangle in Poincaré disk.

In the example of our interest, the triangle $T \subset \mathcal{F}_{Bolza}$ has angles

$$\alpha_1 = \pi/8, \alpha_2 = \pi/8, \alpha_3 = \pi/2.$$

In general, $\alpha_1 + \alpha_2 + \alpha_3 < 1$. We want T to be the conformal image of

$$z = f_T(\xi), \quad \xi \text{ in the upper half plane.} \quad (12)$$

The vertices will correspond to

$$a_1 = 0, a_2 = \infty, a_3 = 1$$

on the real axis:

$$A_1 = f(0), A_2 = f(\infty), A_3 = f(1) \quad (13)$$

Proposition 1 *The conformal map will be given by*

$$z = f(\xi) = \gamma F_1(\xi)/F_2(\xi) \quad (14)$$

where F_1, F_2 are specially chosen (N. p. 206, p. 314) linearly independent solutions of the hypergeometric equation²¹

$$\xi(1-\xi)F''(\xi) + [c - (a+b+1)\xi]F'(\xi) - abF = 0 \quad (15)$$

with parameters

$$\begin{aligned} a &= \frac{1}{2}(1 - \alpha_1 + \alpha_2 - \alpha_3) \\ b &= \frac{1}{2}(1 - \alpha_1 - \alpha_2 - \alpha_3) \\ c &= 1 - \alpha_1. \end{aligned} \quad (16)$$

²⁰We follow the notes by Harmer and Martin.

²¹<https://dlmf.nist.gov/15>

https://en.wikipedia.org/wiki/Hypergeometric_function

<https://mathworld.wolfram.com/HypergeometricFunction.html>

<https://www.mathworks.com/help/symbolic/hypergeom.html>

<https://keisan.casio.com/exec/system/1349143084>

To grit,

$$\begin{aligned} F_2(\xi) &= F(\xi; a, b, c) \quad (\text{the hypergeometric}) \\ F_1(\xi) &= \xi^{1-c} F(\xi; a', b', c) \quad (\text{note that } 1 - c = \alpha_1) \end{aligned} \quad (17)$$

where

$$\begin{aligned} a' &= a - c + 1 = \frac{1}{2}(1 + \alpha_1 + \alpha_2 - \alpha_3) \\ b' &= b - c + 1 = \frac{1}{2}(1 + \alpha_1 - \alpha_2 - \alpha_3) \\ c' &= 2 - c = 1 + \alpha_1 \end{aligned} \quad (18)$$

Finally, for the geodesic triangle T , one obtains

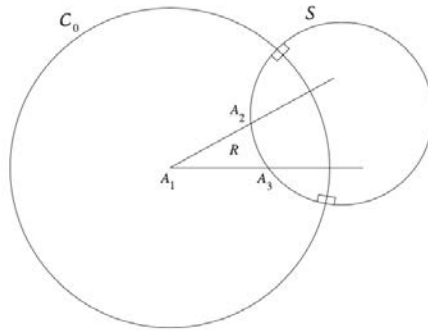
$$\gamma_T = \sqrt{\frac{\cos(\pi\alpha_1 + \pi\alpha_2) + \cos(\pi\alpha_3)}{\cos(\pi\alpha_1 - \pi\alpha_2) + \cos(\pi\alpha_3)}} \frac{\Gamma(1 - \alpha_1)}{\Gamma(1 + \alpha_1)} \frac{\Gamma(\frac{1}{2}(1 + \alpha_1 + \alpha_2 + \alpha_3))}{\Gamma(\frac{1}{2}(1 - \alpha_1 + \alpha_2 + \alpha_3))} \frac{\Gamma(\frac{1}{2}(1 + \alpha_1 + \alpha_2 - \alpha_3))}{\Gamma(\frac{1}{2}(1 - \alpha_1 + \alpha_2 - \alpha_3))}. \quad (19)$$

(20)

(using the Gamma function relations with the hypergeometric equation²²).

Outline of the proof. Since $0 < \alpha_1 < 1$, we have $0 < c(= 1 - \alpha_1) < 1$. We choose the branch of ξ^{1-c} so that ξ^{1-c} is real on the positive real axis and $z^{1-c} = |z|^{1-c} e^{i\pi(1-c)}$ on the negative real axis.

It is known that F_1 is a linearly independent solution of the hypergeometric equation with the same parameters (a , b and c) as F_2 .



The auxiliary circle C_o is centered in A_1 and intersects S at right angles.

²²https://en.wikipedia.org/wiki/Gamma_function
<https://keisan.casio.com/exec/system/1180573444>

It follows from the properties of the hypergeometric ODE that

Lemma 1 For $\gamma = 1$

$$A_1 = 0$$

$$\begin{aligned} A_3 &= f(1) = F(1; a', b', c')/F(1; a, b, c) \quad (\text{in the positive real axis}) \\ &= \frac{\Gamma(1 + \alpha_1)}{\Gamma(1 - \alpha_1)} \frac{\Gamma(\frac{1}{2}(1 - \alpha_1 + \alpha_2 + \alpha_3))}{\Gamma(\frac{1}{2}(1 + \alpha_1 + \alpha_2 + \alpha_3))} \frac{\Gamma(\frac{1}{2}(1 - \alpha_1 - \alpha_2 + \alpha_3))}{\Gamma(\frac{1}{2}(1 + \alpha_1 - \alpha_2 + \alpha_3))} \end{aligned}$$

$$A_2 = e^{i\pi\alpha_1} \frac{\Gamma(1 + \alpha_1)}{\Gamma(1 - \alpha_1)} \frac{\Gamma(\frac{1}{2}(1 - \alpha_1 + \alpha_2 + \alpha_3))}{\Gamma(\frac{1}{2}(1 + \alpha_1 + \alpha_2 + \alpha_3))} \frac{\Gamma(\frac{1}{2}(1 - \alpha_1 - \alpha_2 + \alpha_3))}{\Gamma(\frac{1}{2}(1 + \alpha_1 + \alpha_2 - \alpha_3))} \quad (21)$$

A_1A_2 and A_1A_3 are straight lines, and by construction the the angles at A_1, A_2 and A_3 are the correct ones.

It remains only to find the scale factor γ . This is achieved by the following clever argument.

Rescale $f \rightarrow \gamma f$ so that the radius of C_o equals 1.

Then C_o can be interpreted as Poincaré disk and the triangle A, A_2, A_3 is a geodesic triangle. The hyperbolic cosine rule²³ gives

$$\cosh(\rho(A_1, A_2)) = \frac{\cos(\pi\alpha_1) \cos(\pi\alpha_2) + \cos(\pi\alpha_3)}{\sin(\pi\alpha_1) \sin(\pi\alpha_2)}$$

On the other hand the Euclidian length is $\tanh(\rho(A_1, A_2)/2)$ which is

$$\tanh(\rho(A_1, A_2)/2) = \sqrt{\frac{\cosh(\rho(A_1, A_2)) - 1}{\cosh(\rho(A_1, A_2)) + 1}} = \sqrt{\frac{\cos(\pi\alpha_1 + \pi\alpha_2) + \cos(\pi\alpha_3)}{\cos(\pi\alpha_1 - \pi\alpha_2) + \cos(\pi\alpha_3)}}$$

Comparing with the value of $|A_2|$ above, we get

$$\gamma = \sqrt{\frac{\cos(\pi\alpha_1 + \pi\alpha_2) + \cos(\pi\alpha_3)}{\cos(\pi\alpha_1 - \pi\alpha_2) + \cos(\pi\alpha_3)}} \frac{\Gamma(1 - \alpha_1)}{\Gamma(1 + \alpha_1)} \frac{\Gamma(\frac{1}{2}(1 + \alpha_1 + \alpha_2 + \alpha_3))}{\Gamma(\frac{1}{2}(1 - \alpha_1 + \alpha_2 + \alpha_3))} \frac{\Gamma(\frac{1}{2}(1 + \alpha_1 + \alpha_2 - \alpha_3))}{\Gamma(\frac{1}{2}(1 - \alpha_1 + \alpha_2 - \alpha_3))}$$

. \square

²³A. F. Beardon. The Geometry of Discrete Groups. Springer-Verlag, Berlin, 1983.

Triangle P in the w -plane.

The map $w = f_P(\xi)$ is defined in the same way - and the scale factor is easier to find.

For an 'honest' pizza slice (such that $0 < \alpha_1 < 1$) and $\alpha_2 = \alpha_3 = 1/2$, the same formulas (14, 15, 16, 17, 18) hold. In the Bolza surface $\alpha_1 = 1/8$. We have:

$$|A_2| = |A_3| = \frac{\Gamma(1 + \alpha_1) \Gamma(\frac{1}{2}(2 - \alpha_1)) \Gamma(\frac{1}{2}(1 - \alpha_1))}{\Gamma(1 - \alpha_1) \Gamma(\frac{1}{2}(2 + \alpha_1)) \Gamma(\frac{1}{2}(1 + \alpha_1))} \quad (22)$$

In the hypergeometric functions F_1, F_2 (17) we insert

$$a = \frac{1}{2}(1 - \alpha_1), \quad b = -\frac{\alpha_1}{2}, \quad c = 1 - \alpha_1 \quad (23)$$

and the scaling factor is (all arguments of the Gamma functions in (22) are positive)

$$\gamma_P = 1/|A_2| \quad (\text{with the above } A_2). \quad (24)$$

Differentiating $z = f_T(\xi)$ and $w = f_P(\xi)$

The procedures are the same. Our functions are of the same form, namely quotient of linearly independent solutions of the same hypergeometric ODE,

$$f(\xi) = \gamma F_1(\xi)/F_2(\xi)$$

Then

$$df/d\xi = \gamma \frac{W(F_1, F_2)}{F_2^2}$$

where

$$W(F_1, F_2) = F_{1,z}F_2 - F_{2,z}F_1$$

is the Wronskian. But it is known that the Wronskian of two solutions of the *same* hypergeometric equation satisfies the linear ODE

$$dW/d\xi = \frac{c - (a + b + 1)\xi}{\xi(1 - \xi)} W.$$

and it follows that²⁴

$$W(F_1, F_2) = \alpha_1(1 - \xi)^{\alpha_3 - 1} \xi^{\alpha_1 - 1} \quad (25)$$

This trick expedites using the differentiation formula for a hypergeometric function²⁵.

²⁴<https://dlmf.nist.gov/15.10>, formula 15.10.3 .

²⁵<https://dlmf.nist.gov/15.5>

von Kármán vortex street and the induced flutter

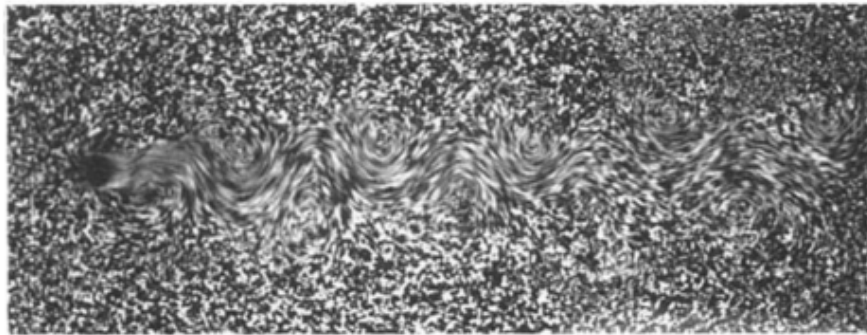
AERODYNAMICS

*Selected Topics in the Light of
Their Historical Development*

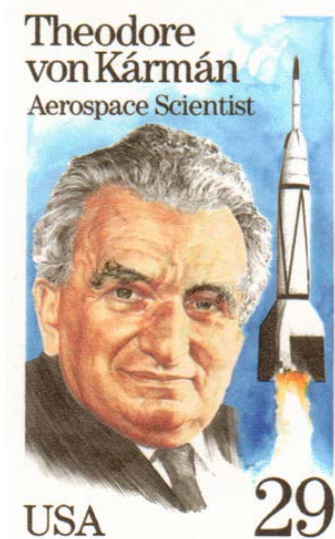


Fig. 32. Double rows of alternating vortices; symmetric (*upper*) and asymmetric (*lower*) arrangements.

Theodore von Kármán

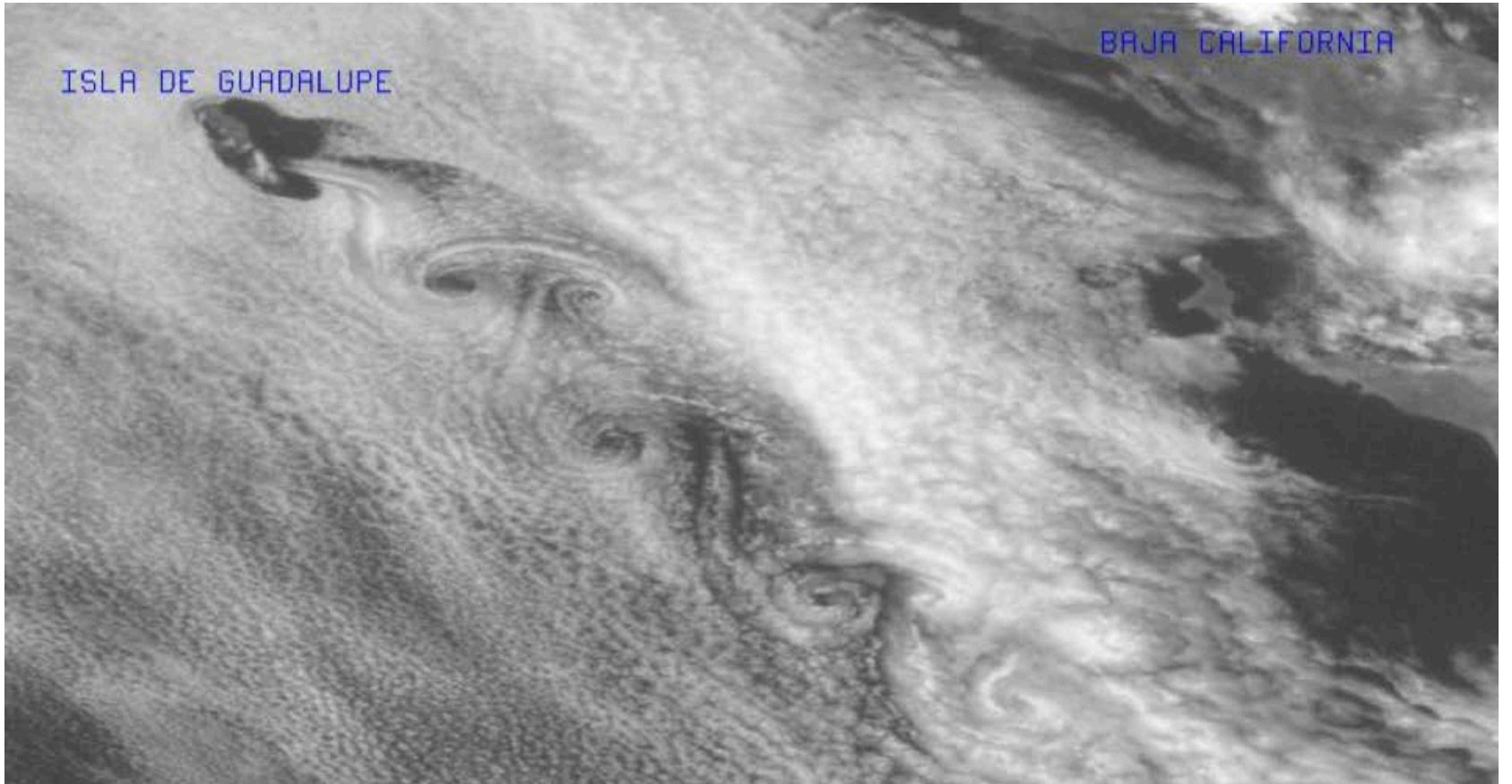


I. Tani, *Fluid Mechanics* [in Japanese], [copyright 1951, Iwanami Shoten], by permission.



ISLA DE GUADALUPE

BAJA CALIFORNIA

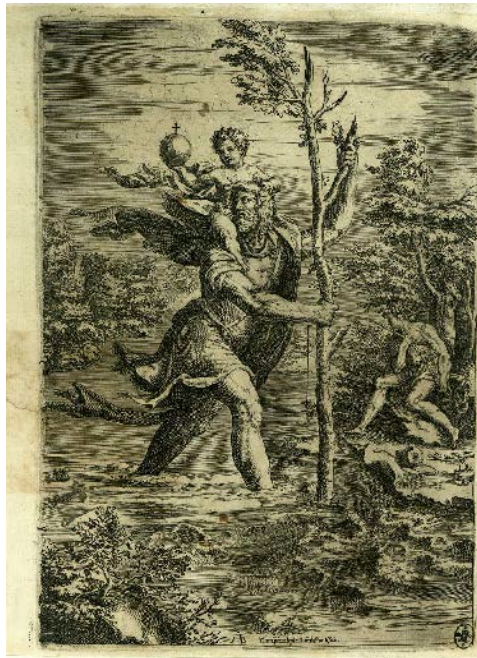


O Santo protetor

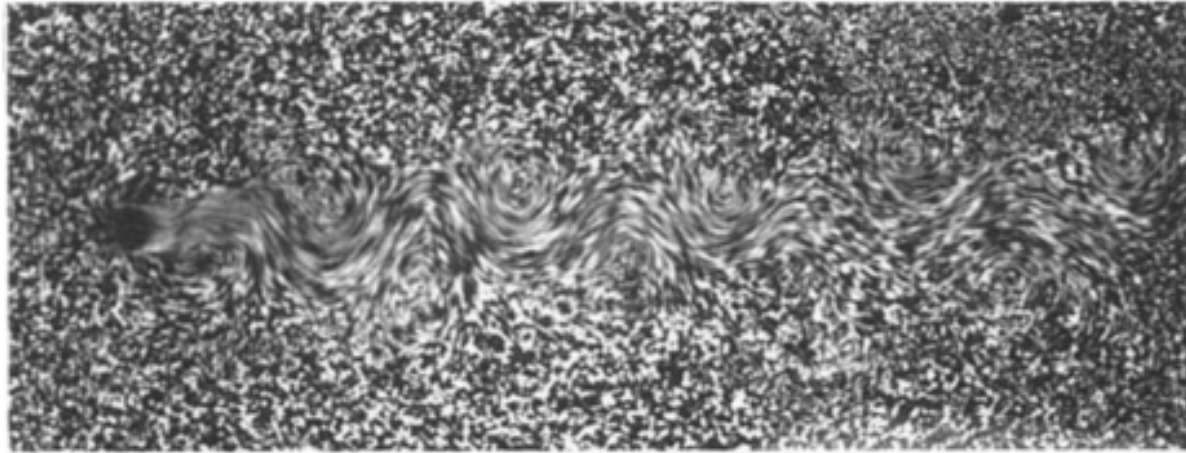
The search

'I bought Kármán's Aerodynamics in 1966 and was captivated by the story about St Christopher. During the 70s, I went twice to Bologna and was unable to trace St Christopher in any of the churches. In the 80s, Professor Buresti of the University of Pisa suggested the help of his relative, a cardinal in the Vatican. The answer came that, although a long list of St Christopher's paintings exists, none is in Bologna. My wife spotted St Christopher in a 1420-30 manuscript held at the Fitzwilliam museum in Cambridge. It was a book illumination on vellum and behind St Christopher's feet only two alternating eddies are depicted.

In the late 90s, Professor Mizota of Fukuoka Institute of Technology came on sabbatical to England. He was fascinated and decided to renew the search. He found a life-size St Christopher in the badly damaged fifteenth century mural in the Basilica di San Domenico in Bologna. Miraculously, the best preserved part is the wake in the mural, see above. The procession of eddies along the wake is now called the Kármán-Bénard eddy street. (Bénard's sketches and photo from (1908J) and (1913J) were reproduced in Vol. 1, Figs 1.7 and 18.4, p. 11 and 511, respectively.)'



Mizota et al. (2000J), *Nature*, **404**, No. 6775, p. 226.



I. Tani, *Fluid Mechanics* [in Japanese], [copyright 1951, Iwanami Shoten], by permission.

The arrangement of the vortices shown in Fig. 31 is connected with my name; it is usually called a *Kármán vortex street* or a *Kármán vortex trail*. But I do not claim to have discovered these vortices; they were known long before I was born. The earliest picture in which I have seen them is one in a church in Bologna, Italy, where St. Christopher is shown carrying the child Jesus across a flowing stream. Behind the saint's naked foot the painter indicated alternating vortices. Alternating vortices behind obstacles were observed and photographed by an English scientist, Henry Reginald Arnulph Mallock (1851-1933) (Ref. 3), and then by a French professor, Henri Bénard (1874-1939) (Ref. 4). Bénard did a great deal of work on the problem before I did, but he chiefly observed the vortices in very viscous fluids or in colloidal solutions and considered them more from the point of view

of experimental physics than aerodynamics. Nevertheless, he was somewhat jealous because the vortex system was connected with my name, and several times—for example, at the International Congresses for Applied Mechanics held in Zurich (1926) and in Stockholm (1930)—claimed priority for earlier observation of the phenomenon. In reply I once said, “I agree that what in Berlin and London is called ‘Kármán Street’ in Paris shall be called ‘Avenue de Henri Bénard.’” After this wisecrack we made peace and became quite good friends.

What I really contributed to the aerodynamic knowledge of the observed phenomenon is twofold (Ref. 5): I think I was the first to show that the symmetric arrangement of vortices (Fig. 32, *upper*), which would be an obvious possibility to replace the



Fig. 32. Double rows of alternating vortices; symmetric (*upper*) and asymmetric (*lower*) arrangements.

vortex sheet, is unstable. I found that only the asymmetric arrangement (Fig. 32, *lower*) could be stable, and only for a certain ratio of the distance between the rows and the distance between two consecutive vortices of each row. Also, I connected the momentum carried by the vortex system with the drag and showed how the creation of such a vortex system can represent the mechanism of the wake drag—a point for which neither Mallock nor Bénard cared very much.

Herr Hiemenz: “It always oscillates”

to the surface of a body. Prandtl had a doctoral candidate, Karl Hiemenz (Ref. 6), to whom he gave the task of constructing a water channel in which he could observe the separation of the flow behind a cylinder. The object was to check experimentally the separation point calculated by means of the boundary-layer theory. For this purpose, it was first necessary to know the pressure distribution around the cylinder in a steady flow. Much to his surprise, Hiemenz found that the flow in his channel oscillated violently.

When he reported this to Prandtl, the latter told him: “Obviously your cylinder is not circular.”

However, even after very careful machining of the cylinder, the flow continued to oscillate. Then Hiemenz was told that possibly the channel was not symmetric, and he started to adjust it.

I was not concerned with this problem, but every morning when I came in the laboratory I asked him, “Herr Hiemenz, is the flow steady now?”

He answered very sadly, “It always oscillates.”¹

Now, I thought, if the flow always oscillates, this phenomenon must have a natural and intrinsic reason. One weekend I tried to calculate the stability of the system of vortices, and I did it in a very primitive way. I assumed that only one vortex was free to move, while all the other vortices were fixed, and calculated what would happen if this vortex were displaced slightly. The result I got was that, provided a symmetric arrangement was assumed, the vortex always went off from its original position. I obtained the same result for asymmetric arrangements but found that, for a definite ratio of the distances between the rows and between two consecutive vortices, the vortex remained in the immediate neighborhood of its original position, describing a kind of small closed circular path around it.

I finished my work over the weekend and asked Prandtl on Monday, "What do you think about this?"

"You have something," he answered. "Write it up and I will present your paper in the Academy."

This was my first paper on the subject. Then because I thought my assumption was somewhat too arbitrary, I considered a system in which all vortices were movable. This required a little more complicated mathematical calculation, but after a few weeks I finished the calculation and wrote a second paper.

Some people asked, "Why did you publish two papers in three weeks? One of them must be wrong." Not exactly wrong, but I first gave a crude approximation and afterward refined it. The result was essentially the same; only the numerical value of the critical ratio was different.

Now these vortices have many physical applications. Shortly after the publication of my paper, Rayleigh (Ref. 7) got the idea that the alternating vortices must give the explanation of the Aeolian harp—the singing wires. Some people will still remember the singing wires of the biplane cellules. The singing comes from the periodical shedding of vortices. When certain struts used on an underwater vehicle sang a high tune, Gongwer (Ref. 8) showed experimentally that the vibration was caused by the periodical shedding of vortices, which occurred when the trailing edges were not properly sharp. This also explains the singing of marine propellers, as was previously found by Gutsche (Ref. 9).

A French naval engineer told me of a case where the periscope of a submarine was completely useless at speeds over 7 knots under water, because the rod of the periscope produced periodic vortices whose frequency at a certain speed was in resonance with the natural vibration of the rod. Radio towers have shown resonant oscillations in natural wind. The galloping motion of power lines also has some connection with the shedding of vortices. The collapse of the bridge over the Tacoma Narrows was also caused by resonance due to periodic vortices. The designer wanted to

build an inexpensive structure and used flat plates as side walls instead of trusses. Unfortunately, these gave rise to shedding vortices, and the bridge started torsional oscillations, which developed amplitudes up to 40° before it broke. The phenomenon was a combination of flutter and resonance with vortex shedding. I am always prepared to be held responsible for some other mischief that the Kármán vortices have caused!



Some fear flutter because they do not understand it. And some fear it because they do.

— *Theodore von Karman* —



Jane Mansfield
from Hollywood
with an admirer
from Caltech